

DESIGN, MODELLING AND CONTROL OF AN AUTONOMOUS UNDERWATER VEHICLE

Louis Andrew Gonzalez

Bachelor of Engineering Honours Thesis 2004

Mobile Robotics Laboratory,
Centre for Intelligent Information Processing Systems,
School of Electrical, Electronic and Computer Engineering,
The University of Western Australia.



Supervisor

Associate Professor Thomas Bräunl

Letter of Transmittal

Louis Gonzalez
12 St John Rd
Wattle Grove WA 6107

31st October 2004

The Dean
Faculty of Engineering, Computing and Mathematics
University of Western Australia
Crawley WA 6009

Dear Professor Mark Bush,

It is with great pride and honour that I submit this thesis entitled *Design, Modelling and Control of an Autonomous Underwater Vehicle* to the University of Western Australia as partial fulfilment of the requirements for a degree of Bachelor of Engineering with Honours.

Yours Faithfully,

Louis Gonzalez

For CIIPS and the Mobile Robot Lab

Thomas, I hope that the founding of Project Mako will begin a long running tradition for the Mobile Robotics Lab with many students eager to participate in this exciting and rewarding ongoing underwater project every year.

It has been a sheer pleasure in establishing and participating in UWA's first ever AUV project and developing one of the largest and most distinctive robotic vehicles to have come out of the laboratory.

Abstract

Autonomous underwater vehicles are currently being utilised for scientific, commercial and military underwater applications. These vehicles require autonomous guidance and control systems in order to perform underwater tasks. Modelling, system identification and control of these vehicles are still major active areas of research and development.

This thesis is concerned with the design and development of an AUV specifically intended for entry into international underwater vehicle competitions. The thesis consists of two phases; the first involves the design and construction of the vehicle while the second phase is concerned with the modelling and system identification of the vehicle, as well as the simulation of a control system.

The design and development of the vehicle consisted of implementing a mechanical and electrical system, as well as the integration of subsystems. The development of these systems has resulted in a low-speed, bottom-heavy, open-frame underwater vehicle named the *Mako* that exhibits high symmetry, modularity and stability.

The modelling of the *Mako* was then performed which involved the application of the dynamic model of an underwater vehicle and the consequent identification of the relevant parameters. The system identification of the vehicle parameters consisted of using onboard sensors to perform static and dynamic experiments. Least squares estimation was used to estimate the parameters from the experimental data obtained.

For the control system of the *Mako*, a PID tracking controller based on computed torque control was adopted. The controller was applied to the vehicle's dynamics and simulated using the parameters found in the system identification process. The results of the simulations demonstrate that this type of controller could indeed be successfully implemented on the vehicle.

The undertakings in this thesis have resulted in a functioning autonomous underwater vehicle that has undergone modelling, system identification and preliminary control analysis. The groundwork has indeed been laid for the *Mako's* entry into future underwater competitions.

Acknowledgements

There are a number of people that deserve mention and gratitude for their help, guidance and support during the course of this thesis project.

Firstly, I would like to give thanks to my fellow submariners, Minh Nguyen, Daniel Lim and Evan Broadway whom undertook the sonar, vision and communications projects respectively. Despite the odds and sheer size of the project, we held our heads up high and our uncompromising perseverance, determination and teamwork brought about the success and realisation of the *Mako* AUV.

I would like to give many thanks to my supervisor, Associate Professor Thomas Bräunl. His expertise, knowledge and his confidence in not only myself, but the whole project, despite its enormity and many setbacks, was vital and greatly aided in the project's success. Thankyou also for putting up with the 'renovations' in your lab. Thanks must also go to my co-supervisor by default, Chris Croft, for helping me acquire access to the water tanks in the hydraulics lab for testing the vehicle.

Many thanks go to the gentlemen in the mechanical and electronic workshops, particularly to Mark Henderson and Ivan Neubronner whom I collaborated closely with and whom helped me in realising the mechanical and electrical requirements of my AUV design using their expertise and first-rate skills. I also thank them for putting up with my persistent scrutinising of their work and my frequent adjustments and modifications. Without their dedication and commitment to detail, the AUV would not be as great as it is. I learnt many things from these gentlemen, namely that the gap between theory and practice is much larger than I had so naively believed it to be.

Thanks also go to my fellow colleagues, particularly Noah Ong and Christian Schmitz, whom were great sources of help and of support.

Thankyou also to my parents for their unconditional love, support and understanding throughout the year. Thanks for especially understanding my stress and neurosis, as well as putting up with my arriving home late (or early depending on your perspective) on numerous occasions. Thanks as well to my brother Christian and his wife Kathy for allowing me to use their pool for testing purposes.

Contents

1	Introduction	1
1.1	Autonomous Underwater Vehicles	1
1.1.1	Commercial and Research AUVs	2
1.1.2	Technology	2
1.2	AUV Systems and Components	3
1.3	Modelling and System Identification	3
1.4	Control Systems	4
1.5	Underwater Vehicle Competitions	4
1.5.1	AUVSI	4
1.5.2	Australasian Competition	4
1.6	Project Motivations and Objectives	5
1.7	Outline of Thesis	5
2	Design Essentials and Concepts	7
2.1	AUV Coordinate System	7
2.2	Factors Affecting an Underwater Vehicle	8
2.2.1	Buoyancy	8
2.2.2	Hydrodynamic Damping	9
2.2.3	Stability	9
2.2.4	Coriolis	10
2.2.5	Added Mass	10
2.2.6	Environmental Forces	11
2.2.7	Pressure	11
2.3	General Design of an AUV	11
2.3.1	Hull Design	11
2.3.2	Propulsion	11
2.3.3	Submerging	12
2.3.4	Electric Power	12
2.4	IAUVC Vehicle Designs	13
2.4.1	Massachusetts Institute of Technology	13
2.4.2	University of West Florida	14
2.4.3	Cornell University	14

2.4.4	University of Florida	15
2.4.5	Remark on Vehicle Designs	15
2.5	Summary	16
3	Mechanical and Electrical Design	17
3.1	Choosing the Final Design	17
3.2	Mechanical System Design	18
3.3	Electrical System Design	18
3.4	Mechanical and Electrical Systems Outline	20
3.4.1	Propulsion	21
3.4.2	Range of Motion	21
3.4.3	Upper Hull - Electronics	22
3.4.4	Lower Hull - Batteries	22
3.4.5	Skeletal Frame	22
3.4.6	Through-hull Connections	23
3.4.7	Power System	23
3.4.8	Controllers	24
3.4.9	Motor Controllers	25
3.4.10	Depth Sensor	25
3.4.11	Digital Magnetic Compass	26
3.4.12	Velocity Sensor	26
3.4.13	Leak Monitor	26
3.4.14	Power Monitor	27
3.5	Integration of Subsystems	27
3.5.1	Vision System	27
3.5.2	Sonar System	28
3.5.3	Communications System	28
3.6	Summary	29
4	Modelling and Control of AUVs	31
4.1	Control Problems	31
4.2	Control Techniques	31
4.3	State Vector Representation	32
4.3.1	Reference Frames	33
4.3.2	Notation of Transformations	33
4.3.3	Attitude and Euler Angles	33
4.3.4	State Space Representation	35
4.3.5	Position State Vector Transformation	36
4.3.6	Velocity State Vector Transformation	37
4.4	AUV Dynamic Model	39
4.4.1	Mass and Inertia Matrix	39

4.4.2	Coriolis and Centripetal Matrix	40
4.4.3	Hydrodynamic Damping Matrix	41
4.4.4	Gravitational and Buoyancy Vector	42
4.4.5	Forces and Torque Vector	42
4.5	Summary	43
5	Modelling the <i>Mako</i>	45
5.1	Assertions on Dynamics	45
5.1.1	Low Speed	46
5.1.2	Roll and Pitch	46
5.1.3	Symmetry	46
5.1.4	Posture	46
5.1.5	Environmental Disturbances	46
5.1.6	Sway	47
5.1.7	Decoupling	47
5.2	Simplifying the Dynamic Model Matrices	47
5.2.1	Mass and Inertia Matrix	48
5.2.2	Hydrodynamic Damping Matrix	49
5.2.3	Gravitational and Buoyancy Vector	49
5.2.4	Forces and Torque Vector	50
5.3	System Identification Approach	51
5.3.1	Model for Each Degree of Freedom	51
5.3.2	Least Squares Estimation	52
5.3.3	Static Experiment	52
5.3.4	Dynamic Experiment	53
5.4	Summary	54
6	System Identification	55
6.1	Thrust Measurement	55
6.1.1	Thrust Experiment	55
6.1.2	Remark on Thrust Outputs	56
6.2	Testing and Control	56
6.2.1	Communications	59
6.2.2	Remotely Controlling the <i>Mako</i>	59
6.2.3	Sensor Limitations	60
6.2.3.1	Magnetic Compass	60
6.2.3.2	Velocity Sensor	61
6.2.3.3	Depth Sensor	61
6.3	System Identification Results	61
6.3.1	Static Experiments	61
6.3.1.1	Surge Static Experiment	62

6.3.1.2	Heave Static Experiment	63
6.3.1.3	Yaw Static Experiment	65
6.3.2	Dynamic Experiments	66
6.3.2.1	Surge and Heave Inertial Parameters	66
6.3.2.2	Yaw Inertial Parameters	68
6.4	<i>Mako</i> Dynamic Model Parameters	68
6.5	Summary	69
7	Controller Simulation	71
7.1	Computed Torque Control	71
7.2	Applying Computed Torque Control to the <i>Mako</i>	72
7.2.1	PD Tracking Controller	72
7.2.2	PID Tracking Controller	73
7.3	Trajectory Generation	74
7.4	Controller Simulation	75
7.4.1	Simulator Implementation Issues	75
7.4.1.1	Simulating Feedback	75
7.4.1.2	Degrees of Freedom	75
7.4.1.3	Model Parameters	76
7.4.1.4	Realism	76
7.4.1.5	Trajectory Generation	76
7.4.2	Simulation Study	76
7.5	Analysis of Simulation	77
7.5.1	Overshoot	77
7.5.2	Thrust Output	82
7.5.3	Final Remark	82
7.6	Limitations of Simulation	82
7.6.1	Thrust Output	83
7.6.2	Heading Drift	83
7.6.3	Position	83
7.7	Controller Implementation	83
7.8	Summary	85
8	Conclusion	87
8.1	Contributions of the Thesis	87
8.2	Discussion on Outcomes	88
8.2.1	Mechanical System	88
8.2.2	Electrical System	88
8.2.3	Subsystems	89
8.2.4	Simplification of the Dynamic Model	89
8.2.5	Thrust Measurement	89

8.2.6	Remote Control	90
8.2.7	System Identification	90
8.2.8	Control System Simulation	90
8.3	Recommendations and Future Work	90
8.3.1	Mechanical System	91
8.3.2	Electrical System	91
8.3.3	Sensors	91
8.3.4	System Identification	91
8.3.5	Communications System	92
8.3.6	Control System	92
8.4	Final Word	92
A	IAUVC Rules and Mission 2004	93
A.1	Mission	93
A.1.1	Breakdown of Mission	93
A.1.2	Size and Weight Constraints	94
A.1.3	Other Restrictions	94
A.2	Placement of Elements in the Arena	95
A.2.1	Validation Gate	95
A.2.2	Target	95
A.2.3	Markers	96
A.2.4	Pinger	96
A.2.5	Recovery Zone	96
B	Electronic Components	97
B.1	Thrusters	97
B.2	Batteries	97
B.3	Computer/Microcontroller	98
B.4	Digital Magnetic Compass	99
B.5	Echo Sounder	99
B.6	Velocity Sensor	99
C	Design Concepts	101
C.1	Torpedo Shape	101
C.2	One Hull, Four Thrusters	102
C.3	Two Hulls, Four Thrusters	102
C.4	Two Hulls, Two Rotating Thrusters	103
C.5	Comparison of Designs	104
D	Mechanical System Design	105
D.1	Mechanical Requirements	105
D.2	Mechanical Design	106

D.2.1	Overview of Design	106
D.2.2	Material Selection	107
D.2.2.1	Hulls	108
D.2.2.2	Frame	108
D.2.3	Motor Selection	108
D.2.4	Hull Sizes	108
D.2.5	Mass and Volume Relationship	108
D.2.5.1	Total Expected Mass	109
D.2.5.2	Total Expected Volume	110
D.3	Comments on Design	110
E	Electrical System Design	113
E.1	Motion Control	113
E.2	Sonar and Vision Processing	114
E.3	Measuring Depth	114
E.4	Attitude	115
E.5	Velocity Sensor	115
E.6	Hull Breaches	115
E.7	Power Monitor	116
E.8	Power Supply	117
E.9	Through-hull connections	117
F	Construction Process	119
F.1	Construction of Components	119
F.1.1	Hulls	119
F.1.2	Through-hull Connections	120
F.1.3	Motors	120
F.1.4	Frame	121
F.1.5	Motor Controllers	122
F.1.6	Power Board	123
F.1.7	Regulators	123
F.2	Uniting the Components	123
F.3	Summary of Design and Construction	125
G	CDROM Listing	129
	References	131

Nomenclature

Acronyms

AUV	Autonomous Underwater Vehicle
ROV	Remotely Operated Vehicle
UWA	University of Western Australia
MIT	Massachusetts Institute of Technology
AUVSI	Association for Unmanned Vehicle Systems International
IAUVC	International Autonomous Underwater Vehicle Competition
nDOF	n Degrees of Freedom
PVC	Polyvinylchloride
PC	Personal Computer
RAM	Random Access Memory
ROM	Read Only Memory
LCD	Liquid Crystal Display
PD	Proportional Derivative
PID	Proportional Integral Derivative
ADC	Analog-to-Digital Converter
PWM	Pulse Width Modulation
Ah	Amp-hour

Nautical Terminology

Bow	Front side of vehicle
Stern	Back side of vehicle
Starboard	Right side of vehicle
Portside	Left side of vehicle
Surge	Motion in the longitudinal or x direction
Sway	Motion in the lateral or y direction
Heave	Motion in the vertical or z direction

Variable Table

SYMBOL	NAME	DESCRIPTION
W	weight	Magnitude of the weight of vehicle
B	buoyant force	Magnitude of the weight of water displaced by vehicle
g	gravitational acceleration	Acceleration due to gravity
RM	righting moment	The magnitude of the moment created by a distance existing between a body's centre of mass and centre of buoyancy
m	mass	Mass of vehicle
ρ	density	Density of seawater
V	volume	Volume of vehicle
c_D	drag coefficient	The coefficient of drag due to movement of a body underwater at constant speed
s	speed	Speed of vehicle in an arbitrary direction
A	area	The surface area of an arbitrary face of the vehicle
$\{B\}$	body frame	The Cartesian reference frame positioned on the vehicle
$\{W\}$	world frame	The Cartesian reference frame positioned on the surface of the world
\mathcal{R}	rotation matrix	Matrix for converting from body to world coordinates. The inverse is used to convert from world to body coordinates.
\mathcal{P}_B	position state vector	The position state vector corresponding to the vehicle
\mathbf{x}_B	position vector	Vector defining the position of the vehicle in Cartesian coordinates
Θ_B	attitude vector	Vector defining the attitude in Euler angles of the vehicle
x	x position	Position along the x axis
y	y position	Position along the y axis
z	z position	Position along the z axis
ϕ	roll Euler angle	Angle of rotation about the x axis
θ	pitch Euler angle	Angle of rotation about the y axis
ψ	yaw Euler angle	Angle of rotation about the z axis

SYMBOL	NAME	DESCRIPTION
\mathcal{V}_B	velocity state vector	The velocity state vector corresponding to the vehicle
v_B	linear velocity vector	Vector defining the linear velocities of the vehicle along the Cartesian axes
ω_B	angular velocity vector	Vector defining the angular velocities of the vehicle about the Cartesian axes
u	surge	The vehicle's linear velocity along the x axis
v	sway	The vehicle's linear velocity along the y axis
w	heave	The vehicle's linear velocity along the z axis
p	vehicle roll rate	The vehicle's angular velocity about the x axis
q	vehicle pitch rate	The vehicle's angular velocity about the y axis
r	vehicle yaw rate	The vehicle's angular velocity about the z axis
\mathcal{T}_B	force/torque state vector	The force and torque state vector corresponding to the vehicle
\mathcal{F}_B	force vector	Vector defining the forces applied to the vehicle along the Cartesian axes
\mathcal{W}_B	torque vector	Vector defining the torques or moments applied to the vehicle about the Cartesian axes
X		Force applied to vehicle along the x axis
Y		Force applied to vehicle along the y axis
Z		Force applied to vehicle along the z axis
K		Torque applied to vehicle along the x axis
M		Torque applied to vehicle along the y axis
N		Torque applied to vehicle along the z axis
$\dot{\phi}$	roll rate	Angular velocity about the world frame's x axis
$\dot{\theta}$	pitch rate	Angular velocity about the world frame's y axis
$\dot{\psi}$	yaw rate	Angular velocity about the world frame's z axis
\mathcal{W}		Matrix for converting body angular velocities to world angular velocities. The inverse is used to convert from world to body angular velocities.
M	mass and inertia matrix	Matrix that defines the mass and inertia of the vehicle
M_{RB}	rigid body mass matrix	Matrix defining the mass and inertia of the vehicle when viewed as a rigid body
M_A	added mass matrix	Matrix used to account for the added mass like effect that occurs during acceleration underwater

SYMBOL	NAME	DESCRIPTION
I_x		Mass moment of inertia coefficient about the x axis
I_y		Mass moment of inertia coefficient about the y axis
I_z		Mass moment of inertia coefficient about the z axis
$C(\mathcal{V})$	Coriolis and centripetal matrix	Matrix that defines the Coriolis and centripetal effects affecting the vehicle underwater
$C_{RB}(\mathcal{V})$	rigid body Coriolis and centripetal matrix	Matrix that defines the rigid body Coriolis and centripetal effects induced by M_{RB}
$C_A(\mathcal{V})$	Coriolis-like matrix	Matrix that defines the Coriolis effects induced by M_A
$D(\mathcal{V})$	hydrodynamic damping matrix	Matrix that defines the damping effects due to underwater drag
G	gravitational and buoyancy vector	Vector matrix that defines the gravitational and buoyant forces acting on the vehicle
f_B	buoyant force vector	Vector matrix denoting the buoyant forces acting on the vehicle
f_G	gravitational force vector	Vector matrix denoting the gravitational forces acting on the vehicle
r_B	centre of buoyancy vector	Vector matrix defining the position of the vehicle's centre of buoyancy
r_G	centre of gravity vector	Vector matrix defining the position of the vehicle's centre of gravity
x_B		Distance along x axis from origin of vehicle's reference frame to centre of buoyancy
y_B		Distance along y axis from origin of vehicle's reference frame to centre of buoyancy
z_B		Distance along z axis from origin of vehicle's reference frame to centre of buoyancy
L	thrust mapping matrix	Matrix that maps the thrusts produced by the vehicle's thrusters to external forces and torques on the vehicle along and about the Cartesian axes
U	thrust vector	Vector matrix that defines the thrusts produced by each of the vehicle's thrusters
m_ξ		Inertial parameter for a particular degree of freedom
$m_{RB,\xi}$		Rigid body inertial parameter for a particular degree of freedom
$m_{A,\xi}$		Added mass parameter for a particular degree of freedom

SYMBOL	NAME	DESCRIPTION
d_ξ		Linear damping coefficient for a particular degree of freedom
$d_{\xi \xi }$		Quadratic damping coefficient for a particular degree of freedom
g_ξ		Gravitational and buoyancy coefficient for a particular degree of freedom
τ_ξ		Input force/torque for a particular degree of freedom
$\dot{\xi}$		Velocity for a particular degree of freedom
$\hat{\Lambda}$		Estimate of parameter used in least squares estimation
$\hat{\sigma}_\Lambda$		Standard deviation of estimated parameter
$\hat{\sigma}^2$		Estimated Gaussian zero mean measurement noise variance
ς		Error of estimated parameter
\mathcal{T}'		Variable used in linearising nonlinear system in computed torque control
\mathcal{P}_d		Desired position vector for tracking controller
\mathcal{V}_d		Desired velocity vector for tracking controller
$\dot{\mathcal{V}}_d$		Desired acceleration vector for tracking controller
ϵ		Position error vector for tracking controller
$\dot{\epsilon}$		Velocity error vector for tracking controller

Chapter 1

Introduction

The robotics world has reached a stage where the remotely operated vehicle (ROV) industry is very well established with thousands upon thousands of ROVs having been created and deployed since the dawn of this industry. The need for autonomy in robots and vehicles, however, is becoming more and more a prevalent issue in many situations and environments worldwide. The ability to communicate between the operator and the vehicle is one of the main factors affecting whether a vehicle is to be designed as an ROV or as an autonomous vehicle. For instance, in environments where communication with a vehicle is inhibited or not possible, autonomous control is then required as opposed to remote control.

One of the environments in which communication is very much constrained is underwater. Underwater vehicles are playing a vital role in underwater exploration and allowing humans to explore great depths. ROVs have been used in the offshore industry since the late 1960s and are well established and specialised vehicles for deepwater missions. However, their constraints such as the need for a communications tether and a control platform have limited their use and capabilities.

1.1 Autonomous Underwater Vehicles

To overcome the deficiencies of ROVs, autonomous underwater vehicles (AUVs) have stepped to the forefront of deepwater exploration. AUVs are untethered, fully automated submersible platforms capable of performing underwater tasks and missions with their onboard sensor, navigation and payload equipment [1]. Despite an AUV's increased complexity, particularly with respect to its programming, its advantages over an ROV far outweigh the added complexity of designing and building one.

Today, the AUV industry is growing dramatically with the increase in the reliability and technical abilities of these vehicles. The goal in underwater robotics at present is to create fully self-contained, intelligent, decision-making AUVs [2]. In order to accomplish this goal, much research is being carried out worldwide with particular emphasis on autonomy, navigation, object detection, energy sources and information systems.

1.1.1 Commercial and Research AUVs

AUVs are not merely restricted to scientific underwater exploratory applications. They are also used for military purposes, inspection of underwater structures, as well as being largely utilised in the mining and oil industries [3]. Many countries have intensive AUV research and development programs. This is a clear indication of the growing importance and significance of these vehicles.

Bluefin Robotics is a corporation that was developed from the AUV laboratory at Massachusetts Institute of Technology (MIT) and is a world leader in underwater vehicle development. It commenced building AUVs in 1989 and its success in this area has led to the deployment of these vehicles all over the world [4].

The Naval Postgraduate School of California is an institute with its own AUV department and is currently undergoing intensive research into navigation, control, fault detection, computer simulations and various other areas for these vehicles. At present the department has two main AUVs (Figure 1.1). The *ARIES* is being used to develop and test underwater navigation systems while the *Phoenix* is used as a testbed for underwater vehicle control systems.

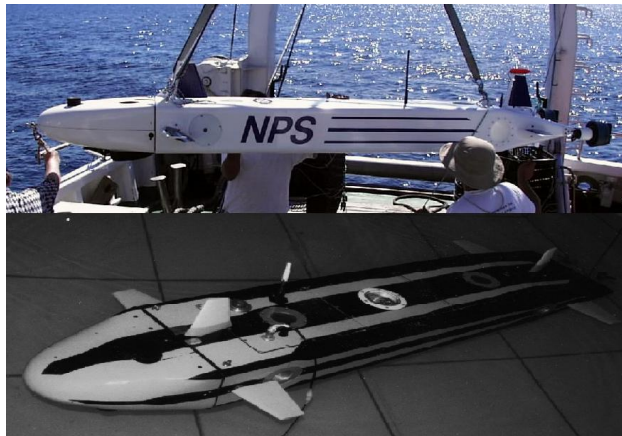


FIGURE 1.1: (Top) The *ARIES*. (Bottom) The *Phoenix* [5].

The Defence Advanced Research Projects Agency of the United States began an AUV program in the late 1980s specifically oriented toward military applications. At present, the vehicles built by the agency are the largest and more versatile of any AUVs built anywhere else. They have been used in testing advanced underwater technologies and systems, and have proven instrumental in advancing developments in underwater vehicles worldwide.

1.1.2 Technology

Many new underwater technologies are being explored and applied to AUVs. For instance, hybrid underwater vehicles utilising both ROV and AUV technologies are currently being used by The Monterey Bay Aquarium Research Institute of California. MIT is working

on fish tail propulsion systems to use on their vehicles while institutes such as Nekton Research have been developing miniature AUVs (Figure 1.2) that can travel in groups, communicate with each other and provide researchers with simultaneous data over a large volume of water [6]. AUV research and technology is definitely on an upward curve.

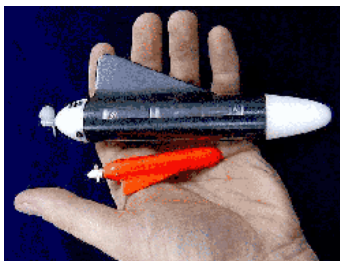


FIGURE 1.2: Nekton Research's miniature AUV prototype [6].

1.2 AUV Systems and Components

The only means by which an AUV can control and navigate itself successfully underwater is by obtaining real-time data and conditions from its immediate surrounding environment. It attains the necessary information via its onboard sensors and systems. Every AUV at its most basic form must have some sort of navigation system, propulsion system and a dry, watertight environment to house onboard components. In addition, an AUV will usually possess the following systems and components as seen in Figure 1.3.

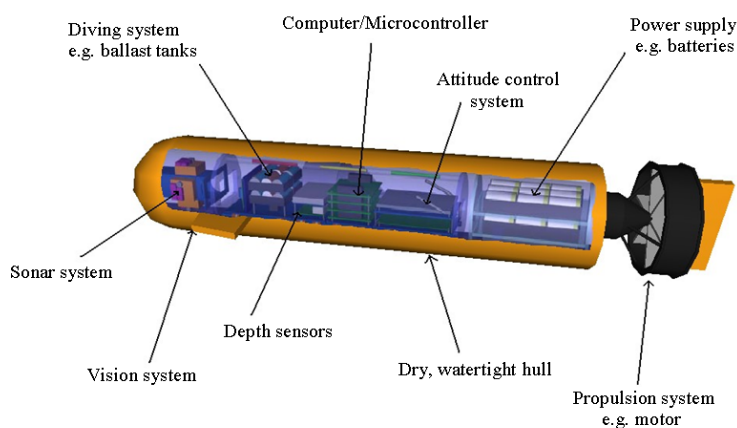


FIGURE 1.3: AUV systems and components.

1.3 Modelling and System Identification

In order to design, simulate and develop control systems for underwater vehicles, a dynamic model must first be identified and the relevant parameters found by performing system

identification [7]. System identification approaches for modelling AUVs have been undertaken extensively for various types of underwater vehicles [8–11]. Modelling of underwater vehicles in the past has mainly consisted of data acquisition from a mathematical model. Present day techniques mostly involve identification through onboard sensors [12]. This technique allows modelling to occur in a timely manner and avoids complex mathematical modelling techniques.

1.4 Control Systems

Once modelling and system identification has been undertaken, a control system can then be designed for an underwater vehicle. Control systems are required to provide signals to the actuators in order to achieve the desired positions and velocities for the vehicle. Controlling underwater vehicles is very challenging due to the nature of underwater dynamics. Control systems for AUVs have therefore been an area of much research with many different techniques having been proposed in the literature to provide autonomy [13–16]. Current state of the art technology is focused on using intelligent controllers to provide autonomous underwater vehicles with superior control capabilities over ROVs.

1.5 Underwater Vehicle Competitions

Vehicle competitions around the world have had a profound influence on research into robotic vehicle systems [17]. With the advent of AUVs, underwater vehicle competitions have been gaining momentum.

1.5.1 AUVSI

The Association for Unmanned Vehicle Systems International (AUVSI) is dedicated to advancing and promoting unmanned system technologies worldwide [18]. One way it achieves this is by holding vehicle competitions annually. With regard to AUVs, it holds an underwater competition called the International Autonomous Underwater Vehicle Competition (IAUVC) in which academic institutions from around the world can compete.

The competition varies slightly from year to year, however, the theme remains fairly constant. The objective is to design and implement an AUV to navigate a course by using a variety of onboard sensors and equipment, and perform certain tasks such as locating a target and dropping a marker on it. A summary of the 2004 competition’s mission, rules and requirements can be found in Appendix A.

1.5.2 Australasian Competition

An underwater vehicle competition has been proposed for the Australian and Asian-Pacific region [19]. The competition will involve both physical and simulated tasks. Proposed tasks for AUVs to perform include wall following, pipeline following, target finding and

object mapping. It is intended that this competition will promote research into underwater robotic technologies.

1.6 Project Motivations and Objectives

The University of Western Australia (UWA) showed interest in and was keen to design and implement its own AUV primarily for entering the international underwater competitions, but also to undertake and promote research into underwater robotics.

To realise this aspiration a small team was established. *Project Mako*, as this endeavour came to be known, would involve implementing a control, sonar, vision and communications system, not to mention implementing the actual vehicle itself. It became the aim of the team to lay the groundwork for UWA's entrance into the following year's AUV competitions.

The objectives of this thesis project were to:

- Design and develop the mechanical and electrical systems of an AUV
- Integrate the vision, sonar and communications subsystems into the vehicle
- Perform system identification and modelling of the vehicle
- Apply and simulate a control system for the vehicle

As such, this project can be seen as having been divided into two phases. The first phase involved the design and construction of the *Mako* AUV, including not only the mechanical system, but also the electrical system of the vehicle. The overall vehicle was developed so as to adhere to the rules and regulations of the IAUVC. The second phase involved the system identification, modelling and preliminary control analysis of the vehicle using onboard sensors and software.

This thesis did not directly involve the implementation of the sonar, vision or communications systems. These three sections were each implemented by the other team members involved in the *Mako* project. However, the mechanical and electrical designs had to take into account the components required for these systems so as to be able to successfully accommodate and unite all the systems in the final stages of the development of the vehicle.

1.7 Outline of Thesis

In accordance with the actual stages entailed in the project, this thesis firstly details the design and development of the vehicle, and then proceeds onto the modelling and control simulations.

Chapter 2 introduces fundamental ideas and concepts regarding underwater vehicles and their design. The designs of IAUVC vehicles are also considered and examined closely.

Chapter 3 presents the final design chosen for the *Mako* with a detailed outline of the mechanical and electrical systems that were developed. The integration of the subsystems is also discussed.

Chapter 4 discusses the problem of controlling AUVs and common control techniques used. The state vector representation and dynamic model for an underwater vehicle is then presented.

Chapter 5 discusses the simplification and application of the dynamic model to the *Mako*. Also presented is a system identification approach that exploits the characteristics of a low-speed underwater vehicle to significantly simplify overall modelling.

Chapter 6 discusses the testing and remote control of the *Mako* with associated problems. The results of the system identification process on the *Mako* are then presented with a discussion on the problems encountered.

Chapter 7 proposes the use of a PID tracking controller for the control system of the *Mako*. This controller is simulated in software with the results presented and discussed.

Chapter 8 summarises the overall results and undertakings in this thesis, with suggestions for further work and areas of research for future versions of the *Mako* AUV.

Chapter 2

Design Essentials and Concepts

In order to design any vehicle, it is essential to have background knowledge and fundamental concepts about the processes and physical laws governing the vehicle in its environment. With regard to an AUV, factors such as buoyancy, stability, hydrodynamic damping and pressure have to be taken into consideration. This chapter introduces some of these fundamental concepts and ideas about underwater vehicles, and also examines the general design of these vehicles. The mechanical and electrical systems of past IAUVC vehicles are also presented and examined closely to gain insight into different designs.

2.1 AUV Coordinate System

Analogous to flying vehicles, an underwater vehicle has 6DOF; three spatial coordinates, x , y and z ; and three attitude defining Euler angles, roll, ϕ , pitch, θ , and yaw, ψ (Figure 2.1).

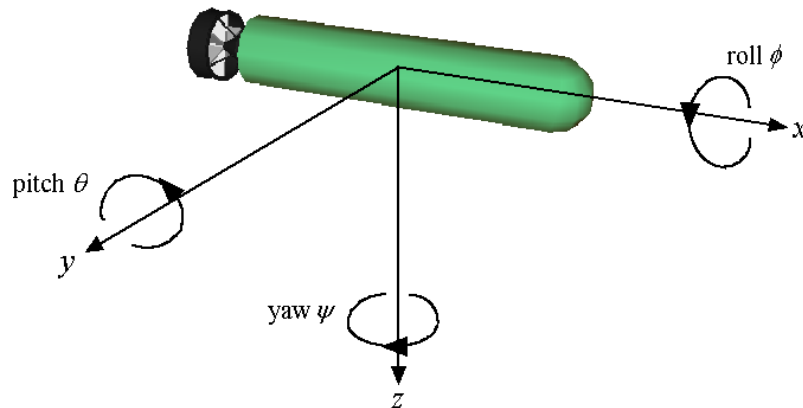


FIGURE 2.1: AUV coordinate system.

The x axis points along the forward direction of the vehicle, defining the vehicle's longitudinal translation. The y axis points through the right hand or starboard side of the

vehicle, defining the vehicle's lateral translation. The z axis defines the vehicle's vertical translation or depth. Note that the z axis is zero at the surface and points downwards; hence, it is positive for increasing depth. This is because the AUV cannot travel further than the surface of the water.

The degrees of freedom that an underwater vehicle has allows it to be quite versatile. This high range of motion, however, can be problematic as it must be considered during the design process how each degree of freedom will be controlled in order to keep the vehicle stable. Most AUVs are designed so as to be able to control as many degrees of freedom as possible.

2.2 Factors Affecting an Underwater Vehicle

Several forces act on an underwater vehicle that require consideration for the design process. These include buoyancy, hydrodynamic damping, Coriolis and added mass. Buoyancy is one of the most important factors which significantly affects the vehicle's ability to submerge as well as its stability. Stability is also affected by external forces. Pressure is another significant factor for underwater vehicles that needs to be taken into consideration in the design process.

2.2.1 Buoyancy

The magnitude of the buoyant force, B , exerted on a body, floating or submerged, is equal to the weight of the volume of water displaced by that body [20]. The ability of an object to float depends on whether or not the magnitude of the weight of the body, W , is greater than the buoyant force. Clearly, if $B > W$, then the body will float, while if $B < W$ it will sink (Figure 2.2). If B and W equate, then the body remains where it is.

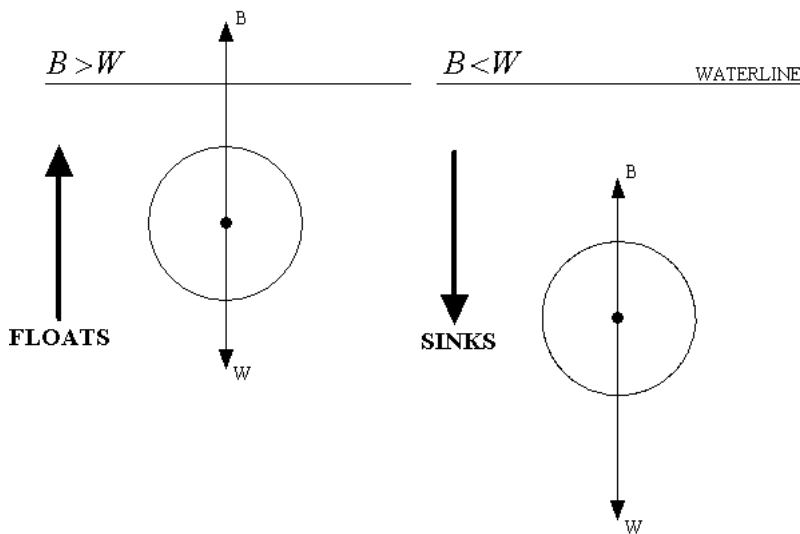


FIGURE 2.2: Effects of buoyancy and weight on an underwater body.

2.2.2 Hydrodynamic Damping

When a body is moving through the water, the main forces acting in the opposite direction to the motion of the body are hydrodynamic damping forces. These damping forces are mainly due to drag and lifting forces, as well as lineal skin friction [21]. Damping forces have a significant effect on the dynamics of an underwater vehicle which leads to nonlinearity. Lineal skin friction can be considered negligible when compared to drag forces, and therefore, it is usually sufficient to only take into account the latter when calculating damping forces.

2.2.3 Stability

Assuming no water movement, the stability of a static body underwater is predominantly affected by the positions of the centres of mass, C_M , and buoyancy, C_B . The centre of buoyancy is the centroid of the volumetric displacement of the body [22]. If C_M and C_B are not aligned vertically with each other in either the longitudinal or lateral directions, then instability will exist due to the creation of a nonzero moment (Figure 2.3).

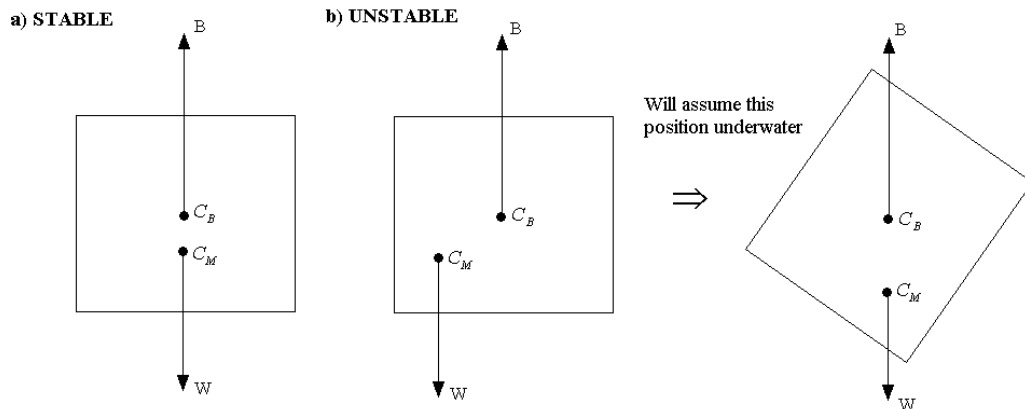


FIGURE 2.3: a) Stable configuration of underwater body. b) Instability of an underwater body through misalignment of centres of mass and buoyancy.

If C_M and C_B coincide in the same position in space, the vehicle will be very susceptible to perturbations. Ideally, the two centroids should be aligned vertically some distance apart from each other with C_M below C_B . This results in an ideal bottom-heavy configuration with innate stability.

As seen in Figure 2.4, this configuration produces a righting moment, RM , when the vehicle rolls or pitches that is directly proportional to the perpendicular distance between C_M and C_B , as well as to both B and W . This moment is conducive to the vehicle's stability, acting as a passive roll and pitch control system. The moment is given by,

$$RM = \frac{1}{2}d(B + W) \quad (2.1)$$

where d is the perpendicular distance between the acting forces B and W .

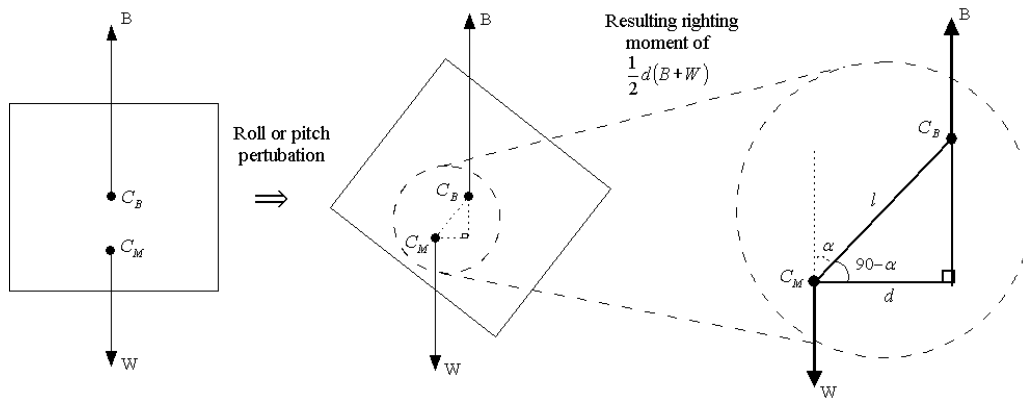


FIGURE 2.4: Righting moment caused by roll or pitch of vehicle.

The magnitude of RM varies sinusoidally with the angle α that the vehicle rolls or pitches. From Figure 2.4, equation 2.1 becomes,

$$RM = \frac{1}{2} l (B + W) \sin \lambda \quad (2.2)$$

where l , B and W are constants for the vehicle; l being the distance between the centres of mass and buoyancy.

In the case of a dynamic underwater body, stability is affected not only by the centres of mass and buoyancy, but also by factors such as external forces and centres of drag. To increase dynamic stability, the centres of drag, determined by the centroids of the effective surface areas of the vehicle, should be aligned with the centres of the externally applied forces. In this manner, the vehicle will not tend to exhibit undesirable characteristics in its motion.

2.2.4 Coriolis

Coriolis is an inertial force that acts perpendicular to the direction of motion of a body. The force is proportional to both the velocity and rotation of the coordinate system. The effect of the Coriolis force then, is that the path of the body is deflected. In reality, however, the path of the body is not actually deflected, but only appears to be. This is due to the motion of the body's coordinate system [23]. Since the coordinate system of an AUV rotates with respect to another reference frame, the effect of the Coriolis force is usually taken into account and included in the equations of motion.

2.2.5 Added Mass

Another phenomenon that affects underwater vehicles is added mass. When a body moves underwater, the immediate surrounding fluid is accelerated along with the body. This affects the dynamics of the vehicle in such a way that the force required to accelerate the water can be modelled as an added mass [24]. Added mass is a fairly significant effect and

is related to the mass and inertial values of the vehicle.

2.2.6 Environmental Forces

Environmental disturbances can affect the motion and stability of a vehicle. This is particularly true for an underwater vehicle where waves, currents and even wind can perturb the vehicle. When the vehicle is submerged, the effect of wind and waves can be largely ignored. The most significant disturbances then for underwater vehicles are currents. In a controlled environment such as a pool, the effect of these environmental forces is minimal.

2.2.7 Pressure

As with air, underwater pressure is caused by the weight of the medium, in this case water, acting upon a surface. Pressure is usually measured as an *absolute* or *ambient* pressure; absolute denoting the total pressure and ambient being of a relativistic nature.

At sea level, pressure due to air is 14.7psi or 1atm. For every 10m of depth, pressure increases by about 1atm and hence, the absolute pressure at 10m underwater is 2atm. Although linear in nature, the increase in pressure as depth increases is significant and underwater vehicles must be structurally capable of withstanding a relatively large amount of pressure if they are to survive.

2.3 General Design of an AUV

There are several aspects in AUV mechanical and electrical design that need to be looked at closely. International Submarine Engineering [25] identifies hull design, propulsion, submerging and electric power as major design aspects.

2.3.1 Hull Design

An AUV must provide a pressure hull to house its components in a dry, watertight environment. The hull must allow components to be easily accessible and maintainable, as well as allowing for modularity in case of future changes or additions. As well as being light and strong, the hull should also be corrosion resistant as it will be subjected to a harsh saltwater environment.

Spherical hulls offer the best structural integrity, however, the shape inhibits the efficient use of the space available as most components and systems are rectangular in shape. Cylindrical hulls provide the best alternative, comprising high structural integrity and a shape conducive to the housing of electronic components.

2.3.2 Propulsion

Some sort of propulsion is required on all AUVs and is usually one of the main sources of power consumption. Most AUVs use motors for propulsion due to the scarcity and cost

of alternative systems.

The location of the motors affects which degrees of freedom can be controlled. The positioning of the motors can also affect noise interference with onboard electronic components, as well as propeller-to-hull and propeller-to-propeller interactions. Propeller-to-hull and propeller-to-propeller interactions can have unwanted effects in the dynamics of an AUV.

When travelling at a constant speed, the thrust produced by the motors is equal to the friction or drag of the vehicle, that is,

$$Thrust = Drag = \frac{1}{2}\rho s^2 A c_D \quad (2.3)$$

where ρ is the water density, s is the speed, A is the effective surface area and c_D is the drag coefficient.

Power consumption for the propulsion system increases dramatically as the speed of the vehicle increases. This is because the thrust power is equal to the product of the thrust and the speed, meaning thrust power is a function of speed cubed,

$$Thrust\ Power = Thrust \times s = \frac{1}{2}\rho s^3 A c_D \quad (2.4)$$

Therefore, because of an AUV's limited energy supply, it must travel at a speed that does not draw too much power, but at the same time does not take too long to complete its mission. Obtaining the ideal speed becomes an optimisation problem.

2.3.3 Submerging

In the case of a submersible vehicle, since the volume of the vehicle remains constant, in order to dive deeper, it must increase the downward force acting upon it to counteract the buoyant force. It can accomplish this either by increasing its mass via the use of ballast tanks or by using external thrusters.

Ballasting is the more common approach for submerging. This method is mostly mechanical in nature and involves employing pumps and compressed air to take in and remove water. The alternative is to use thrusters that point downwards. This is a much simpler system, but is quite inefficient in terms of power consumption and not really suited at great depths.

To reduce the size of ballast tanks or the force required by thrusters for the process of submerging, AUVs are usually designed so as to have residual buoyancy. That is, the weight of the vehicle is made to be more or less equal to the buoyant force.

2.3.4 Electric Power

Electric power is commonly provided via sealed batteries. The ideal arrangement of batteries is to have them connected in parallel with diodes between each one to allow even discharge and to prevent current flow between batteries. Fuses or other protective devices

should also be used to prevent excessive current flow in case of short circuits occurring or components malfunctioning.

The restrictive nature of power on AUVs influences the types of components and equipment that can be utilised. Components and equipment should be chosen so as to draw as little power as possible in order to allow the batteries to provide more than enough time for the vehicle to complete its mission.

2.4 IAUVC Vehicle Designs

Since the *Mako* was being designed to enter the annual AUVSI underwater competition, it was appropriate to look closely at other academic institutions' AUVs to gain insight into and ideas about mechanical and electrical designs. Another reason in doing this is that academic institutions usually find easy to use, innovative and cost-effective alternatives to certain devices and mechanisms. Presented below are some of the mechanical and electrical designs of four AUVs.

2.4.1 Massachusetts Institute of Technology

MIT's *Orca* AUV [26] has two PVC tubes mounted on an aluminium frame. Batteries are situated in the bottom tube to lower the centre of mass and increase the righting moment of the vehicle. Each tube has a sliding card mounted with electronic equipment. These cards use connectors to connect the electronic equipment to the PVC end plate. The end plate contains the external connectors. This configuration eliminates the need for disconnecting cables when removing the cards from the tubes.



FIGURE 2.5: MIT's *Orca* AUV being tested in a swimming pool [27].

Propulsion is provided via two motors mounted on the sides for horizontal movement and two vertical motors for depth control. These thrusters are powered via six 12V, 3Ah batteries while the remaining electronic equipment utilises four other 12V batteries. An onboard monitoring system measures individual voltages and currents for power management purposes.

The AUV has an inertial measurement unit consisting of two gyroscopes and three accelerometers. A compass module assists in attitude determination and navigation while a Doppler Velocity Logger is used to determine the velocity of the vehicle with respect to the bottom. All onboard functions are controlled via a PC running Linux.

2.4.2 University of West Florida

The University of West Florida's *Nautilus* [28] consists of two PVC tubes aligned side by side. Each tube has a rack of electronics that easily slides out for maintenance and inspection, and these connect to external devices via waterproof connectors. A highly buoyant float situated on top of the tubes allows for the vehicle to easily upright itself when it rolls or pitches. A motor at the end of each tube provides longitudinal and lateral motion while a larger one located in the centre of the float provides downward movement.



FIGURE 2.6: The University of West Florida's *Nautilus* [28].

Two computers are used for controlling the AUV; one is used for motor control and the other for sensors. Navigation is provided via an electronic compass that provides information about the three attitude related degrees of freedom, while pressure is measured by two depth sensors. Two 12V, 12Ah batteries provide the necessary onboard power.

2.4.3 Cornell University

Like MIT, Cornell University's AUV [29] is composed of two hulls on top of each other surrounded by an aluminium exoskeleton. Both hulls have a blind-mount interface system for connecting electronic components to external connectors. Electronic components mounted upon sliding racks are inserted into each hull and connect blindly with the end plate, thus avoiding the need for disconnecting cables.

Three 28V, 9Ah batteries supply the necessary power and are located in the lower hull for increased vehicle stability. Two horizontal thrusters and two vertical thrusters mounted on the frame allow for 4DOF; movement in the x and z directions, and control of pitch and yaw. Processing power is provided via two computers, one for vision processing and the other for both motor control and sonar.



FIGURE 2.7: Cornell University's AUV being deployed [30].

2.4.4 University of Florida

The University of Florida's *SubjuGator* [31] consists of an aluminium body with six motors capable of being arranged so as to create different configurations (Figure 2.8). These different configurations enable the vehicle's range of motion to be adjusted for different mission requirements. Two sliding shelves allow components to be mounted inside the hull. Electrical connections located at the opening of the hull allow for easy removal of the shelves.

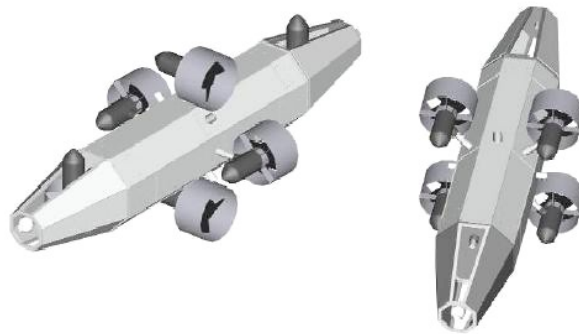


FIGURE 2.8: Two different thruster configurations for The University of Florida's *SubjuGator* AUV [31].

Power is supplied by five 12V, 12Ah batteries located on the lower shelf to provide stability. Sensors include an inclinometer, a digital compass and a pressure sensor. A microcontroller is used for control of the motors while top-level control is maintained by a Pentium-based, Linux-running PC.

2.4.5 Remark on Vehicle Designs

It is clear that many of the entrants' AUVs are far from sleek in design, however, there is little need for this with regard to the requirements of the competition mission. Vehicle features and characteristics also appear to be fairly consistent across the board with

most of the similarities due to limited underwater technologies, the expensive nature of components, and the restrictive rules and regulations of the competition. Motors as a source of propulsion is standard among all AUV entries due to the scarceness and considerable expense of alternative propulsion systems. Hulls are mostly constructed from readily available and cost-effective materials such as aluminium and PVC. Depth sensors, sonar systems and attitude feedback components are also typical among the vehicles. On-board power is supplied by sealed rechargeable batteries on all the vehicles. It is also of interest to note that most of these AUVs do not employ ballast systems and instead make use of some type of motor configuration for depth control.

2.5 Summary

A brief introduction to the fundamental concepts regarding AUVs has been presented in this chapter, as well as an overview of the main factors that should be taken into account when designing these vehicles. The mechanical and electrical systems of a few IAUVC vehicles were also examined to gain insight into different design methodologies. By using the concepts discussed in this chapter, and after thorough research and analysis of AUV designs, several designs were conceptualised for the *Mako*. Some of the more feasible designs are detailed in Appendix C. The following chapter discusses which design was pursued with an outline of the mechanical and electrical systems that were developed for the vehicle.

Chapter 3

Mechanical and Electrical Design

Utilising the concepts presented in Chapter 2, the mechanical and electrical systems for an AUV were designed. These two systems had to be designed and considered simultaneously. As such, they needed to complement each other and were by no means mutually exclusive processes. This chapter presents an overview of the mechanical and electrical systems that were developed for the *Mako*, as well as the entire vehicle itself. Presented as well is the integration of the vision, sonar and communications systems. A more in-depth account of the design and construction processes can be found in the appendices.

3.1 Choosing the Final Design

A two-hull, four-thruster configuration, as detailed in Appendix C, was chosen for the final design because of its significant advantages over the other proposed designs. The two-hull, four-thruster design provided the following:

- Ease in machining and construction due to its simple structure
- Relative ease in ensuring watertight integrity because of the lack of rotating mechanical devices such as bow planes and rudders
- Substantial internal space owing to the existence of two hulls
- High modularity due to the relative ease with which components can be attached to the skeletal frame
- Cost-effectiveness because of the availability and use of common materials and components
- Relative ease foreseen in software control implementation in using a four thruster configuration when compared to using a ballast tank and one thruster system
- High range of motion provided by the four thruster configuration
- Ease in submerging with two vertical thrusters

- Static stability due to the separation of the centres of mass and buoyancy, and dynamic stability due to the simple alignment of thrusters with easily identifiable centres of drag

Precision in controlling the vehicle and overall simplicity were pursued in the mechanical design over speed and sleekness. Although speed and sleekness are generally desirable qualities in AUVs, there is no real need for these as per the tasks required for the underwater competition.

3.2 Mechanical System Design

The mechanical system of the *Mako* sought to fulfil the following main objectives:

- To fit in a rectangular volume 1.8m long, 90cm wide and 90cm deep, as well as being buoyant by at least 0.5% of its mass; both as per IAUVC regulations
- To provide a dry, watertight hull that facilitates the housing of onboard electronic components and that is capable of surviving in a saltwater environment
- To provide a static and dynamically stable vehicle with suitable versatility in its motion to accomplish a wide range of tasks
- To possess the ability to be modular and extensible for future missions

The final hull design intended to achieve the above objectives is shown in Figure 3.1. For a detailed account of the mechanical system design and rationale, the reader is referred to Appendix D.

3.3 Electrical System Design

The electrical system of the *Mako* sought to fulfil the following:

- Provide for motion control
- Provide for sonar and vision processing
- Measure the vehicle's depth
- Discern the vehicle's attitude
- Measure the vehicle's surge velocity
- Detect hull breaches and power shortage
- Supply sufficient power for ample testing periods

The block diagram for the electrical system design intended to achieve the above objectives is shown in Figure 3.2. In the figure, a component surrounded by blue indicates that it is situated externally, that is, in the water. A component surrounded by red indicates the component is located in the lower hull. All other components and devices are situated in the upper hull.

The reader is referred to Appendix E for a more in-depth account of the design and rationale of the electrical system.

3.4 Mechanical and Electrical Systems Outline

Simplicity and modularity were key goals in both the mechanical and electrical system designs. The mechanical design was made symmetrical to not only make construction relatively straightforward, but to also simplify software modelling. The materials chosen were common, cost-effective and easily machineable. Only crucial electronic components were purchased with improvisations made for other components. With the vehicle having a maximum rated depth of 5m, pressure did not pose a major problem to construction.

The *Mako* (Figure 3.3) measures 134cm long, 64cm wide and 46cm tall with a mass of 35kg. The vehicle is buoyant by 4.3% of its mass meaning it will still surface in the unlikely event it loses onboard power.

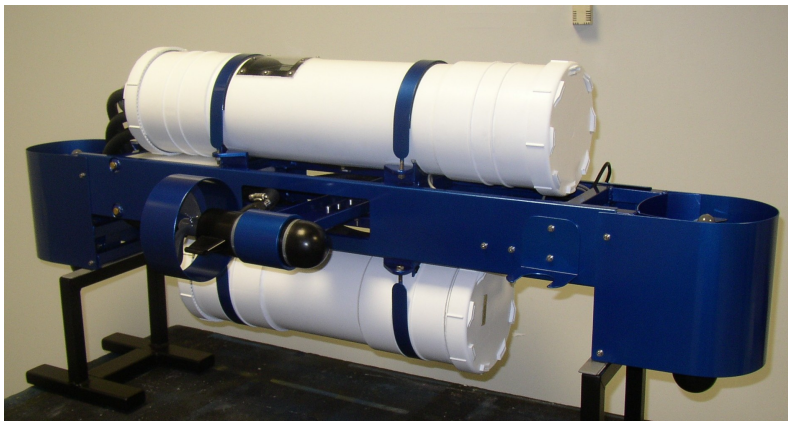


FIGURE 3.3: The *Mako* AUV.

The vehicle comprises two watertight hulls machined from PVC separately mounted to a supporting aluminium skeletal frame. Two thrusters are mounted on the port and starboard sides of the vehicle for longitudinal movement, while two others are mounted vertically on the bow and stern for depth control. The *Mako's* vertical thruster diving system is not power conservative, however, when a comparison is made with ballast systems that involve complex mechanical devices, the advantages such as precision and simplicity that come with using these two thrusters far outweigh those of a ballast system.

3.4.1 Propulsion

Propulsion is provided by four modified 12V, 7A trolling motors (Figure 3.4) that allow horizontal and vertical movement of the vehicle. These motors were chosen for their small size and the fact that they are intended for underwater use; a feature that minimised construction complexity substantially and provided inherent watertight integrity.

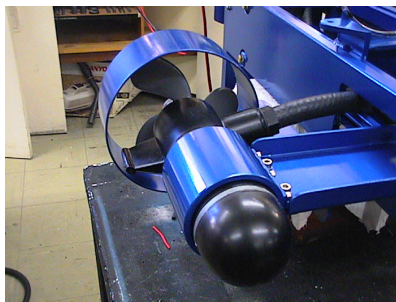


FIGURE 3.4: Close up of starboard motor.

The horizontal motors can be repositioned via an adjustable mount in order to adjust the centre of mass and to also account for drag. All four motors have shrouds surrounding their propellers to not only protect them from damage, but to ensure that human operators are also protected from harm. The shrouds for the vertical motors are built into the skeletal frame. Each motor can be easily removed from the frame for inspection, maintenance or replacement.

3.4.2 Range of Motion

The horizontal motors provide surge control in both forward and reverse directions while the vertical motors provide heave control in both downward and upward directions. Roll and pitch is passively controlled by the vehicle's innate righting moment, although pitch can be controlled by the vertical motors if necessary.

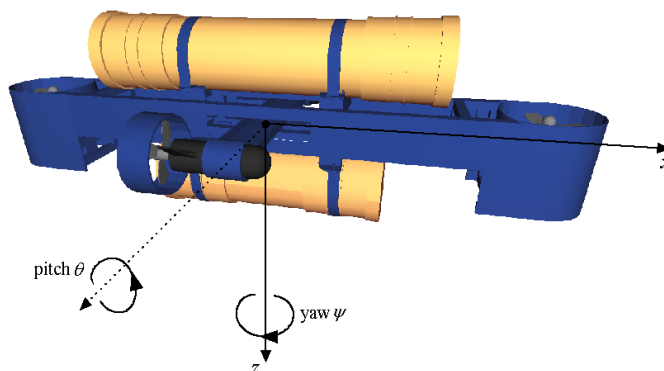


FIGURE 3.5: The *Mako* has 4DOF that can be actively controlled; movement in the x and z directions, that is, surge and heave, as well as pitch and yaw.

Lateral movement is not possible for the vehicle, however, this ability is not necessary as the horizontal motors allow yaw control which permits movement in any global horizontal direction. Overall, this provides the vehicle with 4DOF that can be actively controlled (Figure 3.5). These 4DOF provide an ample range of motion suited to accomplishing a wide range of tasks.

3.4.3 Upper Hull - Electronics

The upper hull is made of PVC and consists of two end caps providing watertight seals. The hull measures 75cm in length with an internal diameter of 15cm. Two aluminium boards sit inside the hull and provide four surfaces on which electronic components can be mounted (Figure 3.6). These boards easily slide in and out of the hull for inspection, maintenance or addition of components. Utilising blind mate connections situated at one end of the hull, the boards can be removed without the need to disconnect any cables by hand.

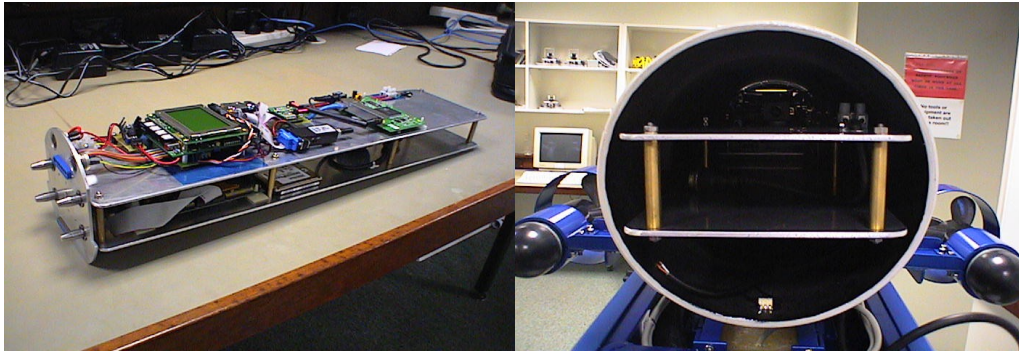


FIGURE 3.6: (Left) The aluminium boards with mounted electronic components. (Right) The boards positioned in the upper hull.

3.4.4 Lower Hull - Batteries

The lower hull is of the same diameter as the upper hull, but is only 50 cm in length. It houses the largest and heaviest components; three sealed lead acid batteries. Situating most of the mass of the components in the lower hull places the centre of mass in the lower half of the vehicle, below the centre of buoyancy. This configuration contributes to the innate metacentric righting moment that passively controls roll and pitch.

3.4.5 Skeletal Frame

The skeletal frame (Figure 3.7) is made from aluminium, chosen especially for its light-weight characteristic as well as its resistance to corrosion which helps protect the frame against the harsh saltwater and chlorine environment in which it is subjected to. As well as supporting the two hulls and four motors, the structure of the frame allows for the simple mounting of external devices and components. The design took into account the

potential need for additional components in the future and for that reason ample space is available on the frame.

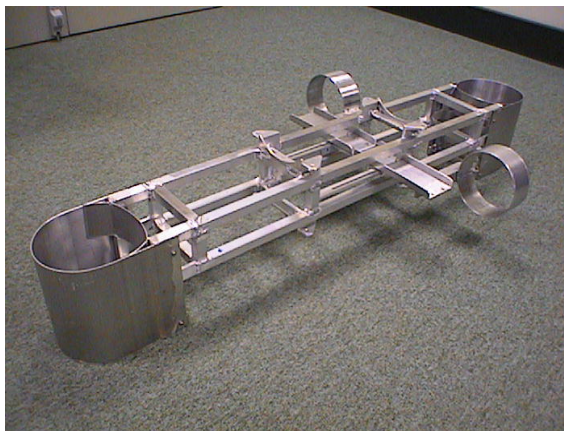


FIGURE 3.7: Aluminium skeletal frame.

The symmetrical and structurally simple nature of the frame design contributed to the relatively straightforward aligning of the thrusters with the centres of drag for increased dynamic stability. The nature of the frame also allowed the thrusters to be easily mounted in positions where they would minimise potential magnetic interference with onboard electronic devices.

3.4.6 Through-hull Connections

External components such as thrusters require external connections to internal hull components. Expensive underwater connectors were avoided by using rubber hosing combined with common plastic plumbing connectors to house cables from each external component to the hull. The same approach was used to connect the power cables from the lower hull to the upper hull as well as other external devices. All through-hull connections occur on one end cap of each hull to allow the other end to be opened with ease.

3.4.7 Power System

The *Mako's* thrusters and electronic components are powered by a bank of one 12V, 7Ah and two 12V, 12Ah batteries connected in parallel (Figure 3.8). Combined, these batteries supply about 31Ah which allows the vehicle to be operated continuously and at maximum specifications for about two hours. The batteries are housed in an aluminium frame for easy removal from the hull.

Each battery connects to a power distribution board attached to the aluminium frame. Power diodes are connected between each battery to prevent the batteries from attempting to charge one another and to ensure even discharge. A fuse also prevents excessive current flow from damaging the batteries and electronic devices in the event of a short circuit or component malfunction, although each onboard device has its own polyswitch. A

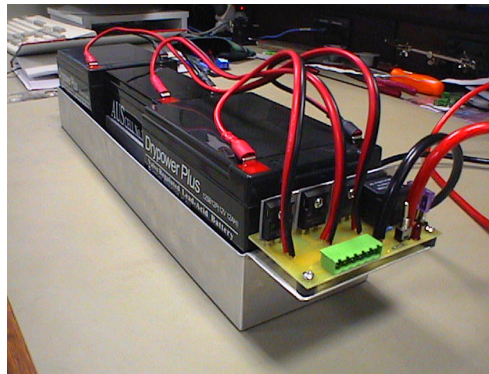


FIGURE 3.8: The bank of one 7Ah and two 12Ah, 12V batteries with power board.

magnetic reed switch located on the board allows the powering down of the whole vehicle via a magnet located externally. A charging port on the power board provides convenience by allowing the batteries to be charged without their removal from the lower hull.

3.4.8 Controllers

The control system of the *Mako* is separated into two controllers; an Eyebot microcontroller and a mini Cyrix PC running Linux (Figure 3.9).

The Eyebot controller runs at 33MHz and comprises 512KB of ROM, as well as 2048KB of RAM. The Eyebot also boasts an LCD screen which allows visual feedback of data. This controller's primary purpose in the *Mako* is in controlling the four thrusters, that is, controlling the vehicle's movement. The Eyebot is also responsible for receiving input from the majority of the onboard sensors.

The mini PC comprises a Cyrix 233MHz processor, 32MB of RAM and a 5GB hard drive. Its function is to provide processing power for the computationally intensive vision system.

Since the thrusters would be in continuous use while the vision system was operational, it was logical to decentralise functions and control over two controllers. This allows a more powerful and concurrent approach to dealing with data and controlling the vehicle.



FIGURE 3.9: (Left) Eyebot controller. (Right) Mini PC.

3.4.9 Motor Controllers

Motor controllers designed and built specifically for the thrusters provide both speed and direction control. Each motor controller interfaces with the Eyebot controller via two servo ports. Due to the high current used by the thrusters, a large amount of heat is produced by each motor controller. To keep the temperature inside the hull from rising too high and damaging electronic components, a heat sink attached to the motor controller circuit board and leading to the outer hull was devised (Figure 3.10). This allows the surrounding water to continuously cool the heat sink and allow the temperature inside the hull to remain at an acceptable level.



FIGURE 3.10: Heat sink located in the centre of the upper hull's end cap.

3.4.10 Depth Sensor

A pressure sensor could not be attained for the determination of depth, however, an improvisation was made. Since the sonar system was utilising an array of Navman Depth 2100 echo sounders (Figure 3.11), the use of one of these was decided upon to provide a crude, but effective depth sensor.

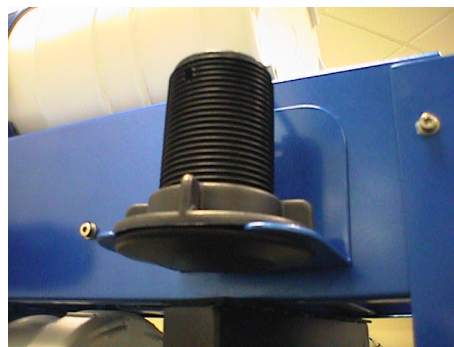


FIGURE 3.11: Navman Depth 2100 transducer.

The echo sounder is positioned pointing downwards on the vehicle. The sensor allows for depth feedback only if the depth of the water is known. Since the echo sounder determines the distance to the bottom, the depth of the vehicle can easily be discerned by

the difference between the depth of the water and the echo sounder reading. However, this system will only work when the depth of the water that the vehicle is being tested in is constant. Therefore, this is a limited and only a temporary solution to depth measurement for the *Mako*.

3.4.11 Digital Magnetic Compass

A low-cost Vector 2X digital magnetic compass module (Figure 3.12) provides for yaw or heading feedback. The small module delivers high accuracy and low power, interfacing with the Eyebot controller via a digital input port.

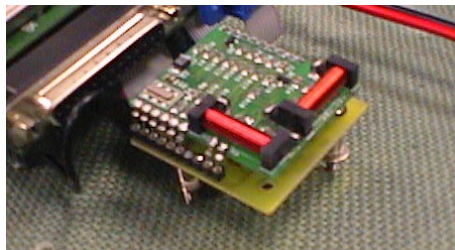


FIGURE 3.12: Digital Magnetic Compass.

3.4.12 Velocity Sensor

A Navman Speed 2100 transducer (Figure 3.13) is used to measure the forward longitudinal velocity of the vehicle. The transducer uses an encoder style paddle wheel mechanism to discern the velocity. The sensor has a resolution of 5cm/s, draws little power and interfaces with the Eyebot controller via an analog-to-digital converter (ADC) channel. Although less accurate and functional than a Doppler Velocity Logger, it is far less costly.

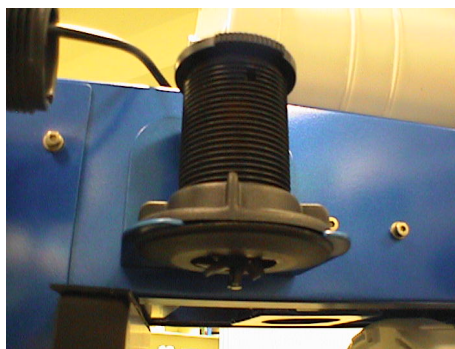


FIGURE 3.13: Navman Speed 2100 transducer.

3.4.13 Leak Monitor

A simple dual water detector circuit connected to ADC channels on the Eyebot controller is used for the unlikely but possible event of a hull breach. Two sets of probes run along

the bottom of each hull. This allows for the location (upper or lower hull) of the leak to be known, therefore saving time in isolating a leak. The Eyebot periodically monitors whether or not the hull integrity of the vehicle has been compromised and if so immediately surfaces the vehicle.

3.4.14 Power Monitor

To ensure adequate power is being supplied to the vehicle, particularly to the motors, a simple power monitor is used to detect when the voltage level drops to unacceptable levels. This is essential as a low voltage will result in the thrust characteristics of the motors drifting from expected values, therefore compromising accurate control of the vehicle.

The power monitor is essentially a voltage divider circuit that connects to an ADC channel on the Eyebot. This allows for the Eyebot to periodically monitor the supply voltage and to surface the vehicle when it senses a low voltage.

3.5 Integration of Subsystems

The integration of the vision, sonar and communications systems occurred throughout the development of the mechanical and electrical systems of the vehicle. The presence of these systems had to be taken into account during the design and construction phases.

3.5.1 Vision System

The vision system consists of the mini PC connected to a standard parallel port web camera. The PC was mounted onto the component boards along with the other electronic components. A chassis made from Perspex and aluminium was built to house the camera in a watertight enclosure. The chassis was attached to the underside of the vehicle's frame (Figure 3.14) so that the camera was pointing directly downwards. A through-hull connection was then made for connecting the camera to the PC located in the upper hull.

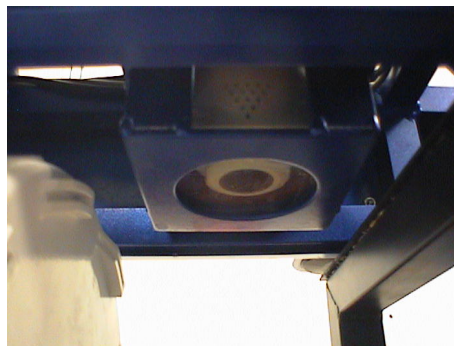


FIGURE 3.14: Camera chassis on underside of frame.

3.5.2 Sonar System

Four echo sounders were envisioned for the sonar system; one pointing forward, one pointing downward, and the other two positioned on either side of the vehicle [32]. However, during the course of the development of the vehicle, only two echo sounders were able to be acquired. These two were attached pointing in the forward (Figure 3.15) and downward directions (Figure 3.11). As previously mentioned, the downward pointing echo sounder was utilised as a temporary depth sensor. Through-hull connections on the end cap of the upper hull were made for the echo sounder cables to connect to onboard circuitry.



FIGURE 3.15: Forward pointing echo sounder.

3.5.3 Communications System

The purpose of the communications system for the *Mako* is essentially to provide operators with the ability to remotely transmit and receive data from the vehicle in order to perform testing with greater ease. Although the communications system has not yet been implemented, communication with the vehicle was needed to perform testing and system identification. A temporary communications system was therefore employed.

To communicate with the Eyebot controller, a Bluetooth dongle was attached to one of the serial ports (Figure 3.16). This system allows:

- Programs to be downloaded onto the Eyebot remotely via a computer
- Stored data to be uploaded to a computer
- Signals to be sent to the Eyebot during test runs

The use of the Bluetooth dongle avoids the need to recover and open the vehicle in order to reprogram the Eyebot or upload data. This system, however, does not work in more than 30cm of water, and hence, can only be used to transmit and receive when the vehicle is surfaced.

The Eyebot can also be controlled by an infrared (IR) remote control. A Perspex cover situated on top of the upper hull not only allows feedback from the Eyebot's screen, but also allows an infrared signal to pass through to a receiver attached to the Eyebot. The IR

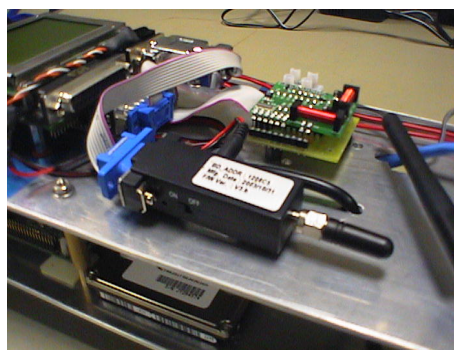


FIGURE 3.16: Bluetooth dongle attached to Eyebot controller.

remote control allows a user to access the Eyebot's menu functions; the primary purpose of this being to set the Eyebot to download and upload modes so that the Bluetooth dongle can then be used to transmit or receive data.

For communicating with the vision system, a wireless router was acquired and attached to the component boards (Figure 3.17). The router allows for the gathering of data and the remote compilation and execution of programs [33]. As with the Bluetooth dongle, the signal to the router attenuates dramatically underwater, and so can only be used when the vehicle is near the surface of the water. However, for testing purposes and requirements the functionality of the router suffices.

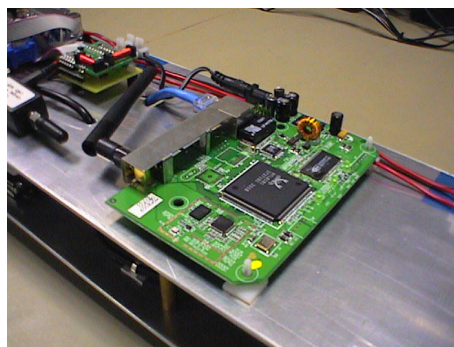


FIGURE 3.17: Wireless router for communicating with the onboard mini PC.

3.6 Summary

An overview of the mechanical and electrical systems of the AUV that was developed has been presented in this chapter. The development of the mechanical and electrical systems has resulted in an AUV that possesses high versatility, modularity and functionality to accomplish a wide range of tasks. The chapters that follow discuss the modelling, identification and control simulations that were performed on this vehicle.

Chapter 4

Modelling and Control of AUVs

Having completed the design and construction of the *Mako*, the next phase involved the modelling and control of the vehicle. Before continuing on, it is appropriate to take a side-step and explore the different controllers that have been implemented on AUVs. As such, this chapter looks at the problems of controlling AUVs and control techniques available and used for these vehicles. The state vector representation of AUV kinematics and the mathematical modelling of their dynamics of motion are then presented. Determining the state vector representation and the modelling of their motion is the first step to controlling these vehicles.

4.1 Control Problems

Underwater vehicles are particularly difficult to control due to the existence of several complex and nonlinear forces acting upon the vehicle. Hydrodynamics is the chief source of nonlinearity in the dynamics of underwater vehicles [8]. What makes control even more complex are the difficulties in observing and measuring underwater vehicle hydrodynamics response [22]. Motion of the vehicle can usually only be viewed by remote means and the acquisition of data is usually very time consuming.

With respect to vehicles in other environments, underwater vehicles are probably the hardest to accurately model. Attaining a correct model is critical in ensuring that major faults do not occur with the vehicle. For instance, most AUVs cannot be allowed to pitch or roll to postures where the angle is very steep; the reason being the potential damage to internal components. An incorrect model could allow this to occur as well as allowing a number of other failures to occur in control, navigation or power which can result in damage or even loss of the entire vehicle.

4.2 Control Techniques

With the advancement of AUV technology and the increase of these vehicles worldwide, there has been a great push towards research in the design and implementation of con-

trollers to accurately model and to improve dynamic response.

Simple control techniques such as PID control have been more commonly used because of the relative ease of implementation. A PID tracking controller has been implemented successfully on an AUV by Wettergreen et al. [34]. The controller is an extension of the control technique of computed torque control which is used in robotics. Simple Linear Quadratic Gaussian controllers have also been developed [7, 35]. Despite the existence of these simple controllers, other more complex control techniques have also been recently utilised for AUVs.

Fuzzy logic controllers have been proposed and implemented with success on AUVs in several cases [14, 36, 37]. The nature of fuzzy logic offers a control solution when a mathematical model is not well known, or not known at all as the case may be. Thus, implementing a controller on an AUV using fuzzy logic can avoid the need for complex hydrodynamic modelling of the vehicle. However, the downside is the implementation of the controller itself poses its own level of complexity.

Adaptive control has also been used, [15, 38–40], with the benefits of this type of control obvious due to the changing dynamics of AUVs in the ocean. For example, the controller can adapt itself to varying ocean currents or to a different vehicle density when ballast tanks are used. Adaptive control is also useful because AUVs are usually refitted with new equipment and adapted for different missions which change their static and dynamic characteristics.

Another technique that has been used is sliding mode control [13, 41, 42]. In this control scheme, the dynamics of the system are altered by the application of high-speed switching control. The system is in essence constrained in such a way so as to exhibit desirable characteristics. This proves useful in the linearisation and hence, controlling of underwater vehicle dynamics.

The different control techniques discussed have more commonly been used in combination with each other. For instance, a neurofuzzy controller has been developed by Mills and Harris [43] for modelling attitude control for an AUV. This involved using a combination of neural networks and fuzzy logic. Filaretov et al. [44] on the other hand implemented a sliding mode adaptive control system for controlling an AUV. The uniting of these different control techniques brings about the advantage of combining the useful properties of each one to improve the robustness and fault tolerance of the overall controller.

4.3 State Vector Representation

Modelling an AUV's dynamics is the first step taken in controlling these vehicles. Although the dynamics and the subsequent system identification can be fairly complex and time consuming, the software implementation becomes relatively straightforward once modelling of the vehicle has been accomplished.

Before proceeding with the dynamic model, it is necessary to firstly define such things

as reference frames and the notation that will be used. The state vector representation of an AUV is also derived in this section.

4.3.1 Reference Frames

In modelling underwater vehicles, two reference frames are commonly used; a world reference frame, $\{W\}$, and a body reference frame, $\{B\}$. The world coordinates are defined with respect to the real world while the body coordinates are defined with respect to the vehicle itself. Both the world and body reference frames are right-handed Cartesian coordinate systems.

For the body reference frame, as explained in Chapter 2, the x axis points in the vehicle's forward pointing direction, the y axis points through the right-hand side of the vehicle, and the z axis points vertically downwards from the vehicle.

The world reference frame is usually defined with the x axis pointing in the northerly direction and the y axis pointing in the easterly direction. The z axis points down towards the earth. Although this is the conventional configuration, the world frame axes can be defined in whatever direction suits the situation.

4.3.2 Notation of Transformations

The following notation for transformations between reference frames is adopted from Silpa-Anan [8]. Define,

$$\begin{aligned} {}^A P &\text{ as a vector } P \text{ in reference frame } A, {}^A P \in \mathfrak{R}^3 \\ {}^A_B R &\text{ as a } 3 \times 3 \text{ rotation matrix of frame } B \text{ relative to frame } A, {}^A_B R \in \mathfrak{R}^{3 \times 3} \end{aligned}$$

The translation of a vector P between two frames is then given by,

$${}^A P = {}^B P + {}^A P_{B_{org}} \quad (4.1)$$

where ${}^A P_{B_{org}}$ is the origin of frame B with respect to frame A . For the rotation of a vector P between two frames,

$${}^A P = {}^A_B R {}^B P \quad (4.2)$$

4.3.3 Attitude and Euler Angles

Euler angles define the rotation angle about the three Cartesian axes, x , y and z . There are many notations for Euler angles, however, the z - y - x form corresponding to rotation angles of yaw, ψ , pitch, θ , and roll, ϕ , respectively, is used here.

The order of rotations is very important when converting from one coordinate system to another. When converting from body to world coordinates, it is conventional in robotics that the first rotation be ψ about the z axis, followed by θ about the intermediate y axis,

and lastly ϕ about the second intermediate x axis. When converting from world to body coordinates, the reverse order is obviously used.

The rotation matrix of frame $\{B\}$ relative to frame $\{W\}$, that is, the rotation matrix for converting from body to world coordinates is given by,

$${}^W_B R = R_z(\psi) R_y(\theta) R_x(\phi) \quad (4.3)$$

where,

$$R_z(\psi) = \begin{bmatrix} \cos \psi & -\sin \psi & 0 \\ \sin \psi & \cos \psi & 0 \\ 0 & 0 & 1 \end{bmatrix} \quad (4.4)$$

$$R_y(\theta) = \begin{bmatrix} \cos \theta & 0 & \sin \theta \\ 0 & 1 & 0 \\ -\sin \theta & 0 & \cos \theta \end{bmatrix} \quad (4.5)$$

$$R_x(\phi) = \begin{bmatrix} 1 & 0 & 0 \\ 0 & \cos \phi & -\sin \phi \\ 0 & \sin \phi & \cos \phi \end{bmatrix} \quad (4.6)$$

The rotation matrix can thus be expressed as,

$${}^W_B R = \begin{bmatrix} \cos \theta \cos \psi & \sin \phi \sin \theta \cos \psi - \cos \phi \sin \psi & \cos \phi \sin \theta \cos \psi + \sin \phi \sin \psi \\ \cos \theta \sin \psi & \sin \phi \sin \theta \sin \psi + \cos \phi \cos \psi & \cos \phi \sin \theta \sin \psi - \sin \phi \cos \psi \\ -\sin \theta & \sin \phi \cos \theta & \cos \phi \cos \theta \end{bmatrix} \quad (4.7)$$

Now that ${}^W_B R$ has been established, it will be denoted simply as \mathcal{R} for the remainder of this thesis for convenience.

Note that the rotation matrix, \mathcal{R} , is orthogonal and hence its inverse will equal the transpose of the matrix, that is,

$$\mathcal{R}^{-1} = \mathcal{R}^T \quad (4.8)$$

This is useful for easily converting from world to body coordinates.

It is important to note that in using Euler angles, \mathcal{R} is plagued by singularity problems at certain angles. This inhibits the conversion of world to body coordinates. However, because the control systems and bottom-heavy configuration of AUVs typically prevent the vehicle from attaining these angles, it is generally sufficient to use Euler angles and not resort to other mathematical techniques such as equivalent angle-axis representations.

In general, an AUV should be restricted to the following rotation angles,

$$-\pi < \phi \leq \pi \quad (4.9)$$

$$-\frac{\pi}{2} < \theta < \frac{\pi}{2} \quad (4.10)$$

$$0 \leq \psi < 2\pi \quad (4.11)$$

These are the permitted ranges of Euler angles that do not result in a singular matrix for \mathcal{R} .

4.3.4 State Space Representation

Let \mathcal{P} be the position state vector, \mathcal{V} the velocity state vector and \mathcal{T} the force and torque vector. Now, define \mathcal{P}_B , \mathcal{V}_B and \mathcal{T}_B to be the position, velocity and force/torque state vectors of the vehicle.

\mathcal{P}_B not only includes the position in Cartesian coordinates, but also includes the attitude in Euler angles. It is defined as,

$$\mathcal{P}_B = \begin{bmatrix} \mathbf{x}_B \\ \Theta_B \end{bmatrix} \quad (4.12)$$

where,

$$\mathbf{x}_B = \begin{bmatrix} x \\ y \\ z \end{bmatrix} \quad (4.13)$$

and,

$$\Theta_B = \begin{bmatrix} \phi \\ \theta \\ \psi \end{bmatrix} \quad (4.14)$$

\mathbf{x}_B defines the position vector while Θ_B represents the attitude vector.

\mathcal{V}_B includes the linear velocities as well as the angular velocities. It is defined as,

$$\mathcal{V}_B = \begin{bmatrix} \mathbf{v}_B \\ \boldsymbol{\omega}_B \end{bmatrix} \quad (4.15)$$

where,

$$\mathbf{v}_B = \begin{bmatrix} u \\ v \\ w \end{bmatrix} \quad (4.16)$$

and,

$$\omega_B = \begin{bmatrix} p \\ q \\ r \end{bmatrix} \quad (4.17)$$

v_B defines the linear velocity vector while ω_B represents the angular velocity vector. u , v and w represent the surge, sway and heave respectively; that is, they define the linear velocities along the x , y and z axes respectively. p , q and r on the other hand represent the roll, pitch and yaw rates respectively; that is, they define the angular velocities about the x , y and z axes respectively.

\mathcal{T}_B represents the force and torque state vectors in Cartesian coordinates. It is defined as,

$$\mathcal{T}_B = \begin{bmatrix} \mathcal{F}_B \\ \mathcal{Q}_B \end{bmatrix} \quad (4.18)$$

where,

$$\mathcal{F}_B = \begin{bmatrix} X \\ Y \\ Z \end{bmatrix} \quad (4.19)$$

and,

$$\mathcal{Q}_B = \begin{bmatrix} K \\ M \\ N \end{bmatrix} \quad (4.20)$$

\mathcal{F}_B represents the force state vector while \mathcal{Q}_B defines the torque state vector.

4.3.5 Position State Vector Transformation

The transformation of the position and velocity state vectors from frames $\{B\}$ to $\{W\}$ is presented in the next two sections.

Using equation 4.1, the linear position of the body relative to frame $\{W\}$ is represented as,

$${}^W x_B = {}^B x_B + {}^W x_{B_{org}} \quad (4.21)$$

However, since the AUV is always situated at the origin of frame $\{B\}$, then ${}^B x_B$ becomes $[0 \ 0 \ 0]^T$ meaning,

$${}^W x_B = {}^W x_{B_{org}} \quad (4.22)$$

That is, the linear position of the vehicle in relation to the world is in effect the position of frame $\{B\}$ with respect to frame $\{W\}$.

With respect to attitude, the attitude transformation is represented simply as \mathcal{R} which was defined in section 4.3.3.

4.3.6 Velocity State Vector Transformation

The world linear velocities can be represented as,

$${}^W v_B = \mathcal{R} {}^B v_B \quad (4.23)$$

That is,

$$\begin{bmatrix} \dot{x} \\ \dot{y} \\ \dot{z} \end{bmatrix} = \mathcal{R} \begin{bmatrix} u \\ v \\ w \end{bmatrix} \quad (4.24)$$

Body linear velocities can be found from the world linear velocities using the inverse (or transpose) of the rotation transformation matrix as such,

$$\begin{bmatrix} u \\ v \\ w \end{bmatrix} = \mathcal{R}^T \begin{bmatrix} \dot{x} \\ \dot{y} \\ \dot{z} \end{bmatrix} \quad (4.25)$$

For the angular velocities, the following linear transformations are used [22],

$$\dot{\phi} = p + q \sin \phi \tan \theta + r \cos \phi \tan \theta \quad (4.26)$$

$$\dot{\theta} = q \cos \phi - r \sin \phi \quad (4.27)$$

$$\dot{\psi} = \frac{q \sin \phi + r \cos \phi}{\cos \theta} \quad (4.28)$$

This allows the world angular velocities to be determined from the body angular velocities via a transformation matrix as such,

$${}^W \omega_B = \mathcal{W} {}^B \omega_B \quad (4.29)$$

That is,

$$\begin{bmatrix} \dot{\phi} \\ \dot{\theta} \\ \dot{\psi} \end{bmatrix} = \mathcal{W} \begin{bmatrix} p \\ q \\ r \end{bmatrix} \quad (4.30)$$

where,

$$\mathcal{W} = \begin{bmatrix} 1 & \sin \phi \tan \theta & \cos \phi \tan \theta \\ 0 & \cos \phi & -\sin \phi \\ 0 & \sin \phi \sec \theta & \cos \phi \sec \theta \end{bmatrix} \quad (4.31)$$

Now, because \mathcal{W} is not orthogonal, then the transpose cannot be used to find the inverse. Equations 4.26 to 4.28 must be rearranged to obtain the following,

$$p = \dot{\phi} - \dot{\psi} \sin \theta \quad (4.32)$$

$$q = \dot{\theta} \cos \phi + \dot{\psi} \sin \phi \cos \theta \quad (4.33)$$

$$r = -\dot{\theta} \sin \phi + \dot{\psi} \cos \phi \cos \theta \quad (4.34)$$

This gives the inverse of \mathcal{W} as,

$$\mathcal{W}^{-1} = \begin{bmatrix} 1 & 0 & -\sin \theta \\ 0 & \cos \phi & \sin \phi \cos \theta \\ 0 & -\sin \phi & \cos \phi \cos \theta \end{bmatrix} \quad (4.35)$$

Therefore, the body angular velocities can be found from the world angular velocities as such,

$$\begin{bmatrix} p \\ q \\ r \end{bmatrix} = \mathcal{W}^{-1} \begin{bmatrix} \dot{\phi} \\ \dot{\theta} \\ \dot{\psi} \end{bmatrix} \quad (4.36)$$

The transformation from the body to world velocity state vector can be represented in a single matrix as such,

$${}^W \mathcal{V}_B = \begin{bmatrix} \mathcal{R} & 0 \\ 0 & \mathcal{W} \end{bmatrix} {}^B \mathcal{V}_B \quad (4.37)$$

or,

$$\begin{bmatrix} \dot{x} \\ \dot{y} \\ \dot{z} \\ \dot{\phi} \\ \dot{\theta} \\ \dot{\psi} \end{bmatrix} = \begin{bmatrix} \mathcal{R} & 0 \\ 0 & \mathcal{W} \end{bmatrix} \begin{bmatrix} u \\ v \\ w \\ p \\ q \\ r \end{bmatrix} \quad (4.38)$$

For converting from the world to body velocity state vector,

$${}^B\mathcal{V}_B = \begin{bmatrix} \mathcal{R}^T & 0 \\ 0 & \mathcal{W}^{-1} \end{bmatrix} {}^W\mathcal{V}_B \quad (4.39)$$

or,

$$\begin{bmatrix} u \\ v \\ w \\ p \\ q \\ r \end{bmatrix} = \begin{bmatrix} \mathcal{R}^T & 0 \\ 0 & \mathcal{W}^{-1} \end{bmatrix} \begin{bmatrix} \dot{x} \\ \dot{y} \\ \dot{z} \\ \dot{\phi} \\ \dot{\theta} \\ \dot{\psi} \end{bmatrix} \quad (4.40)$$

Equations 4.38 and 4.40 define the kinematics equations of motion for an AUV and are extremely useful for testing and analysis of the vehicle, not to mention in computer simulations as well.

4.4 AUV Dynamic Model

The dynamic model of an AUV is presented in this section. A model for a robot is not only useful for formulating control algorithms, but to also perform simulations [45]. The dynamic model presented in this section is based on the underwater robotic models proposed by Fossen [21] and Yuh [46].

The dynamic model is derived from the Newton-Euler motion equation and is given by,

$$M\dot{\mathcal{V}} + C(\mathcal{V})\mathcal{V} + D(\mathcal{V})\mathcal{V} + G = \mathcal{T} \quad (4.41)$$

where M is a mass and inertia matrix, $C(\mathcal{V})$ is a Coriolis and centripetal terms matrix, $D(\mathcal{V})$ is a hydrodynamic damping matrix, G is the gravitational and buoyancy vector, \mathcal{T} is the external force and torque input vector, and \mathcal{V} is the velocity state vector. Note that equation 4.41 does not take into account environmental forces.

4.4.1 Mass and Inertia Matrix

M consists of both a rigid body mass and inertia, M_{RB} , and a hydrodynamic added mass, M_A . That is,

$$M = M_{RB} + M_A \quad (4.42)$$

If frame $\{B\}$ is positioned at the vehicle's centre of gravity, then M_{RB} is expressed as,

$$M_{RB} = \begin{bmatrix} m & 0 & 0 & 0 & 0 & 0 \\ 0 & m & 0 & 0 & 0 & 0 \\ 0 & 0 & m & 0 & 0 & 0 \\ 0 & 0 & 0 & I_x & -I_{xy} & -I_{xz} \\ 0 & 0 & 0 & -I_{xy} & I_y & -I_{yz} \\ 0 & 0 & 0 & -I_{xz} & -I_{yz} & I_z \end{bmatrix} \quad (4.43)$$

where m is the mass of the vehicle while the I terms represent the inertial tensors.

The effect of added mass can be modelled by a matrix such as in equation 4.44. The parameters of the added mass matrix are dependent on the shape of the vehicle, however, they are constants when the vehicle is fully submerged. The parameters are usually in the vicinity of 10% to 100% of the corresponding parameters in the rigid body mass matrix. The added mass matrix, M_A , is denoted as,

$$M_A = \begin{bmatrix} X_{\dot{u}} & X_{\dot{v}} & X_{\dot{w}} & X_{\dot{p}} & X_{\dot{q}} & X_{\dot{r}} \\ Y_{\dot{u}} & Y_{\dot{v}} & Y_{\dot{w}} & Y_{\dot{p}} & Y_{\dot{q}} & Y_{\dot{r}} \\ Z_{\dot{u}} & Z_{\dot{v}} & Z_{\dot{w}} & Z_{\dot{p}} & Z_{\dot{q}} & Z_{\dot{r}} \\ K_{\dot{u}} & K_{\dot{v}} & K_{\dot{w}} & K_{\dot{p}} & K_{\dot{q}} & K_{\dot{r}} \\ M_{\dot{u}} & M_{\dot{v}} & M_{\dot{w}} & M_{\dot{p}} & M_{\dot{q}} & M_{\dot{r}} \\ N_{\dot{u}} & N_{\dot{v}} & N_{\dot{w}} & N_{\dot{p}} & N_{\dot{q}} & N_{\dot{r}} \end{bmatrix} \quad (4.44)$$

4.4.2 Coriolis and Centripetal Matrix

$C(\mathcal{V})$, as with the mass matrix consists of two matrices, $C_{RB}(\mathcal{V})$ and $C_A(\mathcal{V})$, summed together,

$$C(\mathcal{V}) = C_{RB}(\mathcal{V}) + C_A(\mathcal{V}) \quad (4.45)$$

$C_{RB}(\mathcal{V})$ is the rigid body Coriolis and centripetal matrix induced by M_{RB} , while $C_A(\mathcal{V})$ is a Coriolis-like matrix induced by M_A .

If frame $\{B\}$ is positioned at the centre of gravity of the vehicle, then C_{RB} can be expressed as,

$$C_{RB}(\mathcal{V}) = \begin{bmatrix} 0 & 0 & 0 & 0 & mw & -mv \\ 0 & 0 & 0 & -mw & 0 & mu \\ 0 & 0 & 0 & mv & -mu & 0 \\ 0 & -mw & mv & 0 & -I_{yz}q - I_{xz}p + I_z r & I_{yz}r + I_{xy}p - I_y q \\ mw & 0 & -mu & I_{yz}q + I_{xz}p - I_z r & 0 & -I_{xz}r - I_{xy}q + I_x p \\ -mv & mu & 0 & -I_{yz}r - I_{xy}p + I_y q & I_{xz}r + I_{xy}q - I_x p & 0 \end{bmatrix} \quad (4.46)$$

The Coriolis-like matrix, C_A , is expressed as,

$$C_A(\mathcal{V}) = \begin{bmatrix} 0 & 0 & 0 & 0 & -a_3 & a_2 \\ 0 & 0 & 0 & a_3 & 0 & -a_1 \\ 0 & 0 & 0 & -a_2 & a_1 & 0 \\ 0 & -a_3 & a_2 & 0 & -b_3 & b_2 \\ a_3 & 0 & -a_1 & b_3 & 0 & -b_1 \\ -a_2 & a_1 & 0 & -b_2 & b_1 & 0 \end{bmatrix} \quad (4.47)$$

where,

$$\begin{aligned} a_1 &= X_{\dot{u}}u + X_{\dot{v}}v + X_{\dot{w}}w + X_{\dot{p}}p + X_{\dot{q}}q + X_{\dot{r}}r \\ a_2 &= X_{\dot{v}}u + Y_{\dot{v}}v + Y_{\dot{w}}w + Y_{\dot{p}}p + Y_{\dot{q}}q + Y_{\dot{r}}r \\ a_3 &= X_{\dot{w}}u + Y_{\dot{w}}v + Z_{\dot{w}}w + Z_{\dot{p}}p + Z_{\dot{q}}q + Z_{\dot{r}}r \\ b_1 &= X_{\dot{p}}u + Y_{\dot{p}}v + Z_{\dot{p}}w + K_{\dot{p}}p + K_{\dot{q}}q + K_{\dot{r}}r \\ b_2 &= X_{\dot{q}}u + Y_{\dot{q}}v + Z_{\dot{q}}w + K_{\dot{q}}p + M_{\dot{q}}q + M_{\dot{r}}r \\ b_3 &= X_{\dot{r}}u + Y_{\dot{r}}v + Z_{\dot{r}}w + K_{\dot{r}}p + M_{\dot{r}}q + N_{\dot{r}}r \end{aligned}$$

4.4.3 Hydrodynamic Damping Matrix

The hydrodynamic damping matrix represents the drag and lift forces acting on a moving underwater vehicle. However, for a low-speed underwater vehicle, the lift forces can be considered negligible when compared to the drag forces. These drag forces can be separated into two different terms consisting of a linear and quadratic term [10]. That is,

$$D(\mathcal{V}) = \text{diag}\{D_L + D_Q|\mathcal{V}|\} \quad (4.48)$$

where D_L and D_Q are the linear and quadratic damping terms respectively.

The damping matrix, $D(\mathcal{V})$, is given by,

$$D(\mathcal{V}) = \begin{bmatrix} X_u + X_{u|u}|u| & 0 & 0 & 0 & 0 & 0 \\ 0 & Y_v + Y_{v|v}|v| & 0 & 0 & 0 & 0 \\ 0 & 0 & Z_w + Z_{w|w}|w| & 0 & 0 & 0 \\ 0 & 0 & 0 & K_p + K_{p|p}|p| & 0 & 0 \\ 0 & 0 & 0 & 0 & M_q + M_{q|q}|q| & 0 \\ 0 & 0 & 0 & 0 & 0 & N_r + N_{r|r}|r| \end{bmatrix} \quad (4.49)$$

where,

$$D_L = \text{diag}\{X_u \quad Y_v \quad Z_w \quad K_p \quad M_q \quad N_r\} \quad (4.50)$$

and,

$$D_L = \text{diag}\{X_{u|u} \quad Y_{v|v} \quad Z_{w|w} \quad K_{p|p} \quad M_{q|q} \quad N_{r|r}\} \quad (4.51)$$

4.4.4 Gravitational and Buoyancy Vector

The gravitational and buoyancy vector, G , is defined as,

$$G = \begin{bmatrix} f_B + f_G \\ r_B \times f_B + r_G \times f_G \end{bmatrix} \quad (4.52)$$

where f_B is the buoyant force vector, defined as,

$$f_B = \mathcal{R}^{-1} \begin{bmatrix} 0 \\ 0 \\ -B \end{bmatrix} \quad (4.53)$$

and f_G is the gravitational force vector defined as,

$$f_G = \mathcal{R}^{-1} \begin{bmatrix} W \\ 0 \\ 0 \end{bmatrix} \quad (4.54)$$

while r_B is the centre of buoyancy and r_G is the centre of gravity or mass in frame $\{B\}$.

Now, because frame $\{B\}$ is positioned at the centre of gravity, then $r_G = [0 \ 0 \ 0]^T$, and hence G simplifies to,

$$G = \begin{bmatrix} f_B + f_G \\ r_B \times f_B \end{bmatrix} \quad (4.55)$$

Defining r_B as $[x_B \ y_B \ z_B]^T$, that is, the distance in x, y, z coordinates from the origin of frame $\{B\}$, and combining equations 4.53, 4.54, 4.55 and 4.7, G then becomes,

$$G = \begin{bmatrix} (B - W) \sin \theta \\ -(B - W) \sin \phi \cos \theta \\ -(B - W) \cos \phi \cos \theta \\ B \cos \theta (z_B \sin \phi - y_B \cos \phi) \\ B (x_B \cos \phi \cos \theta + z_B \sin \theta) \\ -B (x_B \sin \phi \cos \theta + y_B \sin \theta) \end{bmatrix} \quad (4.56)$$

4.4.5 Forces and Torque Vector

The external force and torque vector produced by the thrusters is defined as,

$$\mathcal{T} = LU \quad (4.57)$$

where L is a mapping matrix and U is a thrust vector.

U is the vector of thrusts produced by the vehicle's thrusters,

$$U = \begin{bmatrix} T_1 \\ T_2 \\ \vdots \\ T_n \end{bmatrix} \quad (4.58)$$

The number of thrust values in U depends on the number of thrusters on the vehicle. The mapping matrix L is essentially a $6 \times n$ matrix that uses U to find the overall forces and moments acting on the vehicle.

4.5 Summary

A brief background on the control of AUVs has been presented in this chapter. The state vector representation and dynamic model of an AUV have also been presented which will be used extensively in subsequent chapters for the modelling, identification and control simulations of the *Mako*. Since the dynamic model presented is fairly complex, the following chapter deals with its simplification and application to the *Mako*.

Chapter 5

Modelling the *Mako*

The dynamic model presented in the previous chapter is quite complex and obtaining many of the parameters is a very time consuming and difficult process. Therefore, simplification of the model was required. This chapter presents some assertions on the dynamics of the *Mako* that simplify the matrices of the dynamic model. Presented as well is a system identification approach that exploits some of the characteristics of a low-speed underwater vehicle. The approach assumes decoupling between the degrees of freedom so that they can be treated independently when performing experiments to identify model parameters.

5.1 Assertions on Dynamics

The following assertions were made for the dynamics of the *Mako* in order to simplify the modelling:

- The vehicle travels at low speeds, that is, less than 2m/s
- Roll and pitch movement is passively controlled and therefore, considered to be negligible
- The vehicle is considered to be symmetrical about its three planes
- During all manoeuvres the vehicle is always maintained in a horizontal posture
- Disturbances from the water environment on the vehicle such as currents and waves are negligible
- Sway, that is, movement along the vehicle's y axis, is negligible
- The vehicle's degrees of freedom are decoupled

The above assertions not only have important ramifications for the modelling of the *Mako*, but also for its control.

5.1.1 Low Speed

The *Mako*'s low speed was verified by testing the vehicle underwater. Even if a high speed was achievable, a lower speed would be desirable to enable precision. As will be seen, the low speed of the vehicle has significant implications for its modelling and parameter identification.

5.1.2 Roll and Pitch

By performing various underwater manoeuvres of the vehicle at full speed, it was observed that the vehicle was very stable, with roll and pitch movements being negligible. This was a direct result of the symmetrical nature of the vehicle, as well as the inherent metacentric righting moment that acted as a passive roll and pitch control system.

Since roll and pitch angles are negligible, then consequently, roll and pitch velocities can also be considered negligible. With roll and pitch movements deemed inconsequential to the modelling of the *Mako*, identification of the corresponding parameters would not be required, thereby decreasing the modelling complexity.

5.1.3 Symmetry

The *Mako* can be considered to be reasonably symmetric about its three planes. By making this assumption, several terms in the dynamic model matrices can be eliminated without serious loss of information. Symmetry also has an important implication for coupling between the degrees of freedom as will be seen.

5.1.4 Posture

Constraining the vehicle to a horizontal posture comes as a direct result of negligible roll and pitch. If roll and pitch were not passively controlled, it would still be desirable to maintain a horizontal posture for the vehicle due to the benefits gained through the simplification of the control software. Since fewer variables are required to be controlled when the vehicle is in a horizontal posture, the easier and more precise the control of the vehicle becomes.

5.1.5 Environmental Disturbances

The assumption that there is negligible water movement is based on the premise that the vehicle will be in a controlled water environment such as a swimming pool when in use. Although modelling water movement is a simple matter of adding another matrix to the dynamic equation, the fact that the perturbation can act from an arbitrary direction makes measuring this perturbation very difficult.

5.1.6 Sway

Analogous to roll and pitch, sway movement was observed to be negligible underwater. This was a consequence of the vehicle's inability to control motion along the y axis via its motors. Although sway could inadvertently be affected by perturbations from the environment, as mentioned, since the vehicle is in a controlled environment, these disturbances can be considered insignificant.

5.1.7 Decoupling

By assuming decoupling between the degrees of freedom, that is, assuming that motion along or about one degree of freedom does not affect another degree of freedom, the dynamic model of an AUV can be significantly simplified.

According to Ridao et al. [10], the justification for the decoupling of the degrees of freedom is based on the fact that:

- The vehicle is fairly symmetrical about its three planes
- The off-diagonal elements of the dynamic model matrices are much smaller than their counterparts
- The hydrodynamic damping coupling is negligible at low speeds

Since the *Mako* is considered to be fairly symmetrical and travels at a low speed, the decoupling for the vehicle's degrees of freedom is valid. The decoupling means that the Coriolis and centripetal terms matrices become negligible and consequently can be eliminated from the dynamic model. The simplified dynamic model for the AUV then becomes,

$$M\dot{\mathcal{V}} + D(\mathcal{V})\mathcal{V} + G = \mathcal{T} \quad (5.1)$$

This means that only the inertial and damping parameters need to be identified for the *Mako*.

5.2 Simplifying the Dynamic Model Matrices

Based on the assertions presented in the previous section, as well as measurements performed on the vehicle, the matrices of the dynamic model from Chapter 4 were simplified and adapted to the *Mako*. These simplified matrices are presented in this section.

Note that since sway, roll and pitch are negligible, then the corresponding parameters in the following matrices have been set to zero since they are not required to be identified for controlling the *Mako*. The inertial and damping parameters for surge, heave and yaw have not been shown below, but rather, their identification and values will be presented in the following chapter.

5.2.1 Mass and Inertia Matrix

With the vehicle frame $\{B\}$ positioned at the centre of gravity and since the vehicle is assumed fairly symmetrical about all axes, then M_{RB} from equation 4.43, can then be simplified to a good approximation to,

$$M_{RB} = \begin{bmatrix} m & 0 & 0 & 0 & 0 & 0 \\ 0 & m & 0 & 0 & 0 & 0 \\ 0 & 0 & m & 0 & 0 & 0 \\ 0 & 0 & 0 & I_x & 0 & 0 \\ 0 & 0 & 0 & 0 & I_y & 0 \\ 0 & 0 & 0 & 0 & 0 & I_z \end{bmatrix} \quad (5.2)$$

Since roll, pitch and sway are considered negligible, then equation 5.2 can be further simplified to,

$$M_{RB} = \begin{bmatrix} 35.3 & 0 & 0 & 0 & 0 & 0 \\ 0 & 0 & 0 & 0 & 0 & 0 \\ 0 & 0 & 35.3 & 0 & 0 & 0 \\ 0 & 0 & 0 & 0 & 0 & 0 \\ 0 & 0 & 0 & 0 & 0 & 0 \\ 0 & 0 & 0 & 0 & 0 & I_z \end{bmatrix} \quad (5.3)$$

or,

$$M_{RB} = \text{diag} \left\{ 35.3 \quad 0 \quad 35.3 \quad 0 \quad 0 \quad I_z \right\} \quad (5.4)$$

where the mass of the *Mako* was measured to be 35.3kg. It can be seen from equations 5.3 and 5.4 that the only parameter that needs identification for this matrix is the inertial moment about the z axis corresponding to yaw.

Analogous to the simplification of M_{RB} , the added mass matrix, M_A , becomes,

$$M_A = \begin{bmatrix} X_{\dot{u}} & 0 & 0 & 0 & 0 & 0 \\ 0 & 0 & 0 & 0 & 0 & 0 \\ 0 & 0 & Z_{\dot{w}} & 0 & 0 & 0 \\ 0 & 0 & 0 & 0 & 0 & 0 \\ 0 & 0 & 0 & 0 & 0 & 0 \\ 0 & 0 & 0 & 0 & 0 & N_{\dot{r}} \end{bmatrix} \quad (5.5)$$

or,

$$M_A = \text{diag} \left\{ X_{\dot{u}} \quad 0 \quad Z_{\dot{w}} \quad 0 \quad 0 \quad N_{\dot{r}} \right\} \quad (5.6)$$

5.2.2 Hydrodynamic Damping Matrix

The hydrodynamic damping matrix, $D(\mathcal{V})$, from equation 4.49 simplifies to,

$$D(\mathcal{V}) = \begin{bmatrix} X_u + X_{u|u}|u| & 0 & 0 & 0 & 0 & 0 \\ 0 & 0 & 0 & 0 & 0 & 0 \\ 0 & 0 & Z_w + Z_{w|w}|w| & 0 & 0 & 0 \\ 0 & 0 & 0 & 0 & 0 & 0 \\ 0 & 0 & 0 & 0 & 0 & 0 \\ 0 & 0 & 0 & 0 & 0 & N_r + N_{r|r}|r| \end{bmatrix} \quad (5.7)$$

or,

$$D(\mathcal{V}) = \text{diag} \left\{ X_u + X_{u|u}|u| \quad 0 \quad Z_w + Z_{w|w}|w| \quad 0 \quad 0 \quad N_r + N_{r|r}|r| \right\} \quad (5.8)$$

5.2.3 Gravitational and Buoyancy Vector

The centre of gravity is denoted as $r_G = [0 \ 0 \ 0]^T$ while the centre of buoyancy is denoted as $r_B = [x_B \ y_B \ z_B]^T$. By experimental verification, r_B was found to be $r_B = [0 \ 0 \ 0.24]^T$ to a good approximation. This shows that the centre of buoyancy is aligned with the centre of gravity along the x and y axes. In fact, the mass and volume of the *Mako* was intentionally distributed in such a way that the only misalignment between the centres of mass and buoyancy was via the z axis. This distance of 24cm between the two centroids provides the metacentric righting moment that passively controls the vehicle's roll and pitch.

The weight of the *Mako* was found to be 345.9N while the buoyant force was measured as 361.0N. Keeping in mind that roll and pitch are negligible, equation 4.56 significantly simplifies to,

$$G = \begin{bmatrix} 0 \\ 0 \\ -15.1 \\ 0 \\ 0 \\ 0 \end{bmatrix} \quad (5.9)$$

The value of -15.1N implies that the vehicle has residual buoyancy just as it was designed to have. The residual buoyancy equates to 4.3% of the vehicle's weight which is more than that required by the underwater competition. Equation 5.9 shows that the gravitational and buoyant forces of the vehicle only affect the heave of the vehicle. This is expected given that the centres of gravity and buoyancy are aligned along the x and y axes, and hence, the gravitational and buoyant forces should then only affect vertical movement.

5.2.4 Forces and Torque Vector

By measuring the positions of the motors on the *Mako*, a layout of the motors depicting their respective distances to the vehicle's centre of gravity was attained. This can be seen in Figure 5.1.

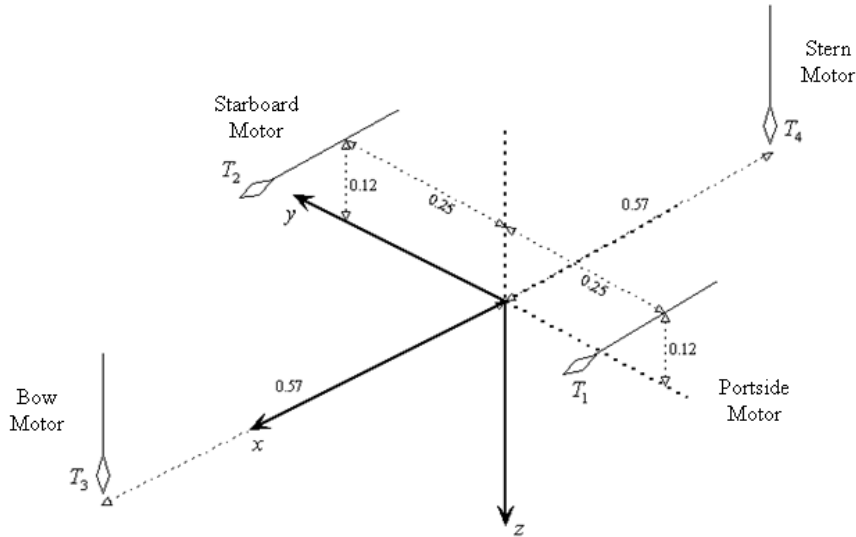


FIGURE 5.1: Positions of motors on *Mako*. Distances are in metres.

From Figure 5.1, the mapping matrix, L , for the *Mako* is given to a good approximation by,

$$L = \begin{bmatrix} 1 & 1 & 0 & 0 \\ 0 & 0 & 0 & 0 \\ 0 & 0 & 1 & 1 \\ 0 & 0 & 0 & 0 \\ -0.12 & -0.12 & -0.57 & 0.57 \\ 0.25 & -0.25 & 0 & 0 \end{bmatrix} \quad (5.10)$$

while the thrust vector is given by,

$$U = \begin{bmatrix} T_1 \\ T_2 \\ T_3 \\ T_4 \end{bmatrix} \quad (5.11)$$

where T_1, T_2, T_3, T_4 represent the thrusts of the portside, starboard, bow and stern motors respectively.

In equation 5.10, the first three rows signify whether or not a particular motor has an effect on the movement of the vehicle along the x, y and z directions. For instance, in the first row, the ones in the first two columns indicate that the horizontal motors are

responsible for surge.

The last three rows of the mapping matrix denote the distances from the centre of gravity to the motors. These values are either positive or negative corresponding to anticlockwise or clockwise moments respectively. The moments that are produced are responsible for affecting the vehicle's attitude.

As can be seen in the fifth row of the mapping matrix, not only do the two vertical motors contribute to pitch, but so do the two horizontal motors. This implies that when the vehicle is surging either forwards or backwards, the horizontal motors will affect the pitch of the vehicle. However, when performing underwater manoeuvres, this effect was not observed, implying that the contribution to pitch by the horizontal motors is not significant. This is most likely attributable to the passive pitch control system.

Also observed in the fifth row is the fact that each vertical motor is equidistant from the centre of gravity. Consequently, applying equal forces to these motors when diving, surfacing or hovering will maintain the vehicle in a reasonably horizontal posture.

5.3 System Identification Approach

The system identification of an AUV is quite complex and requires complete state knowledge, as well as highly complex and expensive equipment [11]. Moreover, the highly configurable and modular nature of the *Mako* would demand system identification of the vehicle more frequently than usual. Therefore, a methodology had to be used that would allow system identification to be relatively simple and not time consuming, as well as not requiring complex and expensive equipment.

An approach by Indiveri [12] for identifying an underwater robotic system's dynamic model exploits some of the characteristics of the vehicle and utilises onboard sensors to successfully and easily identify the vehicle's parameters. The approach assumes decoupling between the degrees of freedom. In the system identification, a combination of static and dynamic experiments are performed with the parameters for each degree of freedom then estimated via least squares estimation utilising the experimental data obtained. This approach was chosen for the *Mako's* system identification due to its simple nature and low loss of information.

5.3.1 Model for Each Degree of Freedom

The above methodology assumes decoupling between the vehicle's degrees of freedom. Since it has been established that the *Mako* can be modelled as a symmetric and decoupled AUV, then this means that each degree of freedom can be treated separately. In this case, the simplified dynamic model in equation 5.1 can then be modified to one applicable to each degree of freedom,

$$m_{\xi}\dot{\xi} + d_{\xi}\xi + d_{\xi|\xi}|\xi| + g_{\xi} = \tau_{\xi} \quad (5.12)$$

In equation 5.12, m_ξ represents the inertial parameters, d_ξ and $d_{\xi|\xi|}$ the linear and quadratic damping parameters respectively, g_ξ the gravitational/buoyancy force, τ_ξ the input force/torque and ξ the velocity component for a particular degree of freedom. From equation 4.42, m_ξ consists of both a rigid body parameter, $m_{RB,\xi}$, and an added mass parameter, $m_{A,\xi}$. The notation for these two parameters will be used later to differentiate between the two inertial parameter values.

5.3.2 Least Squares Estimation

In order to determine the parameters for each degree of freedom, least squares estimation is used to estimate these parameters given a set of experimental data. Equation 5.12 can be written in the regression form,

$$\lambda = H\Lambda \quad (5.13)$$

where λ represents a vector of known values, H is a matrix containing experimentally obtained data, and Λ is a vector containing the unknown parameters.

The estimate of a parameter is found from the following equation [12],

$$\hat{\Lambda} = (H^T H)^{-1} H^T \lambda \quad (5.14)$$

The standard deviation of this estimated parameter is computed as,

$$\hat{\sigma}_\Lambda = \sqrt{\text{diag}(H^T H)^{-1} \hat{\sigma}^2} \quad (5.15)$$

where $\hat{\sigma}^2$ is the estimated Gaussian zero mean measurement noise variance defined as,

$$\hat{\sigma}^2 = \frac{(\lambda - H\hat{\Lambda})^T (\lambda - H\hat{\Lambda})}{\dim \lambda - \dim \Lambda} \quad (5.16)$$

The standard deviation and estimate of the parameter can be used to determine the parameter error which is defined by,

$$\varsigma = \frac{\hat{\sigma}_\Lambda}{|\hat{\Lambda}|} \quad (5.17)$$

5.3.3 Static Experiment

The static experiment involves measuring the velocity of the vehicle under steady-state conditions for a particular degree of freedom. The vehicle has a particular force/torque applied to it and when a constant velocity is reached, this velocity is recorded. The least squares approach described previously is then used to estimate the parameters for the corresponding degree of freedom.

Under steady-state conditions, equation 5.12 simplifies to,

$$d_\xi \dot{\xi} + d_{\xi|\xi} \xi |\dot{\xi}| + g_\xi = \tau_\xi \quad (5.18)$$

as acceleration becomes zero under constant velocity. From equation 5.18 it can be seen that the only unknown parameters are the linear and quadratic damping terms. Utilising equation 5.13, λ becomes,

$$\lambda = \begin{bmatrix} \tau_{\xi,1} - g_\xi \\ \tau_{\xi,2} - g_\xi \\ \vdots \\ \tau_{\xi,n} - g_\xi \end{bmatrix} \quad (5.19)$$

and represents n input forces/torques minus the gravitational/buoyancy force acting along or about the degree of freedom.

The matrix, H , contains the constant velocities obtained experimentally at particular input forces/torques and is denoted as,

$$H = \begin{bmatrix} \xi_1 & \xi_1 |\xi_1| \\ \xi_2 & \xi_2 |\xi_2| \\ \vdots & \vdots \\ \xi_n & \xi_n |\xi_n| \end{bmatrix} \quad (5.20)$$

The vector, Λ , contains the unknown damping parameters,

$$\Lambda = \begin{bmatrix} d_\xi \\ d_{\xi|\xi} \end{bmatrix} \quad (5.21)$$

Equation 5.14 can then be used to estimate the damping parameters given the matrices in equations 5.19 to 5.21.

5.3.4 Dynamic Experiment

The dynamic experiment involves applying a sinusoidal input force/torque to the vehicle about a particular degree of freedom. Since the damping parameters have been estimated from the static experiment, these are now assumed to be correct and can now be used in determining the remaining parameters, that is, the inertial parameters.

Rearranging equation 5.12 in terms of the inertial parameter m_ξ ,

$$m_\xi \dot{\xi} = \tau_\xi - g_\xi - d_\xi \dot{\xi} - d_{\xi|\xi} \dot{\xi} |\dot{\xi}| \quad (5.22)$$

Comparing equation 5.22 to equation 5.13, λ then becomes,

$$\lambda = \begin{bmatrix} \tau_{\xi,1} - g_{\xi} - d_{\xi}\xi_1 - d_{\xi|\xi}|\xi_1| |\xi_1| \\ \tau_{\xi,2} - g_{\xi} - d_{\xi}\xi_2 - d_{\xi|\xi}|\xi_2| |\xi_2| \\ \vdots \\ \tau_{\xi,n} - g_{\xi} - d_{\xi}\xi_n - d_{\xi|\xi}|\xi_n| |\xi_n| \end{bmatrix} \quad (5.23)$$

while,

$$H = \begin{bmatrix} \dot{\xi}_1 \\ \dot{\xi}_2 \\ \vdots \\ \dot{\xi}_n \end{bmatrix} \quad (5.24)$$

and,

$$\Lambda = m_{\xi} \quad (5.25)$$

As with the static experiment, equation 5.14 is then used to find the unknown parameter; in this case, m_{ξ} .

5.4 Summary

The dynamic model presented in Chapter 4 has been significantly simplified and adapted to the *Mako* through assertions made on its dynamics. The majority of these assertions were possible due to the nature of the *Mako's* mechanical configuration. A relatively simple system identification approach has also been identified which will be used in the following chapter to identify the surge, heave and yaw parameters of the vehicle. The parameters presented in the subsequent chapter along with the simplified model presented in this chapter are used in the control simulation study in Chapter 7.

Chapter 6

System Identification

Presented in this chapter are the steps that were undertaken in order to perform the system identification of the *Mako*. Detailed first is the experiment on measuring the thrust outputs of the motors. The testing and remote control of the vehicle is then discussed along with associated problems. The results for the system identification of the *Mako* are then presented for surge, heave and yaw. It is shown that the low resolution and shortcomings of the sensor suite on board the *Mako* resulted in some parameters not being able to be identified.

6.1 Thrust Measurement

Since the dynamic model of an AUV relies on the force input from the motors, it was essential to know what thrust outputs each of the motors on board the *Mako* could produce at different voltages in order to control the vehicle. The thrust outputs of each motor were also required because motors naturally exhibit slightly different characteristics which result in different thrust outputs at respective voltages. For instance, applying the same voltage to the two horizontal motors would not necessarily result in straight line motion of the vehicle. Therefore, it was imperative to know the relation of each motor's thrust characteristics to every other.

6.1.1 Thrust Experiment

In order to measure the thrusts of each motor, an experiment was performed during the construction phase of the AUV that involved placing each motor in a tank of water and measuring the thrust output via a load cell at different voltages. Each motor had their respective shrouds in place during the experiment as propeller-to-hull interactions would have a significant effect on the thrust.

The voltage to the motors was adjusted via the Eyebot controller. The Eyebot uses pulse width modulation (PWM) for adjusting the effective voltage to the motor. This means that the motor is switched on and off at a certain frequency. Depending on how

quickly the motor is switched on and off, the faster or slower that the motor will turn. The Eyebot allows 101 speed settings using PWM for each motor, ranging from 0 to 100 for both forward and reverse mode. This essentially means that 101 different effective voltages can be applied to the motor.

Different speed settings were applied to each motor and the respective thrust outputs were measured. Figures 6.1 to 6.4 show the relation between the speed settings on the Eyebot controller and the motor thrust outputs obtained for the horizontal and vertical motors in both forward and reverse mode.

6.1.2 Remark on Thrust Outputs

As can be seen from the graphs, the thrust for each motor is greatest for an Eyebot speed setting of 0 as opposed to 100. This is due to the reverse logic used on the motor controller circuit boards. What is also noticeable from the graphs is that the majority of speed settings produce no thrust whatsoever. Measurable thrust only occurs between the speed settings of 0 and 40 for the motors in both forward and reverse mode.

Comparing the forward and reverse mode thrust characteristics for both the horizontal and vertical motors, it is clear that in reverse mode, the four motors do not produce considerable thrust when compared to the forward mode. For instance, for the horizontal motors, the maximum thrust in forward mode is 5.07N while in reverse mode it is 1.14N. The low force produced in reverse mode is due to the nature of the propellers that are designed predominantly for forward movement. This feature had an adverse effect on the system identification of the vehicle as will be explained in section 6.3.

Another aspect that can be seen from the graphs is that in forward mode, the vertical motors produce considerably greater thrust than the horizontal motors. The vertical motors at maximum thrust produce 8.18N of force while for the horizontal motors, the maximum thrust is 5.07N. The propeller-to-hull interaction, that is, the interaction between the propeller and the motor's shroud, is the cause for this large difference in thrust. Since the vertical motors have larger and longer shrouds than the horizontal motors, much more water is pushed off the sides of the shroud, contributing to a greater thrust output.

The results of the motor thrust measurements were used in the determination of parameters in the system identification process, as well as ensuring that desired motion, such as straight line motion, was attained for performing the system identification experiments accurately. The thrust results will also prove invaluable in the eventual autonomous control of the vehicle in the future.

6.2 Testing and Control

Once construction of the *Mako* was completed, testing of the vehicle had to occur. In order to test the vehicle software was developed using C++ for the Eyebot controller to control the motors, perform simple manoeuvres and to receive inputs from onboard sensors, as

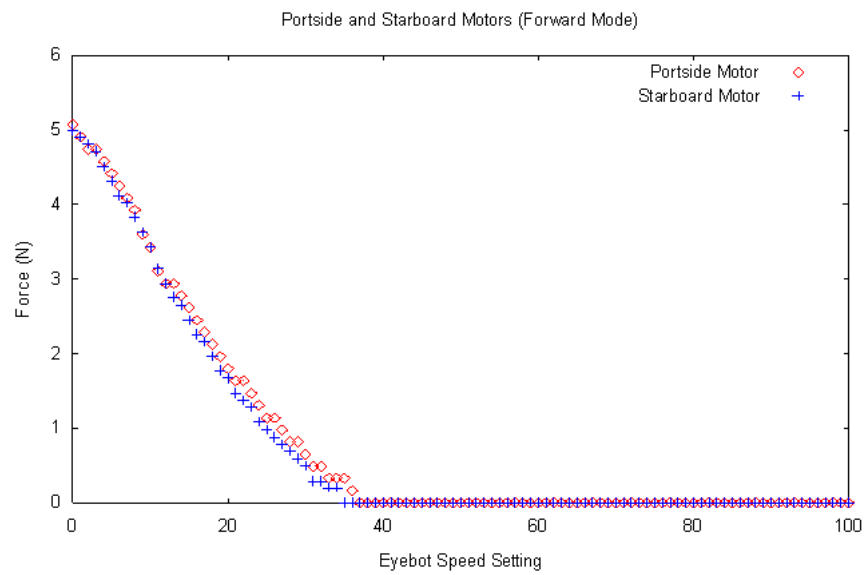


FIGURE 6.1: Thrust output for portside and starboard motors in forward mode.

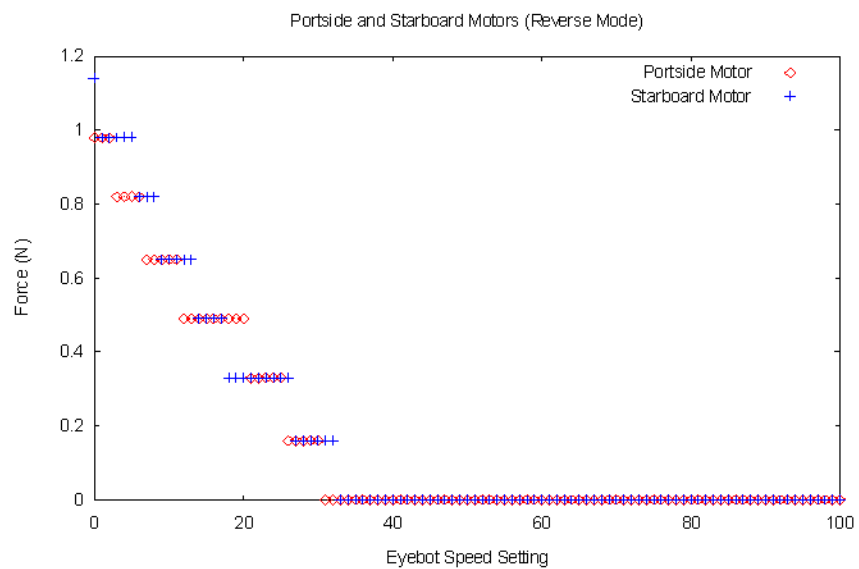


FIGURE 6.2: Thrust output for portside and starboard motors in reverse mode.

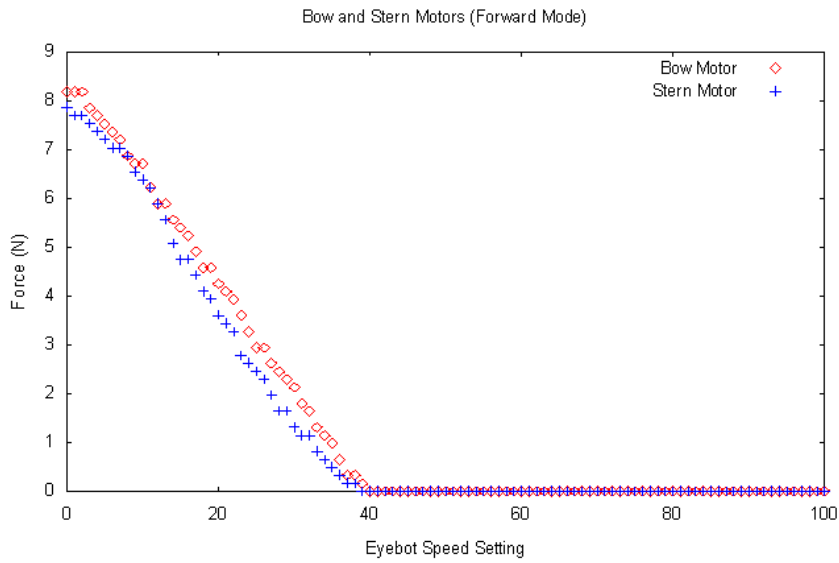


FIGURE 6.3: Thrust output for bow and stern motors in forward mode.

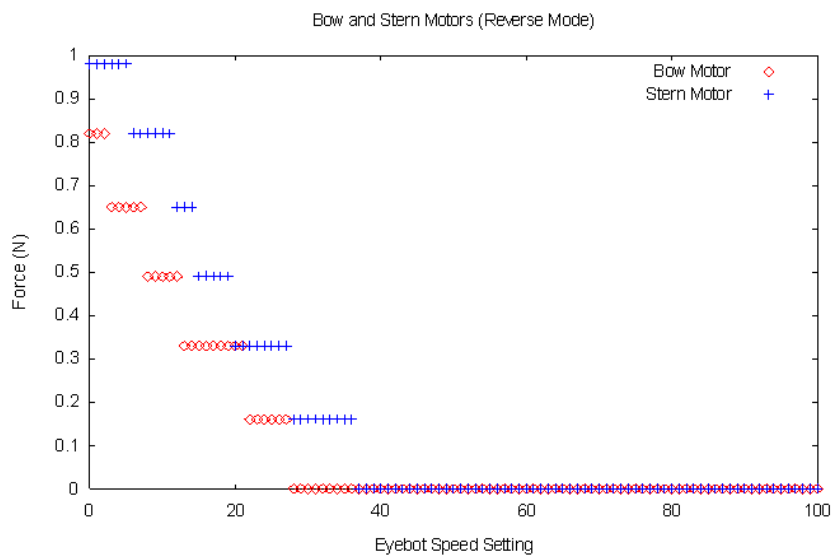


FIGURE 6.4: Thrust output for bow and stern motors in reverse mode.

well as the leak and power monitors.

6.2.1 Communications

Testing was an arduous and time consuming process mainly owing to the underwater environment in which the vehicle had to be tested in. Downloading and uploading data to the vehicle was a necessary aspect of testing. It was not practical to recover the vehicle from the water and open the upper hull every time software had to be downloaded or uploaded to or from the Eyebot controller.

The use of infrared and Bluetooth as a preliminary communications system provided a means with which to download and upload data to the vehicle in a relatively simple manner. Despite the use of this simple communications system, data gathering was still very time consuming and was not real-time. Although the Eyebot controller's LCD screen provided real-time feedback of data, because of the nature of the vehicle's environment, it was not always possible to see the screen. A much more sophisticated communications system is required in the future if testing and control of the vehicle is to be performed with less difficulty and time consumption.

6.2.2 Remotely Controlling the *Mako*

To facilitate testing and system identification, as well as for gaining insight into the manoeuvrability of the *Mako*, software was developed to control the vehicle remotely via the communications system mentioned. The software allows the vehicle to be controlled via infrared or Bluetooth. The following manoeuvres were implemented in software for controlling the vehicle:

- move forward (positive surge)
- move backward (negative surge)
- rotate right (positive yaw)
- rotate left (negative yaw)
- move downward (positive heave)
- move upward (negative heave)
- stop (reset all motors)

In conjunction with the communications project [47], a user interface was developed specifically for controlling the *Mako* via a remote computer using Bluetooth. Screenshots of the interface are shown in Figure 6.5.

On top of performing manoeuvres, the interface also allows each motor to be individually controlled. This is particularly useful for testing purposes and determining optimal speeds for certain manoeuvres.

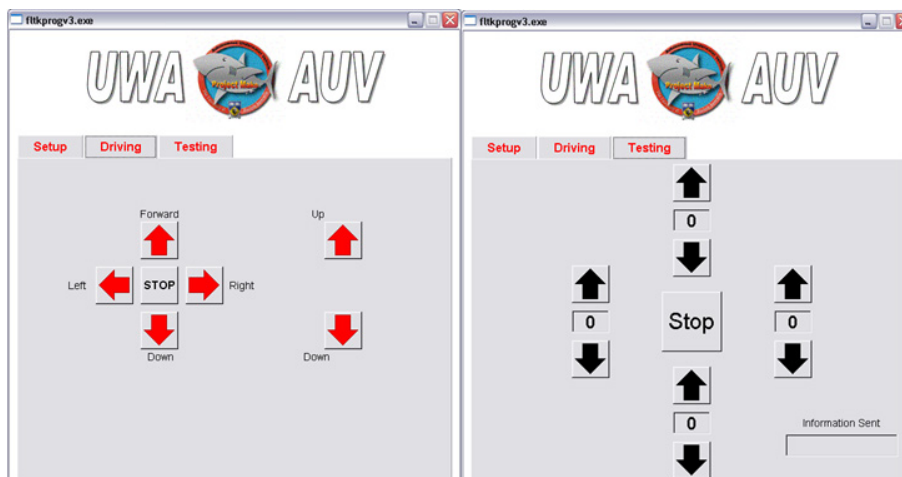


FIGURE 6.5: Left: Interface window for manoeuvring the *Mako*. Right: Interface window for controlling each motor separately [47].

Depending on the inputs received from the user interface, the Eyebot controller either initiates manoeuvres or controls a particular motor. In performing manoeuvres, only one degree of freedom is actively controlled at any one time (Figure 6.6). This not only makes controlling the vehicle easier, but also allows the response of the vehicle to surge, heave and yaw movements to be observed independently.

It was clearly seen through the remote control of the vehicle that the *Mako* was very stable with respect to roll and pitch, and that the degrees of freedom could indeed be considered decoupled.

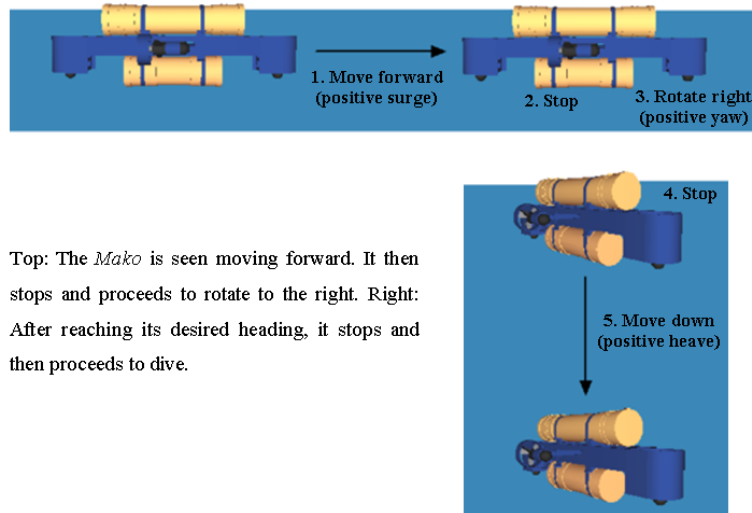
The development of the user interface for controlling the *Mako* was a small step in overcoming some of the difficulties associated with testing. The interface proved particularly useful in the system identification process for effortlessly initiating manoeuvres and obtaining results in a timely manner.

6.2.3 Sensor Limitations

The number of sensors on the *Mako* was limited as well as their capabilities. The sensors available for feedback were a magnetic compass, velocity sensor and echo sounder for depth measurement. Only the magnetic compass and velocity sensor were required in the system identification experiments.

6.2.3.1 Magnetic Compass

The magnetic compass is limited in that it only returns the yaw angle and not roll or pitch angles. The yaw rate can not be obtained directly from the compass, however, by taking the derivative of the yaw angle with respect to time, the yaw rate can be attained indirectly.



Top: The *Mako* is seen moving forward. It then stops and proceeds to rotate to the right. Right: After reaching its desired heading, it stops and then proceeds to dive.

FIGURE 6.6: Example of how the *Mako*'s remotely controlled manoeuvres are performed.

6.2.3.2 Velocity Sensor

The velocity sensor is only able to measure the velocity in one direction. The sensor is currently positioned on the *Mako* so as to measure the forward surge velocity as this is the most important velocity to determine. However, for testing purposes, the sensor has the ability of being rotated so as to measure the velocity in other directions. The sensor's resolution of 5cm/s had an undesirable effect on the system identification results as will be detailed in section 6.3.

6.2.3.3 Depth Sensor

The echo sounder is only able to discern the distance to the bottom and not directly obtain the actual depth of the vehicle. The echo sounder also has a poor resolution of 10cm meaning that any depth control that is attempted with it in the future would result in large fluctuations between the actual and real depths.

6.3 System Identification Results

In this section, the results of the static and dynamic experiments that were performed on the *Mako* are presented. The remote user interface along with software that was written for the Eyebot were used in performing the system identification.

6.3.1 Static Experiments

The following static experiments performed on the *Mako* involved the identification of the damping parameters, d_ξ and $d_{\xi|\xi|}$, for surge, heave and yaw. Presented are the results of these static experiments and the damping parameters identified.

It must be noted that for identifying the parameters for these degrees of freedom, both positive and negative movement along or about the degrees of freedom must be measured. For instance, in performing the surge experiment, both forward and backward movement must be performed as separate experiments. This is because the vehicle is not completely symmetric. Although for model simplification, the vehicle can and was considered to be symmetric, the same argument cannot be used to assume that parameters in positive and negative directions of the vehicle's motion will be the same. Thus, two independent sets of experiments are required for both the static and dynamic experiments for each degree of freedom.

6.3.1.1 Surge Static Experiment

During the surge static experiment (Figure 6.7), the *Mako* had input forces applied to it via its portside and starboard motors. The maximum constant velocity that the vehicle attained was then measured. This experiment was conducted for several different input force values.

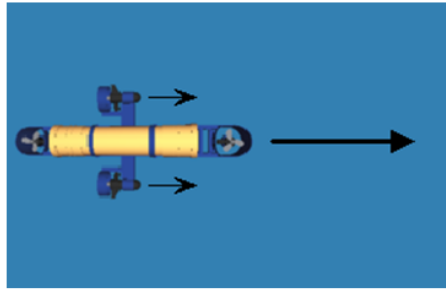


FIGURE 6.7: Graphical representation of positive surge static experiment.

Figure 6.8 shows the results of the forward (positive) surge static experiment with the maximum attained constant velocity of the vehicle versus the total force applied by the horizontal motors.

It can be seen from Figure 6.8 that the velocity remains constant at times even though the force applied by the motors changes. This comes as a direct result of the low resolution of the velocity sensor. Since the velocity sensor was not sensitive enough, it was not able to give accurate readings for particular input forces. For this reason, only the leftmost data points for each velocity change in the graph were used in the calculation of the positive surge damping parameters, d_u^+ and $d_{u|u|}^+$.

Using equations 5.14 to 5.21, the damping parameter estimates, their standard deviations and their errors were computed from the experimental results. These values can be seen in Table 6.1.

It is clear that the quadratic damping term is significantly larger than the linear damping term, implying that the overall damping effect is mainly a result of the square of the vehicle's velocity.

As for the negative surge experiment, a sufficient number of velocity readings could not be attained to justify calculating the corresponding damping parameters. The low number of data values was due to the low resolution of the velocity sensor combined with the low overall force produced by the two motors in reverse.

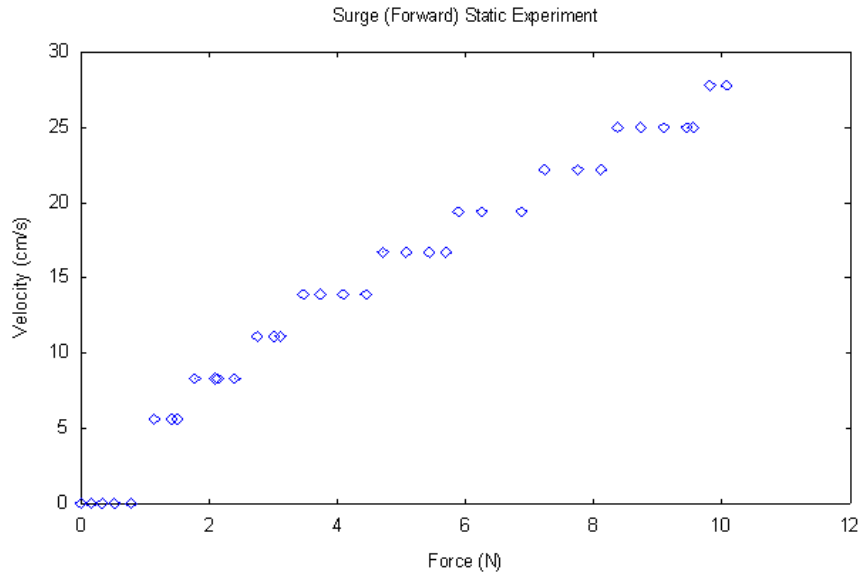


FIGURE 6.8: Positive surge static experiment results.

<i>Positive Surge</i>	d_u^+ (Ns/m)	$d_{u u}^+$ (Ns ² /m ²)
Parameter estimate, $\hat{\Lambda}$	16.8	67.7
Standard deviation, $\hat{\sigma}_\Lambda$	0.8	3.5
Parameter error, ς	4.8%	5.2%

TABLE 6.1: Positive Surge Damping Parameters.

6.3.1.2 Heave Static Experiment

In the heave static experiment, input forces were applied to the *Mako* via the bow and stern motors (Figure 6.9). As with the surge experiment, the maximum constant velocity attained by the vehicle for different input forces was recorded.

Damping parameters had to be found for both upward (negative) and downward (positive) heave. However, since the vertical motors need to be in reverse mode to move the vehicle upwards, and since reverse mode does not provide much force, insufficient data was available to determine the parameters for negative heave. Therefore, only the positive heave damping parameters were able to be found.

With the *Mako* having a residual buoyancy of 15.1N, the overall force required by the bow and stern motors had to be greater than this value to submerge the vehicle for downward movement. Since the two motors combined could only achieve a maximum

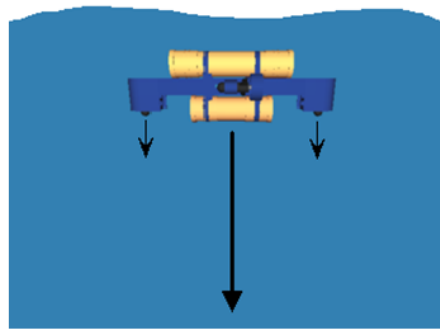


FIGURE 6.9: Graphical representation of positive heave static experiment.

of about 16N of force, only the range of force values from 15.1N to 16N could be used to achieve downward movement. This did not provide many results. However, by adding weights to the vehicle and adjusting the residual buoyancy very close to zero, the full range of force values from 0N to 16N was able to be utilised to achieve downward movement for the vehicle. This resulted in much more data being attained.

Shown in Figure 6.10 are the results of the positive heave experiment with the maximum constant velocity attained by the vehicle for different input forces applied by the vertical motors.

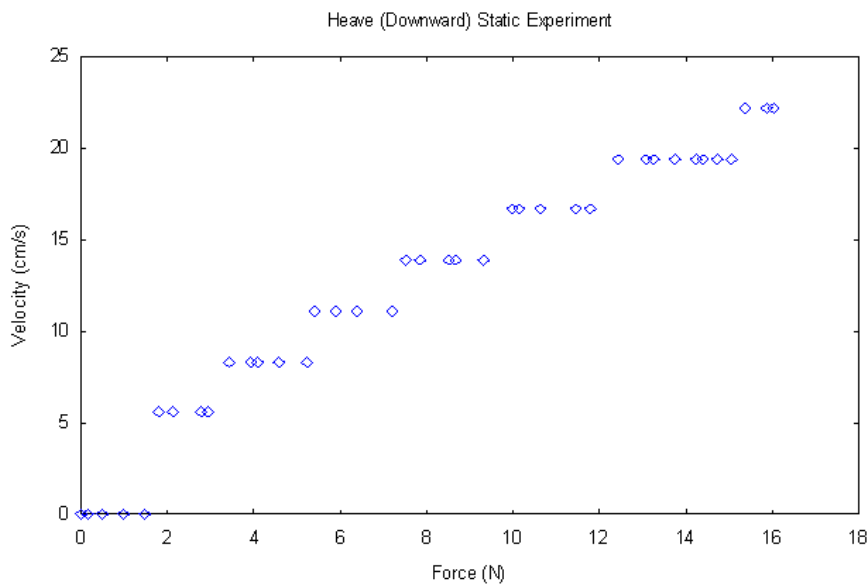


FIGURE 6.10: Positive heave static experiment results.

The positive heave experiment again demonstrated the low resolution of the velocity sensor with repeated velocities being attained for varying input forces. As with the surge experiment, only the leftmost data points were used in the calculation of the heave damping parameters.

Table 6.2 displays the values calculated for the downward heave parameters, d_w^+ and

$d_{w|w}^+$, their standard deviations, and their errors.

<i>Positive Heave</i>	d_w^+ (Ns/m)	$d_{w w}^+$ (Ns ² /m ²)
Parameter estimate, $\hat{\Lambda}$	26.0	196.7
Standard deviation, $\hat{\sigma}_\Lambda$	1.6	8.6
Parameter error, ς	6.2%	4.4%

TABLE 6.2: Positive Heave Damping Parameters.

It can again be seen that the quadratic damping term is significantly larger than the linear damping term; in fact more than seven times larger. The damping parameters for heave are also greater than those for surge indicating that the effective surface area of the vehicle for heave is greater than that for surge. This is indeed the case as the vehicle's surface area in the xy plane is significantly larger than that in the yz plane.

6.3.1.3 Yaw Static Experiment

In the yaw static experiment (Figure 6.11), the *Mako* was made to rotate about its z axis via its portside and starboard motors. Consequently, one motor had to be set in reverse and the other in forward mode. This meant that rotations both clockwise (positive) and anticlockwise (negative) had to be taken into account.

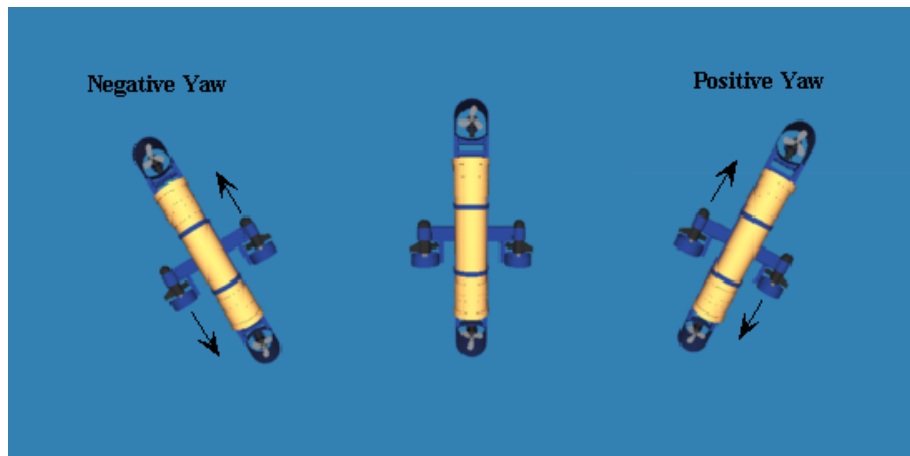


FIGURE 6.11: Graphical representation of yaw static experiments.

Unlike the surge and heave static experiments, the yaw degree of freedom required the measurement of yaw rate and the torque applied to the vehicle, as opposed to velocity and force. The magnetic compass was able to indirectly calculate the yaw rate with a high resolution, and hence, this experiment was not inhibited by the low resolution of a sensor, as was the case with the velocity sensor. Given that the experiment required a torque to be applied to the vehicle, both horizontal motors were not used in reverse mode at the same time, and therefore, the low thrust output present in reverse mode did not hinder the acquirement of data. This meant that experiments for both positive and negative yaw could be used to yield sufficient data.

Figures 6.12 and 6.13 display the results obtained for the positive and negative yaw static experiments respectively. The maximum yaw rate obtained by the vehicle was measured for different input moments.

Using the results in Figures 6.12 and 6.13, the damping parameters for yaw were computed using the least squares estimation equations 5.14 to 5.21. The damping parameters for both positive and negative yaw are displayed in Table 6.3.

<i>Positive Yaw</i>	d_r^+ (Nms/rad)	$d_{r r}^+$ (Nm ² s ² /rad ²)
Parameter estimate, $\hat{\Lambda}$	3.2	1.9
Standard deviation, $\hat{\sigma}_\Lambda$	0.1	0.5
Parameter error, ς	2.9%	26.3%
<i>Negative Yaw</i>	d_r^- (Nms/rad)	$d_{r r}^-$ (Nm ² s ² /rad ²)
Parameter estimate, $\hat{\Lambda}$	3.2	2.0
Standard deviation, $\hat{\sigma}_\Lambda$	0.1	0.4
Parameter error, ς	3.1%	20.0%

TABLE 6.3: Yaw Damping Parameters.

It is clear that the parameters for both positive and negative yaw are quite similar, indicative of the symmetrical nature of the vehicle in the xz plane.

6.3.2 Dynamic Experiments

The dynamic experiments for the *Mako* involve the identification of the inertial parameter, m_ξ , for surge, heave and yaw. As seen in equations 5.22 to 5.25, the identification process for the dynamic experiment involves measuring the acceleration and velocity of the vehicle.

With the velocity sensor on the *Mako* having a low resolution, and since obtaining acceleration readings would require differentiating the velocity with respect to time, the inaccurate readings that would be obtained did not make it practical to perform the surge and heave dynamic experiments.

With regard to yaw, the yaw rate was already being calculated by differentiation of the yaw angle with respect to time. Therefore, differentiating the yaw rate to obtain the yaw acceleration would lead to inaccurate results. Performing the yaw dynamic experiment then, was also impractical.

Although the inertial parameters could not be attained, some estimates were established which will help in their verification when they are determined.

6.3.2.1 Surge and Heave Inertial Parameters

For surge and heave, the rigid body inertial parameter is the mass of the vehicle which has been determined as 35.3kg. Since the added mass parameters range between 10% and 100% of the corresponding rigid body inertial parameters, then it should be expected that the surge and heave added mass parameters, $m_{A,u}$ and $m_{A,w}$, lie between 3.53kg and 35.3kg.

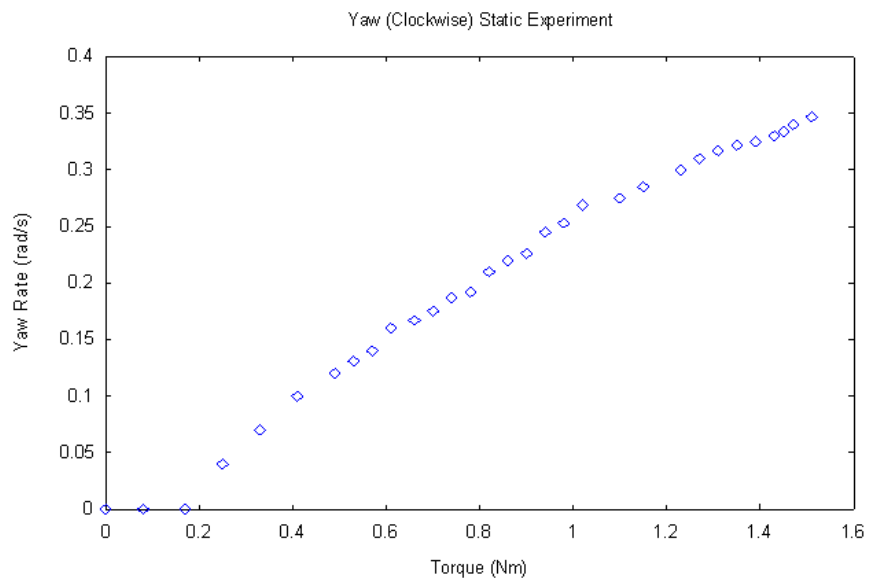


FIGURE 6.12: Positive yaw static experiment results.

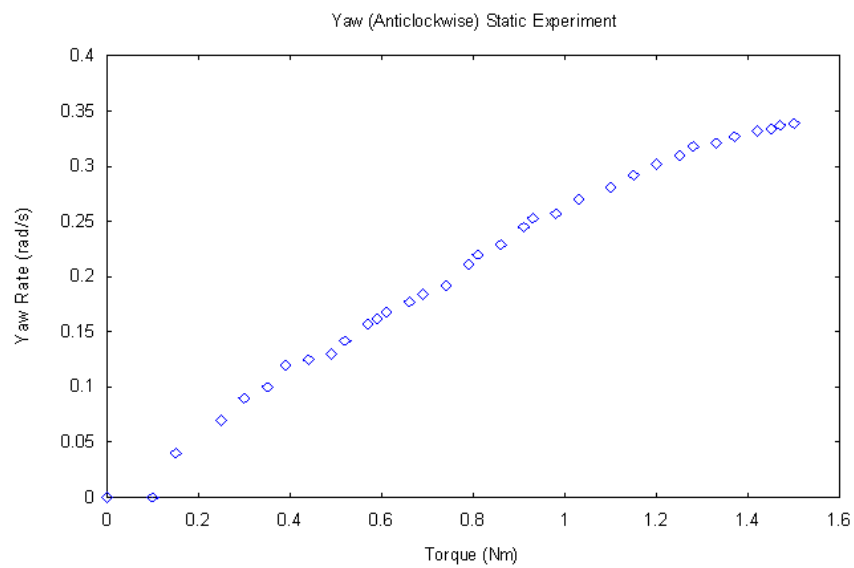


FIGURE 6.13: Negative yaw static experiment results.

6.3.2.2 Yaw Inertial Parameters

The inertial tensor, I_z , for yaw could not be determined due to the composite shape of the vehicle, however, an upper limit on the value can be established by considering an ellipsoid with similar dimensions to the *Mako*.

Imagine an ellipsoid with semi-axes of length a , b and c . The moment of inertia in air for the ellipsoid about the c axis is given as,

$$I_c = \frac{1}{5}M(a^2 + b^2) \quad (6.1)$$

Imagine then that the three axes of the ellipsoid are aligned respectively with the x , y and z axes of the AUV and made the same length. Given that the length of the vehicle's x and y axes are 0.67m and 0.32m respectively, using equation 6.1, an upper bound of 3.9kgm² can be established for the moment of inertia about the z axis in air. Consequently, the added mass parameter for yaw, $M_{A,r}$, will have an upper bound that ranges between 0.39kgm² and 3.9kgm².

6.4 *Mako* Dynamic Model Parameters

Presented below is a table summarising the parameters found or estimated for the relevant degrees of freedom of the *Mako*.

DEGREE OF FREEDOM	RIGID BODY INERTIAL PARAMETER $m_{RB,\xi}$	ADDED MASS PARAMETER $m_{A,\xi}$	GRAVITATIONAL AND BUOYANCY PARAMETER g_ξ	LINEAR DAMPING PARAMETER d_ξ	QUADRATIC DAMPING PARAMETER $d_{\xi \xi }$
<i>Positive Surge</i>	$m_{RB,u}^+$ (kg)	$m_{A,u}^+$ (kg)	g_u^+ (N)	d_u^+ (Ns/m)	$d_{u u}^+$ (Ns ² /m ²)
	35.3	[3.53, 35.3]*	0	16.8	67.7
<i>Negative Surge</i>	$m_{RB,u}^-$ (kg)	$m_{A,u}^-$ (kg)	g_u^- (N)	d_u^- (Ns/m)	$d_{u u}^-$ (Ns ² /m ²)
	35.3	[3.53, 35.3]*	0	–	–
<i>Positive Heave</i>	$m_{RB,w}^+$ (kg)	$m_{A,w}^+$ (kg)	g_w^+ (N)	d_w^+ (Ns/m)	$d_{w w}^+$ (Ns ² /m ²)
	35.3	[3.53, 35.3]*	-15.1	26.0	196.7
<i>Negative Heave</i>	$m_{RB,w}^-$ (kg)	$m_{A,w}^-$ (kg)	g_w^- (N)	d_w^- (Ns/m)	$d_{w w}^-$ (Ns ² /m ²)
	35.3	[3.53, 35.3]*	15.1	–	–
<i>Positive Yaw</i>	$m_{RB,r}^+$ (kgm ²)	$m_{A,r}^+$ (kgm ²)	g_r^+ (N)	d_r^+ (Nms/rad)	$d_{r r}^+$ (Nms ² /rad ²)
	3.9	[0.39, 3.9]*	0	3.4	1.9
<i>Negative Yaw</i>	$m_{RB,r}^-$ (kgm ²)	$m_{A,r}^-$ (kgm ²)	g_r^- (N)	d_r^- (Nms/rad)	$d_{r r}^-$ (Nms ² /rad ²)
	3.9	[0.39, 3.9]*	0	3.2	2.0

* This indicates the range of values that the added mass parameter can attain.

** This value represents an upper bound on the moment of inertia.

TABLE 6.4: Parameters for positive and negative surge, heave and yaw of the *Mako*.

6.5 Summary

The thrust measurements, testing and remote control of the *Mako* have been presented in this chapter. Using the thrust measurements and the remote user interface, the system identification of the vehicle for surge, heave and yaw was undertaken. Although all parameters could not be found due to the shortcomings of the sensor suite, those that were found are used in the control simulation study presented in the following chapter.

Chapter 7

Controller Simulation

Having determined some of the parameters for the *Mako*, it was appropriate then to perform control simulations. The technique of computed torque control is proposed in this chapter for the control system of the vehicle. This technique is relatively simple to implement and has the advantage of making a nonlinear system appear linear. A discussion of how computed torque control is applied to the *Mako* is presented first. A simulation study of the control system is then presented demonstrating that computed torque control does indeed have the ability of controlling the *Mako*.

7.1 Computed Torque Control

Computed torque control is a common technique predominantly used in robotics, particularly for manipulators. The technique allows for the feedback linearisation of a nonlinear system which is very useful in the case of an AUV since its dynamic model is highly nonlinear. By making a nonlinear system appear linear, common and well established linear control techniques such as PID control can then be used in controlling the system.

According to Adams and Rattan [48], the dynamic model for a robot can be expressed as,

$$M(\theta)\ddot{\theta} + N(\theta, \dot{\theta}) = \tau \quad (7.1)$$

where θ is a position state vector, M is a mass and inertia matrix, N is a combined matrix representing the Coriolis, gravitational and friction forces, and τ represents the joint forces and torque vector.

The computed torque control law for equation 7.1 is given as,

$$\tau = \alpha\tau' + \beta \quad (7.2)$$

where α is chosen to be $M(\theta)$ and β as $N(\theta, \dot{\theta})$. An appropriate linear controller for τ' is then chosen. This is the basis of computed torque control.

7.2 Applying Computed Torque Control to the *Mako*

Since equation 7.1 is very similar to the dynamic model of the *Mako*, that is,

$$M\dot{\mathcal{V}} + D(\mathcal{V})\mathcal{V} + G = \mathcal{T} \quad (7.3)$$

then it follows that computed torque control should be able to be applied to the vehicle. Analogous to equation 7.2, the computed torque control law for the *Mako*'s dynamic model is,

$$\mathcal{T} = \alpha\mathcal{T}' + \beta \quad (7.4)$$

where α is chosen to be M and β is chosen as $D(\mathcal{V})\mathcal{V}$.

By choosing an appropriate linear controller for \mathcal{T}' , for instance,

$$\mathcal{T}' = -k_v\mathcal{V} - k_p\mathcal{P} \quad (7.5)$$

then by combining equations 7.3 and 7.4, the following expression is obtained for the system equation,

$$\dot{\mathcal{V}} + k_v\mathcal{V} + k_p\mathcal{P} = 0 \quad (7.6)$$

The parameters, k_v and k_p , are the control gains for the velocity and position state vectors respectively. Equation 7.6 implies the velocity state vector, \mathcal{V} , will reduce to zero which is in fact not very useful if the desired state vector is not a zero vector [8].

7.2.1 PD Tracking Controller

To get around the above problem, Wettergreen et al. [34] made use of desired state vectors and error state vectors to extend the computed torque controller to a tracking controller. By choosing \mathcal{T}' as,

$$\mathcal{T}' = \dot{\mathcal{V}}_d + k_v\dot{\epsilon} + k_p\epsilon \quad (7.7)$$

the computed torque controller is extended to a PD tracking controller where $\dot{\mathcal{V}}_d$ represents the desired acceleration vector, while $\dot{\epsilon}$ and ϵ represent the tracking error vectors for position and velocity respectively.

The error vector for the position state vector is given by,

$$\epsilon = \mathcal{P}_d - \mathcal{P} \quad (7.8)$$

where \mathcal{P}_d represents the desired position vector and \mathcal{P} the current position vector. Note that the position vector not only includes the spatial coordinates, but also the attitude of the vehicle.

The error vector for the velocity state vector is given by,

$$\dot{\epsilon} = \mathcal{V}_d - \mathcal{V} \quad (7.9)$$

where \mathcal{V}_d represents the desired position vector and \mathcal{V} the current position vector. Analogous to the position vector, the velocity vector not only includes the linear velocities, but also the angular velocities.

The error vector for the acceleration can also be defined. It is given as,

$$\ddot{\epsilon} = \dot{\mathcal{V}}_d - \dot{\mathcal{V}} \quad (7.10)$$

The acceleration error vector comes about as a result of combining equations 7.4 and 7.7 with the dynamic model of the *Mako*. The result is a system error equation,

$$\ddot{\epsilon} + k_v \dot{\epsilon} + k_p \epsilon = 0 \quad (7.11)$$

which is used in tracking the position, velocity and acceleration of the AUV for all degrees of freedom. That is, the controller will essentially provide trajectory tracking feedback.

7.2.2 PID Tracking Controller

The linear controller in equation 7.7 works well when the system model is known quite accurately. However, since the system model is usually approximate, the β term in equation 7.4 may not cancel the non-linearity in the system [34]. The use of integral terms in the PD tracking controller can help to minimise the tracking errors.

Integral terms are used for both the position and velocity error vectors. By including these two terms in equation 7.7, the PD tracking controller is extended to a PID tracking controller,

$$\mathcal{T}' = \dot{\mathcal{V}}_d + k_v \dot{\epsilon} + k_{vi} \int \dot{\epsilon} + k_p \epsilon + k_{pi} \int \epsilon \quad (7.12)$$

Equation 7.12 shows that four PID coefficients must be found for the tracking controller. A representation of the PID tracking controller is shown in Figure 7.1.

It is seen in Figure 7.1 that the controller requires a desired position vector, \mathcal{P}_d , a desired velocity vector, \mathcal{V}_d , and a desired acceleration vector, $\dot{\mathcal{V}}_d$, as inputs at any given time. The resulting input forces and torque vector to the AUV is given by,

$$\mathcal{T} = M \left(\dot{\mathcal{V}}_d + k_v \dot{\epsilon} + k_{vi} \int \dot{\epsilon} + k_p \epsilon + k_{pi} \int \epsilon \right) + D(\mathcal{V}) \mathcal{V} + G \quad (7.13)$$

which is a result of combining equations 7.4 and 7.12.

By applying the above forces and torque vector input to the AUV, a position vector and velocity vector is then obtained as an output. The position and velocity state vectors are assumed to be obtained from the vehicle's onboard sensors. The position and velocity are

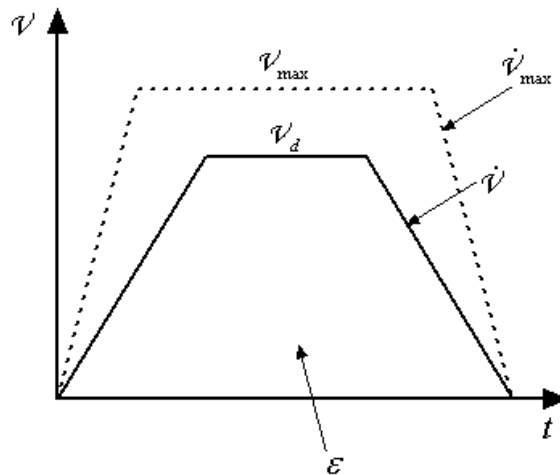


FIGURE 7.2: Velocity profile used for trajectory generation.

7.4 Controller Simulation

The tracking controller in Figure 7.1 was implemented in software. This required the implementation of equations 7.3 and 7.13. The implementation of the kinematics equations of motion presented in Chapter 4 was also required. The parameters for the *Mako* found in Chapter 6 were also used. Furthermore, a trajectory generator was employed to update the desired velocity and acceleration vectors.

7.4.1 Simulator Implementation Issues

Before continuing on with the simulation study, some issues concerning the implementation of the simulator are addressed in this section.

7.4.1.1 Simulating Feedback

The tracking controller assumes position and velocity feedback from the vehicle's onboard sensors. In order to simulate this, theoretical values for position and velocity were computed using the dynamic model and the parameters established for the *Mako*. In reality, the feedback from the vehicle would differ from the theoretical values due to the approximation of the system model and the estimation of the parameters.

7.4.1.2 Degrees of Freedom

Given that it has been established that only surge, heave and yaw for the *Mako* require active control, then the simulation took into account that roll, pitch and sway would not be controlled by the PID tracking controller. This meant that values for the proportional, derivative and integral coefficients for the tracking controller did not have to be found for these degrees of freedom.

7.4.1.3 Model Parameters

Since all the *Mako's* model parameters could not be identified due to the shortcomings of the sensor suite, values were estimated for those parameters that had not been found. The added mass parameters were set at 50% of their corresponding rigid body inertial parameter values. With the negative surge and heave damping parameters not being available, their values were made the same as those for positive surge and heave.

7.4.1.4 Realism

The simulation was made as realistic as possible in the sense that the velocity, acceleration, force and torque values generated were not beyond what the *Mako* is capable of. This allowed a much more realistic analysis to be performed on the PID tracking controller's ability to control the *Mako*.

7.4.1.5 Trajectory Generation

The trajectory generator that was implemented for the simulation is relatively straightforward, using the error in position to determine when to update the desired velocities and accelerations. Whilst the error in position is between 100% and 80%, that is, when the vehicle has not yet travelled 20% of its desired distance, the acceleration is set at a constant value. When the error in position reaches 80%, the desired acceleration becomes zero with a constant desired velocity being set. When the position error reaches 20%, that is, when the vehicle has travelled 80% of the total distance, a constant desired deceleration is set.

Since each degree of freedom has different maximum velocities and accelerations due to the configuration of the vehicle, different maximum velocities and accelerations for the trajectory generator were set for surge, heave and yaw according to what was observed in the system identification results. In essence, a different trajectory generator was used for each degree of freedom.

7.4.2 Simulation Study

The simulation results obtained from the implemented PID tracking controller are presented in this section. Several simulations were performed involving various manoeuvres.

The simulation results presented here involve manoeuvring the *Mako* to a heading of 180 degrees and then moving forward 5m and down 3m. That is, the *Mako's* initial position was set at,

$$\mathcal{P} = \left[0 \ 0 \ 0 \ 0 \ 0 \ 0 \right]^T$$

and the final position was,

$$\mathcal{P} = \begin{bmatrix} -5 & 0 & 3 & 0 & 0 & \pi \end{bmatrix}^T$$

Note that the position of the vehicle is expressed in terms of the world frame, $\{W\}$. Expressing the position in terms of the body frame is impractical as a zero vector would always be obtained. This is because the frame always remains static with respect to the vehicle.

The PID coefficients chosen for the simulation were as follows,

$$k_p = \begin{bmatrix} 0.02 & 0 & 1.5 & 0 & 0 & 0.1 \end{bmatrix}$$

$$k_v = \begin{bmatrix} 0.05 & 0 & 2.0 & 0 & 0 & 0.5 \end{bmatrix}$$

$$k_{pi} = \begin{bmatrix} 0.25 & 0 & 1.5 & 0 & 0 & 0.4 \end{bmatrix}$$

$$k_{vi} = \begin{bmatrix} 0.02 & 0 & 0.8 & 0 & 0 & 0.25 \end{bmatrix}$$

Note that the coefficients for sway, roll and pitch have all been set to zero.

The response of the simulated controller is shown in Figures 7.3 to 7.5. Figure 7.3 shows the velocity with respect to the vehicle's frame while Figure 7.4 shows the vehicle position with respect to the world frame. Figure 7.5 shows the thrust outputs for each of the four motors.

7.5 Analysis of Simulation

From the simulation results, the *Mako* aligns itself according to its desired heading, and then proceeds to move forward and downward at the same time. Since the degrees of freedom on the *Mako* are decoupled to a good approximation, then it is possible for both surge and heave to be controlled at the same time without affecting each other.

7.5.1 Overshoot

From the velocity graphs, it is clear that there exists slight overshoot. However, the velocity definitely remains within attainable values. Figure 7.4 on the other hand, shows that there is little overshoot with regard to position. This is a highly desirable feature as the AUV should not be required to use its thrusters in reverse to backtrack a large distance to its desired position. Having to do so would mean using up valuable time.

Figure 7.6 shows the overshoot caused by using different PID coefficients in the tracking controller. As can be seen, the blue line exhibits the most desired trajectory with regard to position as the vehicle does not overshoot and consequently does not need to significantly reverse its direction of motion to achieve the desired position. The red line shows a highly

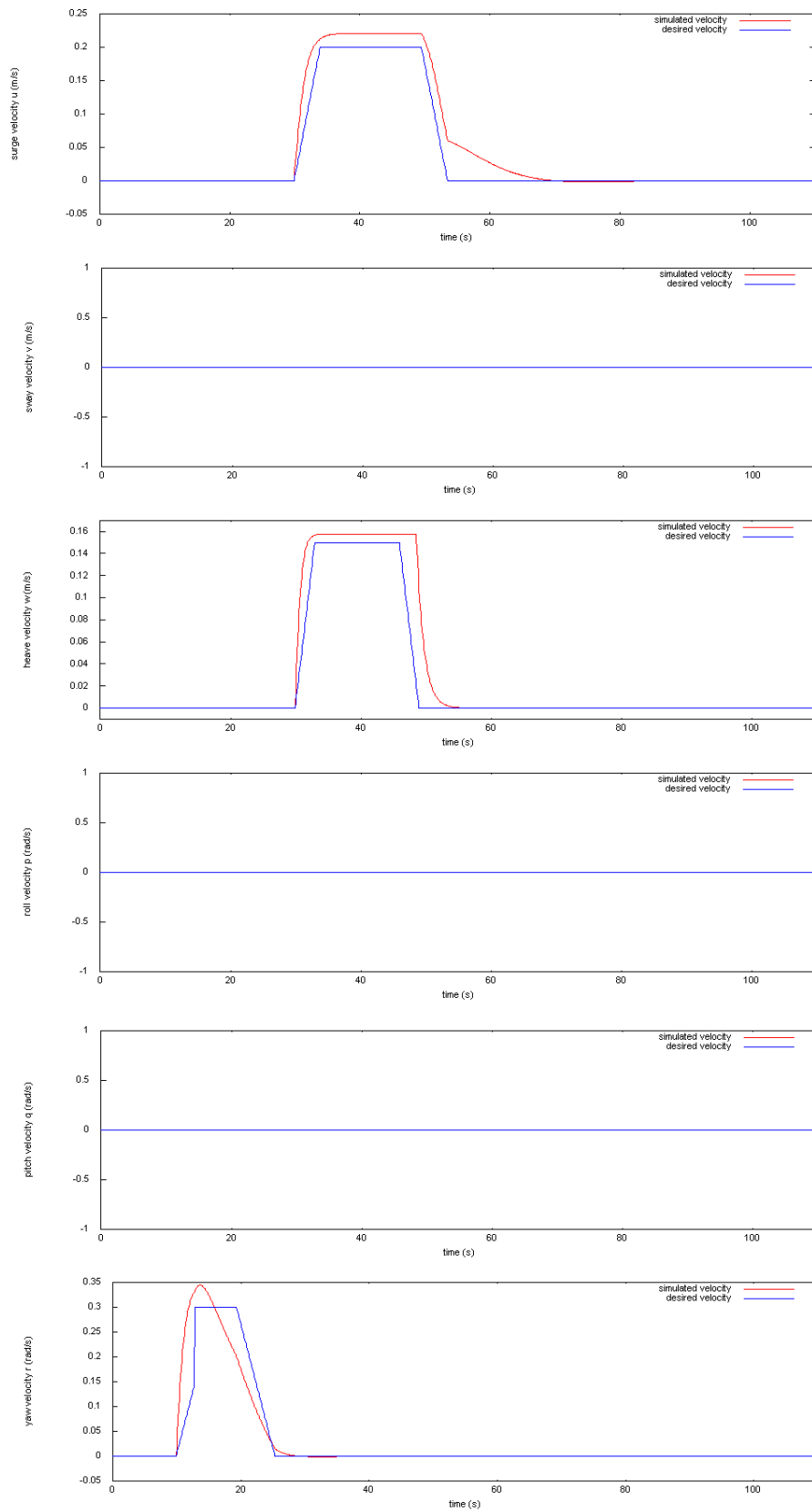


FIGURE 7.3: Simulation results for the velocity for all degrees of freedom.

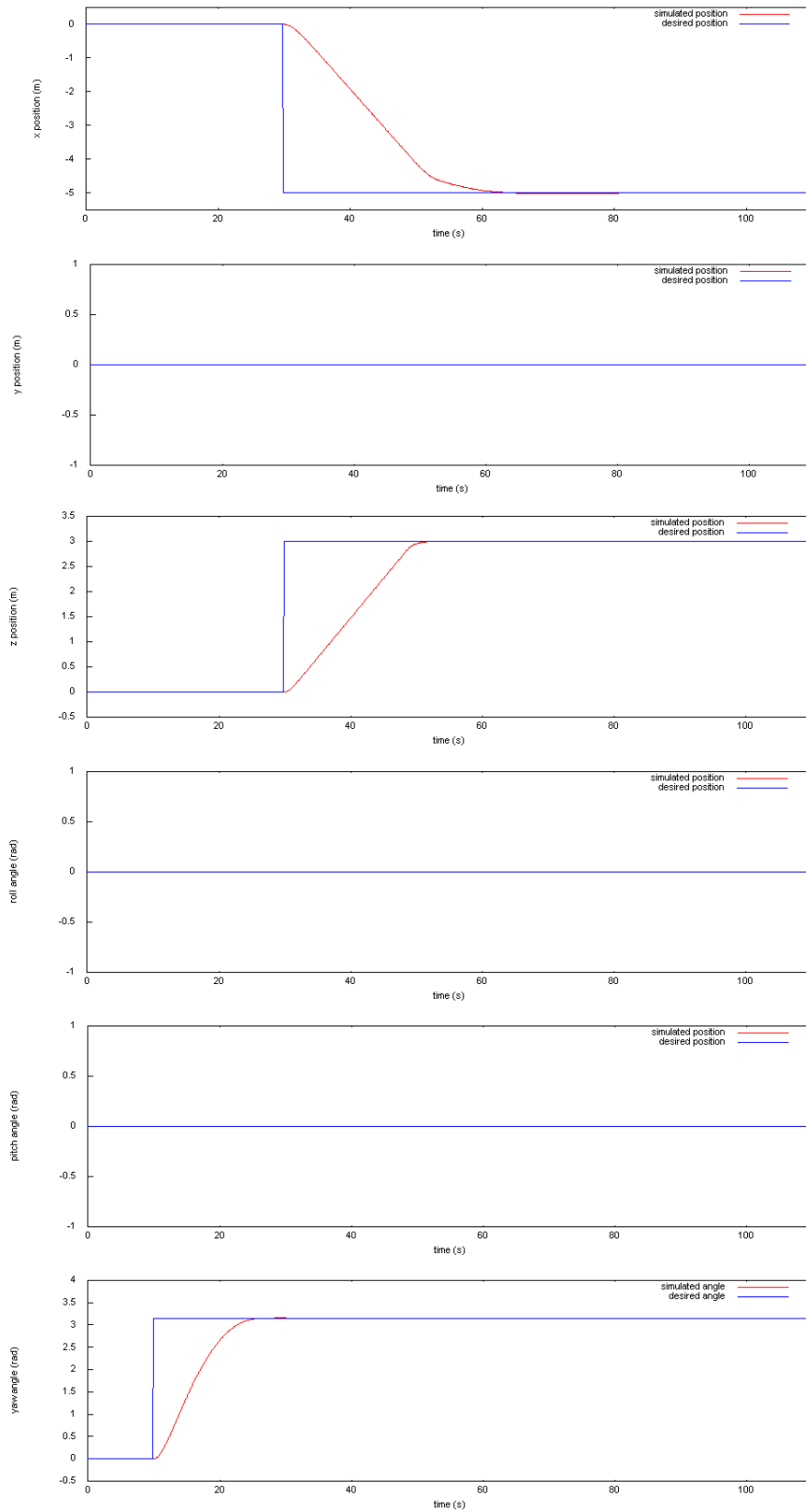


FIGURE 7.4: Simulation results for the position for all degrees of freedom.

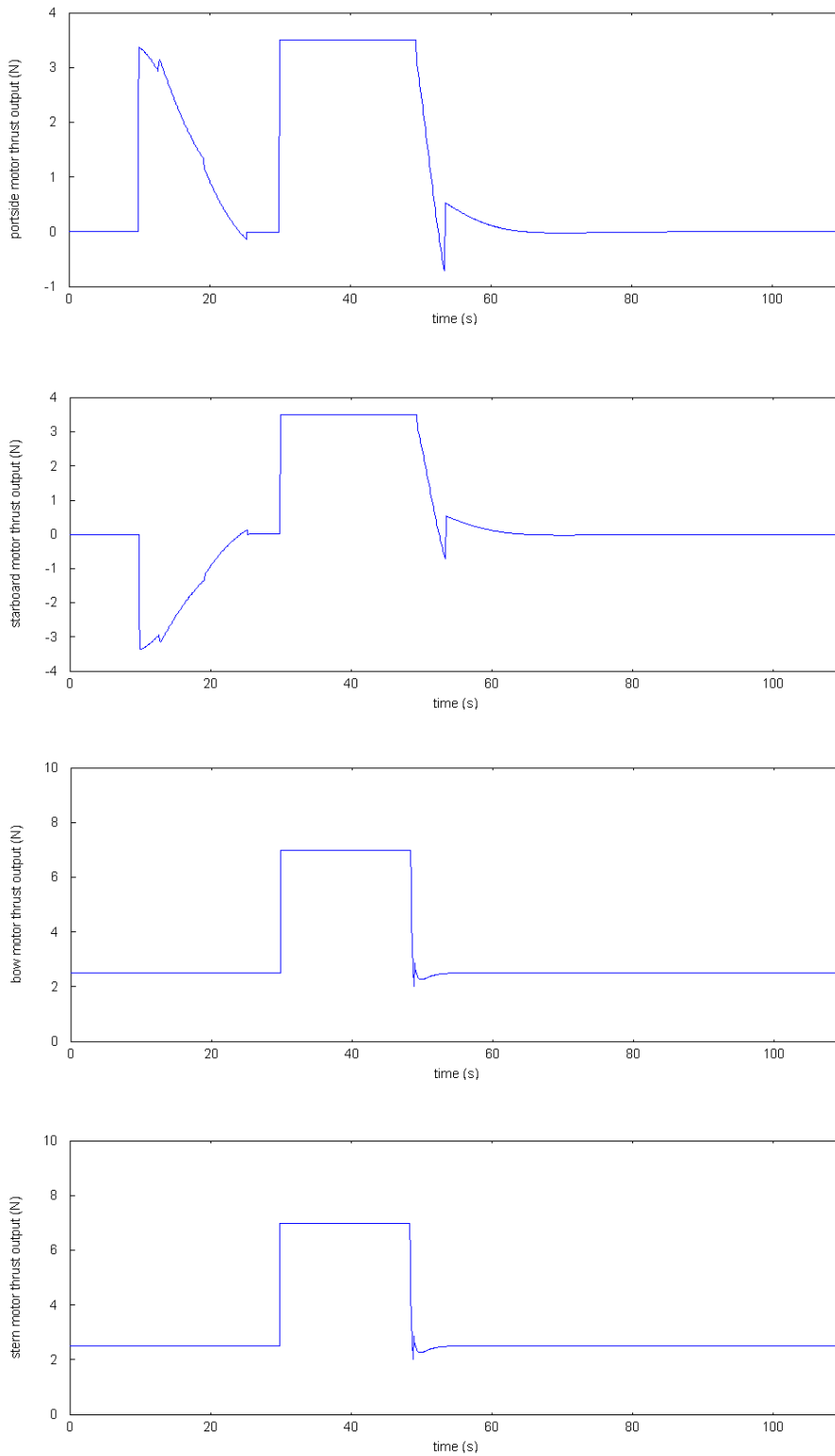


FIGURE 7.5: Simulation results for thrust outputs of the four motors.

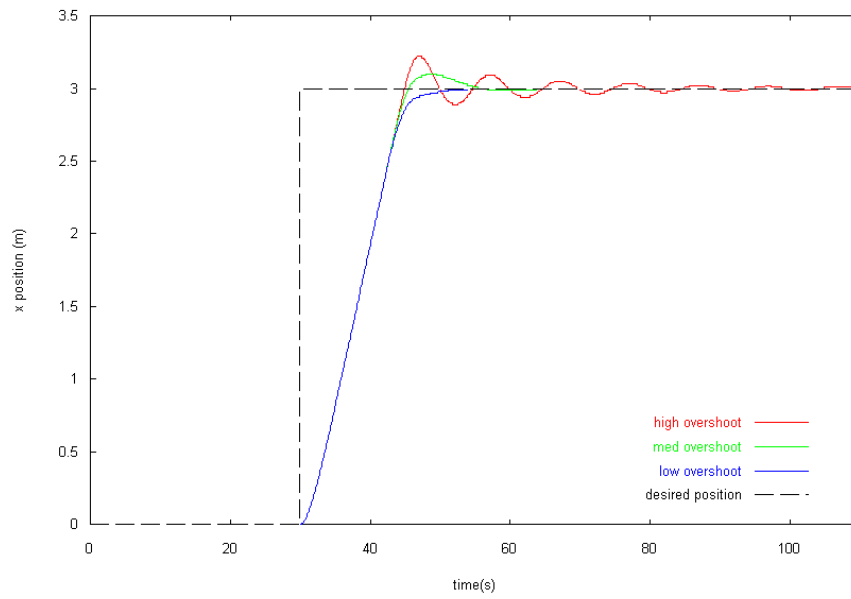


FIGURE 7.6: Varying degrees of overshoot for position.

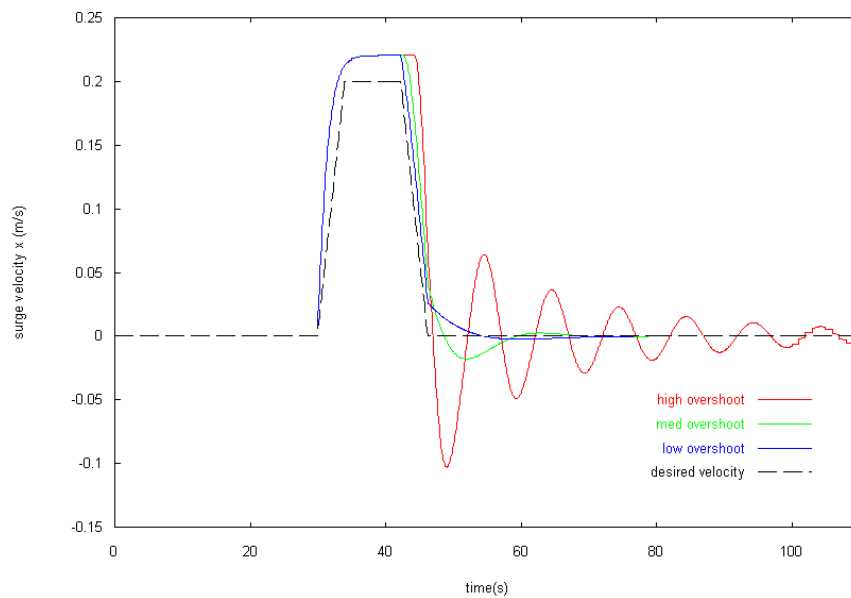


FIGURE 7.7: Varying degrees of overshoot for velocity.

undesirable trajectory with high overshoot which also results in oscillations in the velocity as seen in Figure 7.7.

Appropriate PID coefficients must therefore be chosen in order to minimise overshoot and the time required for the vehicle to achieve its desired position.

7.5.2 Thrust Output

The thrust outputs for the portside and starboard motors are seen to be the same except for the fact that for the starboard motor, the thrust output is negative when the vehicle is aligning itself with its desired heading. Since a moment needs to be generated to rotate the vehicle about the z axis, one motor needs to be set to reverse and the other to forward mode.

For the bow and stern motor graphs, the thrust outputs are the same, indicative of the symmetrical nature of the vehicle. What is also noticeable in these graphs is that the beginning and ending thrust output is 2.5N. This suggests that the effective buoyancy, or equivalently the total thrust needed to keep the vehicle submerged, is 5N as opposed to the 15.1N that was determined for the *Mako*. This is because the effective buoyancy was lowered in the simulation to provide a faster heave response time for the vehicle. In reality, ballast would be added to the *Mako* in order to lower the residual buoyancy as much as possible.

The spikes present in the thrust output graphs signify that the motor directions are reversed within a short amount of time. For instance, when surge is being controlled by the horizontal motors, upon nearing the desired position of 5m, these two motors are quickly set to reverse mode and then set to forward mode again with the thrust decreasing over time to zero. This sequence of events helps to slow down and stabilise the vehicle to its desired position. A parallel can be drawn with satellites, which use a similar succession of thrust outputs to stabilise their orbits.

7.5.3 Final Remark

The results of the simulation do indeed seem to indicate that with an appropriate set of PID coefficients, computed torque control extended to a PID tracking controller could be used on the *Mako*. For all degrees of freedom, velocity and position overshoot is kept to a minimum with velocity and thrust output values well within the capabilities of the *Mako*. There are, however, some limitations to the simulation; the effects of which can only really be accurately observed by implementing and testing the controller on the *Mako*.

7.6 Limitations of Simulation

The limitations of the simulation and their potential effects on the control of the vehicle are discussed in this section.

7.6.1 Thrust Output

From the thrust output graphs in Figure 7.5, it is evident that the simulation assumes that thrust can be generated instantaneously. This is of course not true in reality as it requires time to produce the required thrust. This should have an overall minor effect on the simulation results apart from an increased response time.

The thrust output graphs also show a continuous change in thrust from the motors. The motors on the *Mako* can only be set at discrete speed settings corresponding to discrete thrust values. The result would be that the tracking controller on the *Mako* might not be able to achieve as smooth a response as indicated in the simulations.

7.6.2 Heading Drift

During surge manoeuvres, the thrust output graphs in the simulations indicated that the forces required from the two horizontal motors were exactly the same at any instant in time. In reality, the vehicle's heading would drift over time since the forces applied would not be exactly the same. On top of this the vehicle is not exactly symmetrical.

Therefore, in order for heading to be maintained, the yaw PID tracking controller would have to be used simultaneously with the surge controller. The simultaneous use of these two controllers was avoided in the simulation, however, the implementation of the tracking controller on the *Mako* would have to take this into account

7.6.3 Position

As previously mentioned, the position of the vehicle with respect to the world frame must be known in order to use the PID tracking controller. In the simulation, theoretical values were used. However, in real life the vehicle can only rely on its onboard sensors for feedback as to where it currently is.

The attitude of the vehicle can be easily determined by sensors and then converted to world coordinates, however, the linear position of the vehicle cannot be easily discerned. Finding the linear position requires state estimation. Over time, however, the actual and estimated position values will drift apart mainly due to sensor errors. Nevertheless, if the PID tracking controller is to be implemented on the *Mako*, a state estimator is a necessity.

7.7 Controller Implementation

Due to the shortcomings in the sensor suite, implementing the PID tracking controller on the *Mako* was not possible. However, the simulations performed provided an insight into the performance of the controller and presented encouraging results for the future implementation on the *Mako*.

The block diagram in Figure 7.8 demonstrates how the controller would function given an appropriate sensor suite. Indeed, this block diagram except for the sensor suite block

is representative of what was used in the simulation.

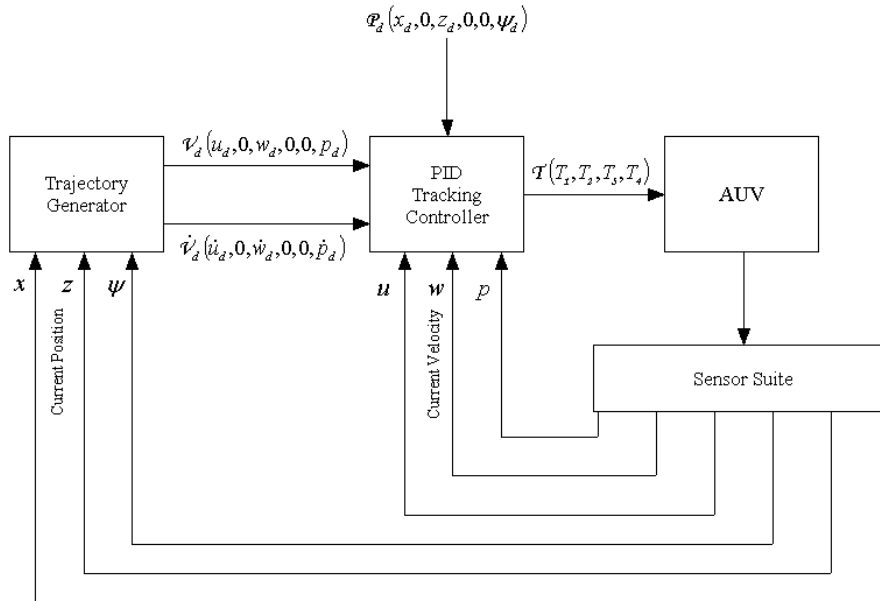


FIGURE 7.8: Block diagram of control system for the *Mako*.

The sensor suite is responsible for feeding back current position and velocity values to the trajectory generator and tracking controller respectively. The trajectory generator is then used to calculate desired velocities and accelerations for the tracking controller. The tracking controller then outputs a thrust value to the motors. The overall input to the system is the desired position of the vehicle.

For the sensor suite, velocity feedback sensors are required for surge, heave and yaw. For the position of the vehicle, position feedback sensors are required for the x and z positions, and for yaw.

With regard to the x axis, position cannot easily be determined by a sensor. Although position sensing sensors could theoretically be used against walls, in an underwater environment surrounding walls are usually quite distant. Therefore, keeping track of the position along the x axis can be very difficult. Determining the surge of the vehicle on the other hand is a simple matter of using a velocimeter positioned along the x axis. The velocity readings can then be integrated with respect to time to find the position which is essentially the state estimation of the vehicle's longitudinal position.

Unlike the x axis, finding the current position along the z axis is much simpler as a pressure sensor can be used to keep track of vertical displacement. State estimation is still required to reduce errors. As with surge, to obtain the current heave velocity, a velocimeter positioned along the z axis of the vehicle can be used.

The determination of the yaw angle and yaw velocity can be accomplished through the use of a magnetic compass. Although, the yaw velocity can be determined indirectly by differentiating the yaw angle with respect to time, it is much more desirable to have a direct form of sensor feedback for this reading. A gyro positioned correctly on the vehicle

can be used to give the yaw velocity.

Although the *Mako*'s magnetic compass is fairly accurate and adequate for obtaining the yaw angle, the velocity sensor and depth sensor are not accurate enough for obtaining the surge velocity and position along the z axis respectively. Furthermore, sensors for heave and yaw velocity are lacking. The sensor suite on the *Mako* needs to be upgraded if the tracking controller is to be implemented.

7.8 Summary

A PID tracking controller extended from computed torque control has been identified and proposed for the control system of the *Mako*. The tracking controller is simple to implement, but requires a trajectory generator. A simple trapezoidal trajectory generator was identified which allows velocity and acceleration updates to be passed to the controller. The tracking controller was simulated in software using the dynamic model of the *Mako* obtained in previous chapters. The simulation shows promising results for the PID tracking controller's eventual implementation on the *Mako*.

Chapter 8

Conclusion

The design, development, system modelling and simulated control of an autonomous underwater vehicle named the *Mako*, has been presented in this thesis. The *Mako* was developed specifically for entering the International Autonomous Underwater Vehicle Competition.

The first phase of this thesis involved the design and construction of the vehicle which took place over a period of half a year. The second phase involved the modelling, system identification and control simulations for the future autonomous control of the vehicle. The culmination of these two phases has resulted in a functioning underwater vehicle that has undergone modelling, system identification and preliminary control analysis.

8.1 Contributions of the Thesis

The following contributions were made in this thesis:

- Design and development of the mechanical system of an AUV that:
 - Provides a dry, watertight hull that facilitates the housing of onboard electronic components and that is capable of surviving in a saltwater environment
 - Provides a statically and dynamically stable vehicle with suitable versatility in its motion to accomplish a wide range of tasks
 - Possesses the ability to be modular and extensible for future missions
- Design and development of the electrical system of an AUV that:
 - Provides for motion control
 - Provides for sonar and vision processing
 - Measures the vehicle's depth
 - Discerns the vehicle's attitude
 - Measures the vehicle's surge velocity

- Detects hull breaches and power shortage
- Supplies sufficient power for ample testing periods

- Integration of sub-systems for a functioning AUV that adheres to IAUVC rules and regulations
- Simplification of the dynamic modelling of the *Mako*
- Thrust output measurements for each motor
- Control of the *Mako* via remote means
- System identification of the vehicle parameters for surge, heave and yaw
- Identification and simulations of a PID tracking controller for the control system of the *Mako*

8.2 Discussion on Outcomes

A discussion on the contributions and outcomes accomplished in this thesis are presented in this section.

8.2.1 Mechanical System

A versatile, modular and durable mechanical system has been designed and developed for the *Mako* with simplicity and symmetry being two prime aspects sought in the design. Comprising of an aluminium frame and two hulls, the mechanical configuration provides a platform conducive to the further development of the vehicle.

The two horizontal and two vertical motors that provide propulsion allow the vehicle to actively control four degrees of freedom in a straightforward and decoupled manner. The separation of the centres of buoyancy and gravity in the design has contributed to a metacentric righting moment that keeps the vehicle very stable during manoeuvres.

Furthermore, the structure of the *Mako's* frame allows external components to be easily attached, thus contributing to modularity and extensibility which will be advantageous in adapting the vehicle to different future missions.

8.2.2 Electrical System

The design and development of the electrical system has resulted in a system with great potential in autonomously controlling the *Mako*. The electrical system consists of an Eyebot controller, an array of sensors, a power system, a vision system, a sonar system and a temporary communications system.

The Eyebot controller provides a versatile platform from which control of the vehicle can easily be achieved. The Eyebot also plays a central role by interfacing with all sub-systems and maintaining top-level control. There is great potential in what the Eyebot can provide for the *Mako* in terms of functionality in future years.

8.2.3 Subsystems

Components for the vision, sonar and communications projects were successfully integrated into the vehicle. The vision system provides for image processing, the sonar system provides for navigation, and the communications system allows testing to occur much more efficiently.

The vision system consists of a mini PC and camera which were incorporated into the electrical and mechanical systems. The PC was linked to the Eyebot and the camera was attached externally on the vehicle's frame. The sonar system consisted of two echo sounders that were mounted to the frame and connected to onboard circuitry.

As a temporary solution to the communications system, Bluetooth and infrared devices were used for downloading and uploading data to the vehicle. This avoided the need to recover the vehicle from the water every time communication with the onboard controllers was required.

8.2.4 Simplification of the Dynamic Model

A dynamic model was identified for use in controlling the *Mako*. The dynamic model, however, was found to be very complex and determination of many of the parameters would be a very difficult and time consuming process. On top of this, highly complex and expensive equipment would be required to perform the necessary system identification.

In order to minimise the number of parameters that would need to be identified and hence, simplify overall modelling, several assertions were made on the dynamics of the *Mako*. The nature of the mechanical structure of the vehicle such as symmetry and stability, allowed for these assertions to be made.

The dynamic model of the *Mako* was broken down to a simpler model that only required the surge, heave and yaw parameters to be found. This allowed the system identification process to be less difficult and time consuming.

8.2.5 Thrust Measurement

The thrust output for each motor at all attainable speed settings was measured. It was shown through this that each motor had slightly different characteristics which would have to be taken into account in order to successfully control the vehicle. The thrust output values of the motors also allowed for parameters to be computed in the system identification process. The results of the thrust measurement will prove extremely useful in the eventual autonomous control of the *Mako*.

8.2.6 Remote Control

Software was written in order to remotely control the *Mako* using Bluetooth via a computer. A user interface was developed in conjunction with the communications project to initiate manoeuvres and to control each motor individually. The remote control of the vehicle not only provided a means of demonstrating the *Mako's* manoeuvring capabilities, but also assisted significantly in the system identification experiments.

8.2.7 System Identification

A system identification process was identified which exploited the characteristic of a low-speed underwater vehicle in order to assume decoupling between the degrees of freedom. By treating each degree of freedom separately, parameters could be found using onboard sensors with relative ease.

Using a series of experiments, damping parameters were found for positive surge, heave and yaw of the *Mako*. Negative yaw damping parameters were also found, however, negative surge and heave parameters could not be identified due to the low resolution of the vehicle's velocity sensor.

The shortcomings of the sensor suite on board the *Mako* prevented the inertial parameters to be found for surge, heave and yaw. Approximations and limits were instead established for these parameters so that their values can be validated in the future when they are identified.

The system identification process used is easily repeatable, which makes it suited for identifying the *Mako's* parameters since the vehicle will be continually subjected to modifications and additions that change its dynamics.

8.2.8 Control System Simulation

Computed torque control was identified as a control technique for controlling the *Mako*. By extending computed torque control to a PID tracking controller, a much more versatile controller was created. Control simulations were performed on the tracking controller using the dynamic model and parameters found for the *Mako*. The simulations had notable limitations, however, they did demonstrate that there was indeed potential for computed torque control to be used in controlling the *Mako*. Although there was overshoot with regard to velocity, by choosing appropriate PID coefficients, while still staying within the actual physical capabilities of the *Mako*, position overshoot was made to be minimal.

8.3 Recommendations and Future Work

This section presents suggestions for further work and research, as well as what is required for the *Mako* if it is to be successful for subsequent years' underwater competitions.

8.3.1 Mechanical System

There is an opportunity to make the mechanical structure of the *Mako* more hydrodynamic by fabricating coverings for the body. Although speed and sleekness are not necessary requirements for the vehicle, increasing the hydrodynamics would increase the velocity, thereby decreasing overall power consumption and increasing efficiency.

8.3.2 Electrical System

The electrical system must be able to cope with the addition of components and sensors in the future. Since the Eyebot is currently handling input and output to most sensors, with most of its ports in use, it is suggested that a second Eyebot controller be installed in the *Mako*. Not only would this second microcontroller be able to handle a numerous number of sensors, it will also be able to run programs concurrently with the other Eyebot, thereby increasing the computational capability of the *Mako*.

To cope with more electronic components, it is also suggested that the lead acid batteries that are currently used for power be upgraded with lithium ion batteries in the future. Not only are lithium ion batteries longer lasting and reliable, but they are also lighter.

8.3.3 Sensors

Several sensors are required for the *Mako* if it is to be successfully controlled. Velocimeters with a relatively high resolution are required as the current velocity sensor's resolution is too low. Velocimeters will greatly aid in system identification, as well as in accurately controlling the vehicle.

A pressure sensor is also required for keeping track of the vehicle's z position. Currently an echo sounder can be used to determine the depth of the vehicle, but only if the depth of the water is known beforehand. On top of this, the resolution of the echo sounder is much too low to enable accurate depth control.

A gyroscope for determining the yaw velocity is also recommended. Although the yaw velocity can be indirectly computed by differentiation of the yaw angle, to enable control to be much more accurate, a direct sensor reading is required.

It is also recommended that accelerometers be obtained so that the system identification of the vehicle can be performed accurately for the inertial parameters.

When a suitable sensor suite has been attained, state estimation software should be developed in order to provide state position and velocity values to the control system. The state estimator is useful in filtering sensor values, modelling noise and determining sensitivity. Its implementation would greatly benefit in accurately controlling the *Mako*.

8.3.4 System Identification

With the attainment of more sensors, the system identification process should be performed for the remaining parameters that could not be identified during the course of this

thesis due to the shortcomings of the sensor suite. If at any time significant modifications and additions are made to the vehicle, then the system identification experiments should be repeated for surge, heave and yaw.

8.3.5 Communications System

To reduce the difficulty and time required in testing the vehicle, a communications system that obtains real-time feedback from onboard components is required. This system should be able to transmit and receive data, as well as change parameters for the vehicle during its underwater testing. An interface should also be developed for the communications system that displays real-time motor, sensor and controller data.

8.3.6 Control System

A control system for controlling the surge, heave and yaw degrees of freedom is required to make the *Mako* autonomous. It is suggested that a PID tracking controller, based on computed torque control, be tested and used for the *Mako's* control system due to its relatively straightforward implementation and promising results obtained in the simulations. However, before its implementation on the vehicle, the identification of the remaining model parameters must be accomplished.

8.4 Final Word

The groundwork has indeed been laid for UWA's entry into the underwater competition for future years with the *Mako*. The majority of future work on the vehicle will lie in implementing a superior sensor suite, implementing an autonomous control system, and further developing the subsystems.

Appendix A

IAUVC Rules and Mission 2004

A summary of the 7th annual International Autonomous Underwater Vehicle Competition main rules and mission as per [49] is presented below.

A.1 Mission

“The fundamental goal of the mission is for an AUV to demonstrate its autonomy by locating a target on the floor of the arena (Figure A.1) and depositing one or two small markers onto the target, proceeding to a recovery zone, and surfacing inside the recovery zone” [49].

A.1.1 Breakdown of Mission

- Each vehicle will have 5 minutes of preparation time and 15 minutes to complete its task once in the water
- The vehicle will be deployed from a launch point
- The vehicle must then pass through a validation gate. If the vehicle breaches the surface, the vehicle’s mission run is declared over
- The vehicle must then locate a target and deploy a maximum of 2 markers onto it
- Having completed this, the vehicle will then proceed to a recovery zone. This zone will have a pinger from which the vehicle will be able to use sonar in order to detect it
- Upon reaching the recovery zone, the vehicle will surface in order to be recovered
- Points are awarded according to different criteria, the main emphasis being placed on the success of the vehicle’s performance in the mission

A.1.2 Size and Weight Constraints

- The vehicle must have a maximum total rectangular volume of 1.8m long, 0.9m wide and 0.9m high
- The vehicle must have total dry mass of no more than 63.5kg. A mass of less than 50kg earns some points, while a mass of less than 32kg earns even more

A.1.3 Other Restrictions

- All vehicles must operate autonomously. No communication, control or guidance is allowed via a person or off-board computer (including GPS)
- Vehicles must be powered via onboard sealed batteries
- Vehicles must be buoyant by at least 0.5% of their mass
- Only compressed air for ballast tanks and markers may be released by the vehicle into the water
- Vehicles must have a clearly labelled switch that disconnects all propulsion and other devices from the batteries

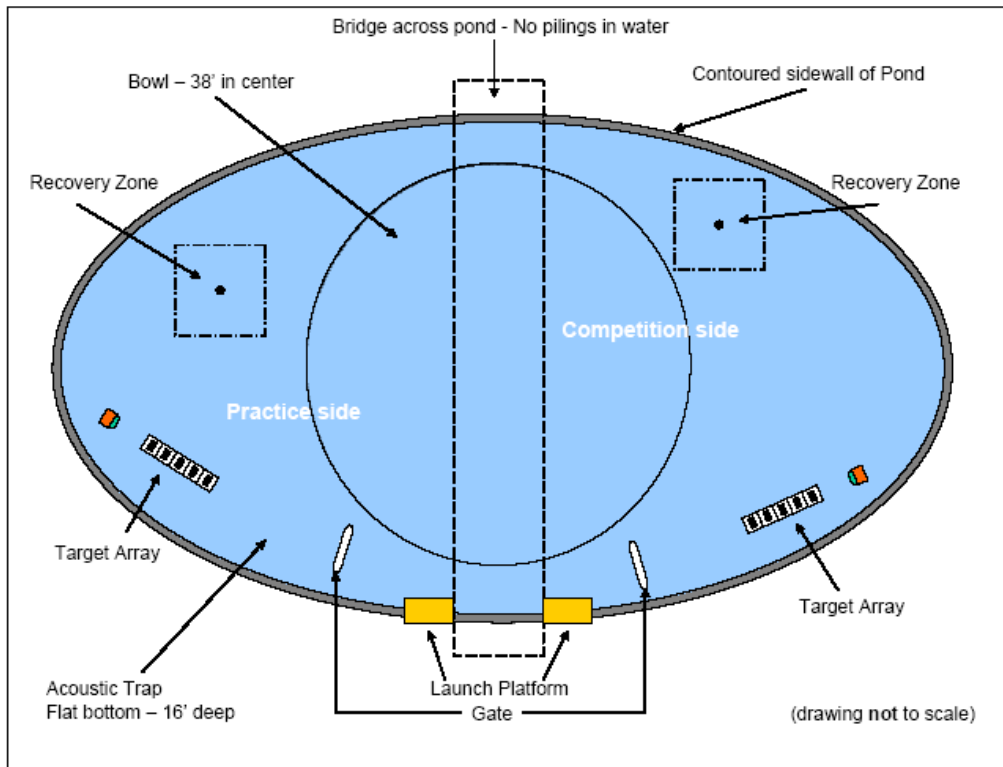


FIGURE A.1: Layout of the arena in which the mission takes place [49].

A.2 Placement of Elements in the Arena

The launch point, validation gate, and target are situated along a relatively straight line as shown in Figure A.1. The recovery zone is some distance away from the target on a new bearing.

A.2.1 Validation Gate

The validation gate (Figure A.2) is made of white PVC tubing. It is 10ft wide and 6ft tall. It is buoyant and anchored to the bottom of the arena.

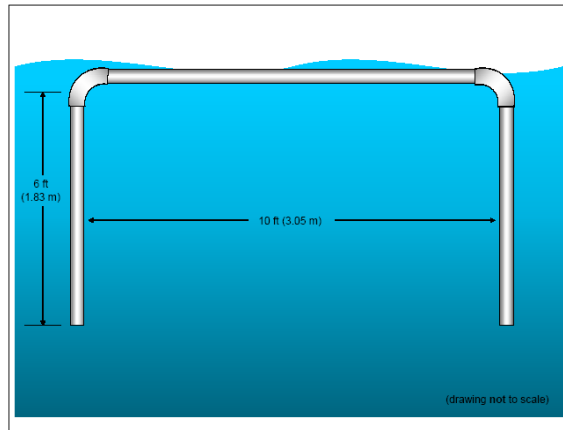


FIGURE A.2: The validation gate dimensions [49].

A.2.2 Target

The target (Figure A.3) consists of a tray containing a row of 5 bins. At one end of the tray, there is an indicator lamp pointing horizontally utilising 60 LEDs. Each bin has a different score value and is $12'' \times 24'' \times 6''$ in dimension. The bin closest to the lamp is worth the most points.

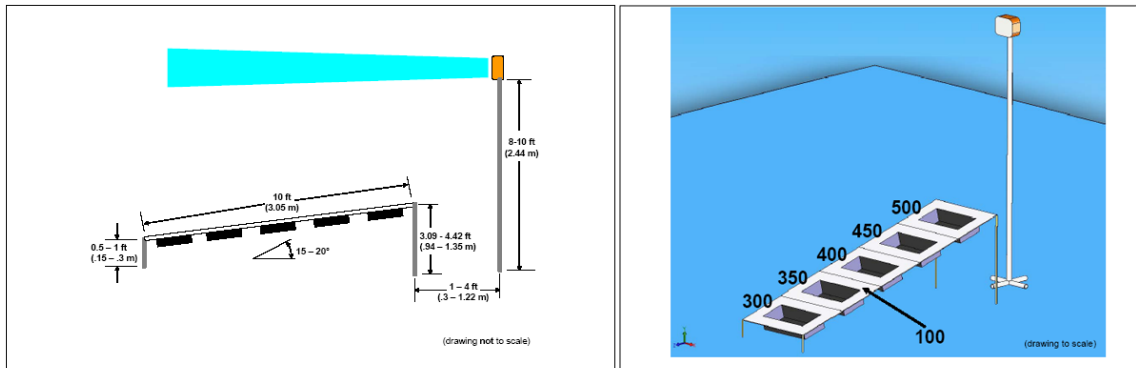


FIGURE A.3: Target and lamp layout [49].

A.2.3 Markers

A vehicle may carry no more than 2 markers. Each marker must fit in a box 1.5" square and 6" long (3.81cm \times 3.81cm \times 15.24cm). Each must weigh less than 1.5lbs (0.68kg) in air.

A.2.4 Pinger

The pinger is situated in the centre of the recovery zone and will be set at a frequency between 22-30 kHz.

A.2.5 Recovery Zone

The recovery zone (Figure A.4) is square with a side length of approximately 20 ft. Floating lines mark the boundaries of the recovery zone.

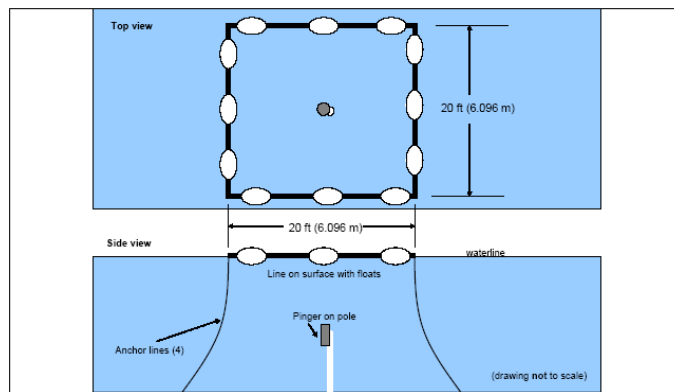


FIGURE A.4: The recovery zone layout [49].

Appendix B

Electronic Components

Thorough research and scouting for components and parts was undertaken very early on in the project. Components were sought from both local and online businesses. Only the most crucial and essential components were acquired. Other components were either built or innovative solutions were found for their absence.

B.1 Thrusters

The thrusters chosen were four Sevylor 12V electric outboard trolling motors (Figure B.1). These trolling motors are conventionally used for small dinghies. They are the smallest trolling motors available on the market. The fact that each motor was already waterproof reduced construction complexity immensely. Each motor was removed from their respective mounts as this was the only part required.

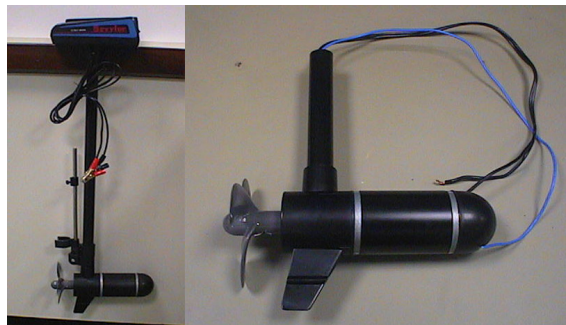


FIGURE B.1: (Left) Sevylor trolling motor. (Right) Motor separated from its mount.

B.2 Batteries

Two 12Ah, 12V Drypower batteries and one 7Ah, 12V AUSCell battery (Figure B.2) were decided upon to supply onboard power to the AUV. Combined, these batteries supply about 31Ah, more than sufficient for the power requirements of all onboard electronic components. Each 12Ah battery has a mass of 4 kg and dimensions of 9.6cm \times 15.0cm \times

10.0cm while the 7Ah battery has a mass of 2.5kg and dimensions of 6.1cm \times 15.0cm \times 10.0cm.



FIGURE B.2: The three batteries lined up together.

B.3 Computer/Microcontroller

Control of different functions on the AUV was decided to be separated and assigned to two different controllers. Movement and direct control of the vehicle is controlled by a microcontroller called a Mark IV Eyebot controller (Figure B.3). Image processing is performed by a Cyrix mini PC running Linux. The need for greater processing power in vision was the main reason for the use of the mini PC.



FIGURE B.3: (Left) Eyebot microcontroller. (Right) Cyrix mini PC .

The Mark IV Eyebot controller was developed at UWA and is the main controller used for robots in the Electrical, Electronic and Computer Engineering department. The Eyebot is developed around the Motorola 68332 32-bit controller. It runs at 33MHz and comprises 512KB flash ROM, as well as 2048KB RAM. Consisting of three serial ports, one parallel port, 16 digital inputs/outputs, 8 analog inputs and 16 I/O ports, the Eyebot is truly a compact yet versatile microcontroller. Both assembly language and C/C++ can be used to create programs for this controller.

The mini PC comprises a Cyrix processor running at 233MHz, 32MB of RAM, as well as a 5GB hard drive. Featuring many characteristics and ports akin to a standard PC, the mini PC provides more than enough functionality for image processing.

B.4 Digital Magnetic Compass

A low-cost Vector 2X digital magnetic compass module (Figure B.4) was chosen to provide yaw or heading control. The compass has an accuracy of 2° and is $1.50'' \times 1.30'' \times 0.39''$ in dimension. The small module requires very little power, running off a 5V source.

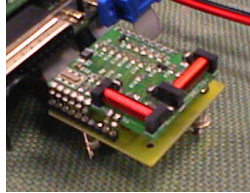


FIGURE B.4: Digital magnetic compass.

B.5 Echo Sounder

An echo sounder (Figure B.5) was used to improvise as a depth sensor. The echo sounder is a Navman Depth 2100 transducer and has a resolution of 10cm. The transducer has a range of 0.6m to over 90m. The echo sounder's beam width is 15° .



FIGURE B.5: Echo sounder.

B.6 Velocity Sensor

The velocity sensor (Figure B.6) is a Navman Speed 2100 transducer that is capable of measuring the velocity of the vehicle to a resolution of 5cm/s via a paddle wheel. It is uni-directional and hence, can only discern the velocity for one degree of freedom at any time.



FIGURE B.6: Velocity sensor.

Appendix C

Design Concepts

After thorough research and analysis of AUV designs, several designs were conceptualised for the *Mako*. Each design concept had its own unique features and varying advantages and disadvantages. Four of the more feasible and physically realisable designs are detailed in this section.

C.1 Torpedo Shape

The torpedo like structure of the design in Figure C.1 provides a sleek, hydrodynamic form that houses components in a high structural integrity, cylindrical hull. Power consumption would be kept to a minimum due to the use of only one motor situated on the stern. Steering would be controlled by a rudder while bow planes and ballast tanks would control depth. Ballast tanks would involve comprising tanks, pumps and compressed air onboard.

Maintenance, inspection and addition of components would be inhibited due to the limited space available. The need for servo-controlled rudders and bow planes would require through-hull connections capable of allowing rotational movement, thus introducing added complexity in ensuring watertight integrity.

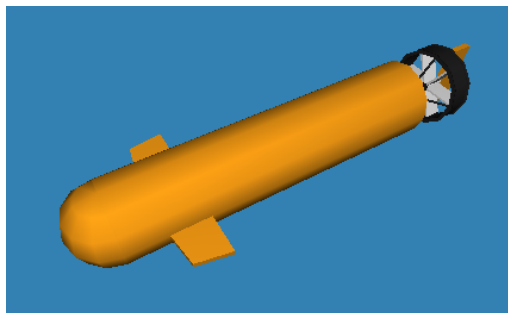


FIGURE C.1: Torpedo shape concept design.

The nature of the vehicle's movement by way of its bow planes, rudder and ballast tanks would introduce a high level of complexity in the control of the vehicle. These mechanisms

would involve intricate modelling in software in order to sufficiently and accurately control the vehicle's motion.

C.2 One Hull, Four Thrusters

The one-hull solution consists of a cylindrical tube with four thrusters attached to a skeletal frame (Figure C.2). Two thrusters would be used for horizontal motion and the other two for depth control. Due to components being housed in just one hull, the need for through-hull connections would be minimal, however, the amount of available space would be restrictive. The stability of the vehicle would also be a problem as the centre of mass would be located very close to the centre of buoyancy.



FIGURE C.2: The one-hull, four-thruster concept design.

Due to the use of four thrusters, power consumption would be far greater than with the torpedo design, hence the need for more batteries and space. On the other hand, the four-thruster configuration would allow for easier modelling and control of the vehicle in software. The frame supporting the hull and thrusters would also allow for modularity and relative ease in attaching external devices.

C.3 Two Hulls, Four Thrusters

The design in Figure C.3 is similar in structure to the one-hull solution, but consists of two hulls; an upper and lower one. The added benefits of this design includes increased space for components and an innate metacentric righting moment produced from a dense lower hull and a highly buoyant upper hull. Batteries would be housed in the lower hull to lower the centre of mass while the remaining components would be situated in the upper hull.

One disadvantage in comprising two hulls would be the need for more through-hull connections to link components in both hulls. Other advantages and disadvantages of this design are akin to those of the one-hull solution.

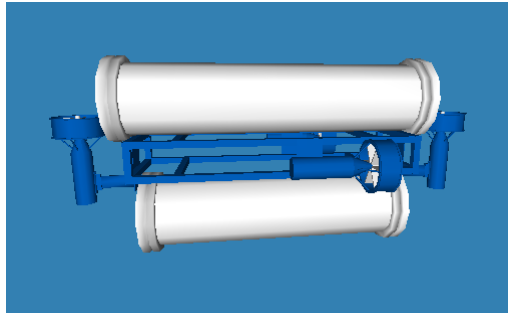


FIGURE C.3: The two-hull, four-thruster concept design.

C.4 Two Hulls, Two Rotating Thrusters

Following in the footsteps of the two hull design above, what makes the design in Figure C.4 unique is its rotational thrusters which allow both horizontal and vertical motion simultaneously. Utilising only two thrusters, this design would require much less power and reduce construction complexity both mechanically and electronically.

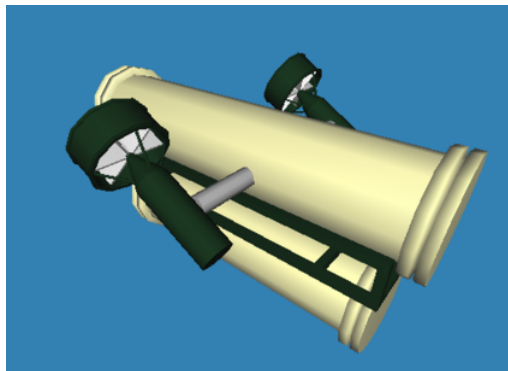


FIGURE C.4: The two-hull, rotational thrusters concept design.

The main disadvantage to this design though would be the need for powerful servos to be able to effectively rotate the thrusters. Another disadvantage would be the difficulty in guaranteeing watertight seals around these rotating mechanisms. Software modelling as well would generate some difficulty mostly attributable to the rotational nature and dynamics of the thrusters.

C.5 Comparison of Designs

A qualitative analysis of the four proposed AUV designs was made based upon particular attributes. A summary and comparison of the main advantages and disadvantages of the four concept designs is presented below in Table C.1.

ATTRIBUTES (DESIRABLE TO HAVE 'HIGH')	TORPEDO SHAPE	ONE HULL, FOUR THRUSTERS	TWO HULLS, FOUR THRUSTERS	TWO HULLS, TWO ROTATING THRUSTERS
Ease of machining and construction	Low	High	High	Moderate
Ease of ensuring water-tight integrity	Low	High	Moderate	Moderate
Power conservation	High	Low	Low	Moderate
Space available	Low	Moderate	High	High
Modularity	Low	Moderate	High	High
Cost-effectiveness	Low	High	High	Moderate
Ease of software control implementation	Low	High	High	Moderate
Range of motion	High	High	High	High
Ease in removing components	Low	Moderate	High	High
Ease in submerging	Low	High	High	High
Ability to withstand high pressure	High	Moderate	Moderate	Moderate
Sleekness/hydrodynamics	High	Moderate	Low	Low
Stability	Moderate	Moderate	High	High
Analysis* (Total Points /13.0)	4.5	9.0	10.0	9.0

* Sum of accumulated points: if 'High' = 1pt, if 'Moderate' = 0.5pt, if 'Low' = 0pt.

TABLE C.1: Comparison of Proposed AUV Concept Designs.

As seen in the preceding table, it is clear the torpedo shape design was not an ideal design to pursue when compared to the other designs. The disadvantages of the torpedo design far outweighed its advantages. The other designs provided a much more feasible and advantageous approach to designing the AUV.

Though Table C.1 did serve as a guide to choosing the final design, many other factors not discussed were also taken into account and considered before making any definitive decision.

Appendix D

Mechanical System Design

The mechanical and electrical designs of the AUV were not mutually exclusive. Each design had to complement the other and hence, there was a need for continuous and simultaneous considerations for both designs.

It is also worthy to note that the vehicle design was continually being subjected to minor changes and modifications in order to obtain an optimal design. Therefore, collaboration with the mechanical and electronic workshops almost everyday during the construction process was essential.

The design sought to develop a simple, easy-to-use and inexpensive AUV with a level of functionality that not only had the potential of accomplishing the 2004 underwater competition, but had enough modularity in order to adapt to different missions.

The budget and time available are usually the controlling factors in a design project. This was certainly true for the *Mako* where the availability of materials, the manufacturability, as well as the cost of components were very important issues in the design. Therefore, a compromise had to be found between cost, functionality and time available to manufacture the vehicle. The limited funds available for the project demanded the search for innovative and inexpensive approaches to solve certain problems.

A detailed summary of the mechanical design process is presented below.

D.1 Mechanical Requirements

Out of the four main proposed designs detailed in Appendix C, the final design was chosen to be the two-hull, four-thruster configuration for its significant advantages over the other designs. The mechanical design of the AUV sought to fulfil the following main objectives:

- To fit in a rectangular volume 1.8m long, 90cm wide and 90cm deep, as well as being buoyant by at least 0.5% of its mass; both as per IAUV C regulations
- To provide a dry, watertight hull that facilitates the housing of onboard electronic components and that is capable of surviving in a saltwater environment

- To provide a static and dynamically stable vehicle with suitable versatility in its motion to accomplish a wide range of tasks
- To possess the ability to be modular and extensible for future missions

More specifically, the design of the frame, the two hulls and position of the motors sought to comprise:

- As low a centre of mass as possible
- As high a centre of buoyancy as possible
- A modular frame to support the two hulls, motors and other external devices
- Centres of drag aligned with centres of thrust
- Shrouds for propellers to not only protect users, but to also avoid possible damage to them
- Symmetry for ease of design and construction, as well as easy modelling
- Adequate internal hull space for electronic components
- Sufficient space to accommodate external devices on the frame
- A longitudinally adjustable centre of mass to assist in static stability

D.2 Mechanical Design

The dimensions and shape of the initial mechanical design seen in Figure D.1 were based on the above specifications as well as the:

- Total expected mass and volume of the vehicle
- Size of onboard and external components
- Commercial availability of materials

D.2.1 Overview of Design

The design incorporates two hulls and four motors attached to a frame in a very symmetrical manner. By comprising two hulls, ample space is provided as well as the opportunity to create a low centre of mass and high centre of buoyancy for enhanced stability.

The existence of four motors provides 4DOF which can be actively controlled. The two horizontal motors control surge and yaw while the two vertical motors control heave and pitch. The positions of these motors are such that they align with the centres of drag and

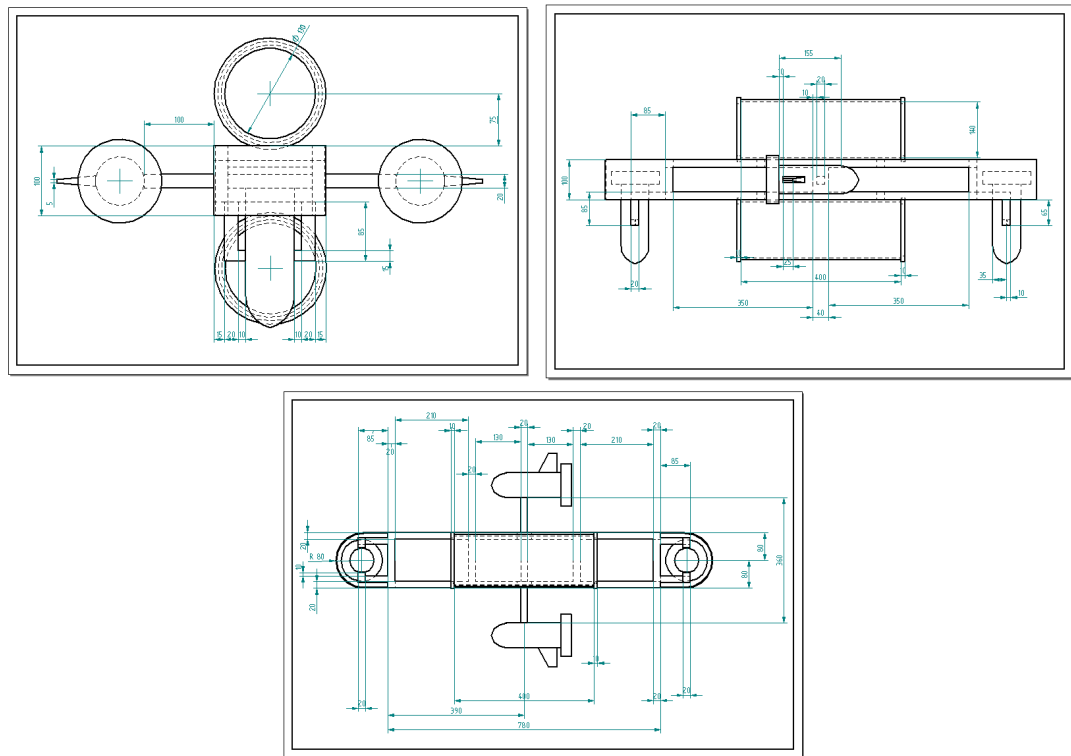


FIGURE D.1: Initial design schematics. (Top Left) Front view. (Top Right) Side view. (Bottom) Top view.

provide a significant amount of force and torque for moving the vehicle. Their positions also allow the relatively straightforward control and modelling of the vehicle.

The frame was designed not only to accommodate the two hulls and motors, but also to allow external components to be easily attached to the vehicle, hence, adding to the vehicle's modularity. The size of the motors and hulls determined the dimensions of the frame to a great extent. Shrouds for the vertical motors were incorporated into the ends of the frame while an adjustable mount was designed for the horizontal motors to adjust the centre of mass in order to maintain the vehicle in a statically horizontal posture.

D.2.2 Material Selection

There were several requirements for the materials to be used in the construction of the vehicle. Firstly, the materials had to be considerate to the overall weight of the vehicle. Materials also had to be corrosion resistant as they would be subjected to a harsh saltwater environment. Durability was also needed from the materials as the vehicle was being designed for several years of use. Furthermore, materials had to be inexpensive and easily machineable. Since the vehicle was not going to be subjected to more than 5m of depth, the materials chosen did not have to withstand significant amounts of pressure.

D.2.2.1 Hulls

The two tubes for the upper and lower hull were chosen to be made out of PVC. This material was preferred over aluminium and Perspex due to its low cost, its high strength and durability, and the ease with which it can be machined.

D.2.2.2 Frame

Aluminium was chosen for the frame due to its lightweight yet high strength qualities. Its resistance to corrosion and ease in machining were also governing factors in its selection.

D.2.3 Motor Selection

For the four motors, Sevylor trolling motors were chosen due to their inherent watertight integrity, their relatively small size and their low cost. Each motor has a mass of 1.5kg and displaces 700cm³ of water. Since the motors are positioned externally, their volume had to be taken into account for designing the overall volume of the vehicle.

D.2.4 Hull Sizes

The two hulls would account for most of the vehicle's volume and so deciding upon their size was critical. The determining factor for the size of the lower hull was the size of the batteries. It was calculated for the dimensions of the batteries that the minimum internal diameter of the lower hull must be 15cm. Now, since each battery was 15cm long, then the length of the lower hull would have to be an absolute minimum of 45cm.

Appraising different dimensions for the two hulls and aiming to obtain maximum possible internal space, while not using too much of the available external volume, resulted in a decision to have each of the two hulls 50cm long with an internal diameter of 15cm.

These dimensions provided a large amount of internal space for components and also used up a volume considerate to the overall available volume. Having the two hulls identical in size not only contributed to symmetry and ease of construction, but also allowed the centres of mass and buoyancy to be easily discerned. The symmetry was also conducive to determining the centres of drag and hence the positioning of the motors.

D.2.5 Mass and Volume Relationship

The total expected mass of the vehicle determined to a great extent the total volume available for the vehicle. This was because of the need for minimal buoyancy. Too much volume as opposed to mass would create too much buoyancy and therefore, the vertical motors would need to use more thrust to keep the vehicle submerged. If on the other hand, the volume was not large enough to counteract the mass, the vehicle would sink.

Since in the competition vehicles must be buoyant by at least 0.5% of their mass, it was desired to have the buoyancy of the AUV as close as possible to this value. Hence, the motors would require minimal thrust in order to keep the vehicle submerged, and if

there was any power failure onboard, the vehicle would still have some residual buoyancy to float back up to the surface.

The volume to mass relationship in order to have at least 0.5% buoyancy is derived as follows. If the vehicle is floating, then the buoyant force equals the vehicle's weight,

$$B = W = mg \tag{D.1}$$

where m is the mass of the vehicle and g is acceleration due to gravity. The buoyant force is determined by the weight of the water displaced by the vehicle, that is,

$$B = \rho g V \tag{D.2}$$

where ρ is the density of saltwater and V is the volume of the vehicle. The density of water varies with temperature, salinity and pressure, however, on average $\rho = 1.02\text{gcm}^{-3}$.

Combining equations D.1 and D.2 with the fact that the buoyant force should be 0.5% greater than the weight gives,

$$\begin{aligned} 1.005mg &\leq \rho g V \\ 1.005m &\leq \rho V \\ 1.005m &\leq \frac{1.02}{10^3} V \\ V &\geq 986m \end{aligned} \tag{D.3}$$

where the volume of the vehicle is measured in cm^3 and the mass is measured in kg. The above inequality states that for every 1kg about 986cm^3 of volume should exist to ensure at least 0.5% buoyancy.

D.2.5.1 Total Expected Mass

Determining the total expected mass of the vehicle was critical to ensure that inequality D.3 was not exceeded by too much. Although weights can be used to adjust the buoyancy of the vehicle as close as possible to 0.5%, if too much buoyancy exists, significant weight must be added to the vehicle to reduce this buoyancy. This is not ideal as unnecessary mass must be added to the vehicle.

However, at the same time the volume of the vehicle should be large enough to enable the addition of more components in the future without violating equation D.3. Factoring in a potential future addition of mass in the vicinity of 5kg leads to the following equation,

$$V = 986(m + 5) \tag{D.4}$$

The above equation states that to enable the addition of 5kg of mass in the future, the

volume of the vehicle must be designed so that it is $V = 986(m + 5)\text{cm}^3$. Hence, the buoyancy of the vehicle becomes,

$$1.005 \left(\frac{m + 5}{m} \right) \tag{D.5}$$

Therefore, because the buoyancy of the vehicle will be greater than 0.5% to allow for future increases in mass, the use of weights totalling a maximum of 5kg can be used to lower the buoyancy to a residual amount.

The total expected mass of the vehicle was found by weighing what components were on hand and estimating the mass of components yet to be obtained. Table D.1 presents the estimated mass of the components.

COMPONENT	MASS (kg)
Motors	~ 6
Batteries	~ 10.5
Two hulls	~ 4
Frame	~ 2
Electronic components	~ 1
Other	~ 1
Total Mass	~ 24.5

TABLE D.1: Estimated mass of components.

Estimating a total expected mass of about 25kg and using equation D.4,

$$V = 986(25 + 5) = 29580\text{cm}^3$$

Hence, a total volume of about 29500cm^3 would be desirable for the vehicle.

D.2.5.2 Total Expected Volume

The main components of the vehicle that would take up most of the volume were the two hulls, the frame and motors. Other external components such as the camera, cabling and through-hull connections would account for a comparatively small amount of volume. A summary of the estimated expected volumes for different components is shown in Table D.2.

Therefore, the final volume of the vehicle was estimated to be about 28500cm^3 which is quite close to the previously derived desirable volume of 29500cm^3 .

COMPONENT	VOLUME (cm ³)
Two hulls	~ 22000
Motors	~ 2800
Frame	~ 2500
Other	~ 1000
Total Volume	~ 28300

TABLE D.2: Estimated volume of components.

D.3 Comments on Design

The design shown in Figure D.1 aimed to incorporate and fulfil the requirements and specifications mentioned in section D.1. For instance, to ensure symmetry, the horizontal motors are positioned laterally and vertically equidistant from both hulls, while the vertical motors are positioned longitudinally equidistant from the hulls. Each hull is also positioned inline with one another for symmetry. With the highly symmetrical nature of the vehicle, stability and modelling would be less problematic. The symmetry also consequently aligns the centres of drag with the centres of thrust.

Due to the symmetry of the vehicle, the centre of buoyancy is located between the two hulls. Thus, to contribute to innate stability, the vertical motors were positioned so that their centres of mass were more or less in line with the lower hull's centre of mass. This configuration would allow the overall centre of mass of the vehicle to be lowered, producing a vertical displacement between the centres of buoyancy and mass.

Adequate spacing on the frame was incorporated in the design to allow for the mounting of components. Sufficient space was also left at the ends of each hull to allow internal components to be removed and at the same time allow external devices to be mounted on the frame.

With modifications and changes being made to the design during the construction process, the final design differed in certain respects, however, the basic structure of the vehicle remained the same. These modifications and their rationale are detailed in Appendix E along with the construction of the vehicle.

Appendix E

Electrical System Design

The electrical system design of the AUV needed to consider the functionality and tasks required of it not only for the requirements of the underwater competition, but also for basic functionality such as manoeuvring and navigation. At the same time, the restrictions that were present for the mechanical system such as cost and manufacturability, were a controlling factor in what could be done with respect to the electrical system. With this in mind, the electrical system sought to fulfil the following basic capabilities:

- Provide for motion control
- Provide for sonar and vision processing
- Measure the vehicle's depth
- Discern the vehicle's attitude
- Measure the vehicle's surge velocity
- Detect hull breaches and power shortage
- Supply sufficient power for ample testing periods

The block diagram of the electrical system layout designed to meet the above requirements is shown in Figure E.1. A component surrounded by blue indicates the component is located externally on the vehicle while those components surrounded by red are situated in the lower hull. All other components are located in the upper hull.

E.1 Motion Control

An Eyebot controller was chosen for the task of controlling the vehicle's four thrusters. The Eyebot provides a small, easy-to-use and highly functional platform on which to perform this task. Since the voltage of the onboard power supply was 12V, a regulator was needed to maintain the voltage at about 7V with a current of 0.25A.

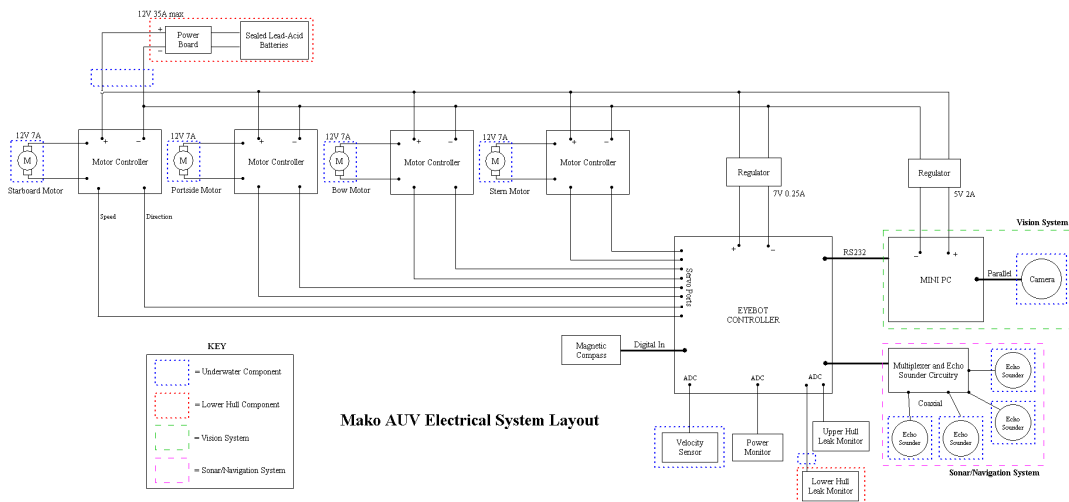


FIGURE E.1: Block diagram of electrical system.

Although the Eyebot has the capability to control motors via two built-in motor controllers, the fact that the AUV utilised four motors, and that each motor drew a maximum of 7A at 12V, required the design of a separate circuit board for four motor controllers. These motor controllers interface with the Eyebot controller via eight servo ports with each pair of ports controlling the speed and direction of each motor.

E.2 Sonar and Vision Processing

For both the sonar and vision systems, the other team members sourced their own required hardware. The objective was to integrate these systems into the vehicle. For the vision system a mini PC was selected for image processing. The Eyebot controller was not chosen for the vision system as image processing requires intensive computation and greater processing power. A parallel port web camera was chosen for the capturing of images. The camera attaches easily to the parallel port of the mini PC. The mini PC communicates with the Eyebot controller via a RS232 serial link.

For the sonar system, four echo sounders were chosen for navigating the AUV. These were integrated into the mechanical and electrical systems of the vehicle. As of yet, the sonar system is not fully functional.

E.3 Measuring Depth

For measuring the depth of the vehicle, a Navman Depth 2100 echo sounder was chosen for the task. These devices were chosen as part of the sonar and navigation system, however, it was decided to utilise a downward pointing echo sounder to detect the distance to the bottom. In this manner, if the height of the water is known, then the current depth of the vehicle can be discerned by subtracting the height of the water from the current reading

of the echo sounder.

The reason for this improvisation with an echo sounder and not resorting to a proper underwater pressure sensor was due to budgetary and time constraints. Since the sonar system is inherently utilising echo sounders which can determine the distance to objects, it made sense to exploit one of the echo sounders for determining depth. The drawback obviously is that the depth of the water must be known initially. The depth of the water must also remain constant. For testing purposes the depth of the water can easily be discerned. As for the requirement for a constant depth of water, the vehicle would have to be restricted to a body of water with constant depth if the depth sensor is to be used.

The echo sounder transmits data in serial form via its own data line. With the programming of the Eyebot controller being relatively straightforward, it became logical to use one of the serial ports not being utilised on the Eyebot for the echo sounder's data line.

E.4 Attitude

A low-cost Vector 2X digital magnetic compass module was chosen to provide yaw or heading control. The small module delivers high accuracy and low power, interfacing with the Eyebot controller via a digital input port.

Due to a low budget and time restrictions, a compass capable of acquiring all three Euler angles was not able to be attained. However, since the mechanical design of the vehicle sought to create a statically and dynamically stable vehicle with a passive roll and pitch control system, roll and pitch would be kept to a minimum and consequently only yaw would need to be actively controlled.

E.5 Velocity Sensor

A Navman Speed 2100 transducer was chosen for measuring the surge or forward velocity of the vehicle. The transducer uses a paddle wheel to measure the speed of the water. The device interfaces with an ADC channel on the Eyebot where the number of spins of the paddle wheel, and hence the velocity over a period of time, is able to be determined.

E.6 Hull Breaches

In order to avoid potential damage to electronic components in the event of a hull breach or leak, some sort of water detector was required. A simple water detector circuit as shown in Figure E.2 that connects to an ADC port on the Eyebot was designed to solve this problem. To detect in which hull a leak occurs, two sets of probes were required; each attached to different ADC ports. Knowing in which hull a leak occurs would save time in trying to isolate the leak. In the event a leak is detected, the idea is for the Eyebot to

immediately cease its program and send commands to the vertical thrusters to surface the vehicle for recovery.

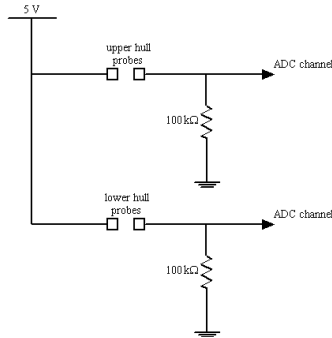


FIGURE E.2: Water detector circuits for upper and lower hulls.

E.7 Power Monitor

Due to the fact that the motors each draw 7A, it was not feasible to regulate their voltage at 12V because of the immense amount of heat that would need to be dissipated. Another problem would be the unacceptable noise levels that would be encountered in designing a regulator of the required size.

The reason for regulating the voltage in the first place is to ensure the voltage is kept constant and does not drop below unacceptable levels. If the voltage does drop significantly below 12V, the output thrust from the motors will drift from expected values. When this occurs the Eyebot controller loses the ability to accurately control the vehicle's motion.

To prevent the above situation from occurring, a power monitor was designed to detect when the power supply voltage drops to 11.5V. It was determined that at this voltage, the thrust outputs from the motors will begin to significantly drift from their expected values. The power monitor circuit (Figure E.3) is essentially a voltage divider circuit that connects to an ADC channel on the Eyebot controller.

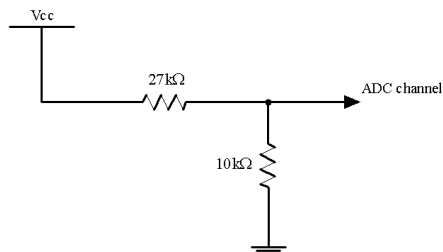


FIGURE E.3: Power monitor circuit.

The idea is for the Eyebot controller to periodically read the value on the ADC channel and detect when the voltage on the channel falls below 11.5V. At this point the Eyebot will immediately cease its program and send commands to the vertical thrusters to surface the vehicle for battery charging.

E.8 Power Supply

Three 12V sealed lead acid batteries totalling 31Ah were chosen to provide power for all onboard electronic components. A power distribution board (Figure E.4) was designed to connect all three batteries in parallel with diodes between each one to prevent the batteries trying to charge one another. A charging port, fuse and magnetic reed switch were also incorporated in the design. The charging port eliminates the need to remove the batteries from the hull for charging, the fuse prevents excessive current flow and the reed switch acts as an overall vehicle kill switch.

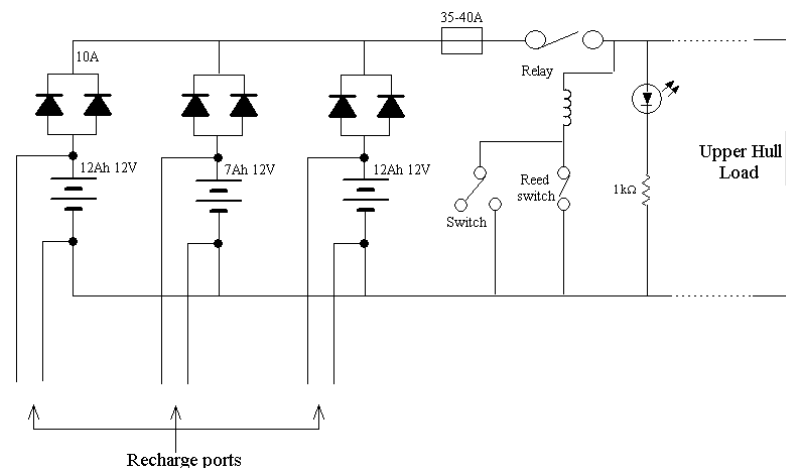


FIGURE E.4: Power distribution board circuit.

E.9 Through-hull connections

Due to external devices such as the motors and camera requiring connections to internal components, through-hull connections were required. Through-hull connections were needed for:

- Power supply from lower to upper hull
- Leak monitor for lower hull
- Four motors
- Camera
- Velocity sensor
- Echo sounders

The lower hull requires only one through-hull connection that handles both the power cables and the lower hull leak monitor probes. The upper hull, however, requires eleven through-hull connections; one for power, four for the motors, one for the camera, one for the velocity sensor and four others for the echo sounders.

Appendix F

Construction Process

Construction of the vehicle and its components took place over a period of several months. Close collaboration with the mechanical and electronic workshops during construction was a necessity to not only ensure a realisation that fulfilled the mechanical and electrical design requirements, but to also ensure mechanical and electronic components were built in a manner complementary to each other.

It is worthy to note that as with many designs on paper, the final product is never exactly the same. As such, the constructed AUV differed slightly in dimensions to the design schematics. Minor changes and modifications were continually being made to the AUV to improve certain aspects as well as to account for unforeseen assembly problems. The limited funds available for the project also demanded the search for innovative and inexpensive approaches to solve certain problems.

Presented below is a brief account of the construction process; the parts built and used, how the vehicle was put together, the problems encountered and the solutions around these problems.

F.1 Construction of Components

Several components had to be constructed and machined for the AUV. This section presents an outline of the main components and how they were manufactured for the vehicle.

F.1.1 Hulls

The upper and lower hulls were made from PVC tubing utilising threaded end caps (Figure F.1) with O-ring seals for easily opening and closing each end of the hull, but at the same time ensuring watertight integrity. Each tube measured 50cm in length with an internal diameter of 15cm.

To support the electronic components inside the upper hull, two Perspex boards were machined to size and PVC supports were attached inside the tube to allow the boards to



FIGURE F.1: (Left) The two PVC tubes. (Right) Tube with end caps in place.

be held in place and to easily slide in and out.

In order to position the three batteries in the lower hull, an aluminium rack was made to hold the batteries together. Supports were attached inside the tube to prevent the bank of batteries moving from side to side.

F.1.2 Through-hull Connections

Rubber hosing was used to house cables leading from external devices to the hulls. This was a relatively cheap and innovative alternative to using proper underwater connections. Through-hull connections were made with plastic plumbing connectors which allowed the rubber hosing to connect easily. Hose clamps were used around each connector to increase watertight integrity.

F.1.3 Motors

Each motor had to attach to the frame, but at the same time had to be removable in the event inspection, maintenance or replacement was necessary. Therefore, a clamp was made for each motor (Figure F.2) which could be bolted easily onto the frame. To connect the motor's cables to the upper hull, each motor was opened up and a threaded plastic connector was attached to the top of each motor. This allowed rubber hosing to be used to house cables from each motor to the end cap of the upper hull (Figure F.3). Each plastic connector had a sealant applied to it to ensure watertight integrity.



FIGURE F.2: Motor with clamp.

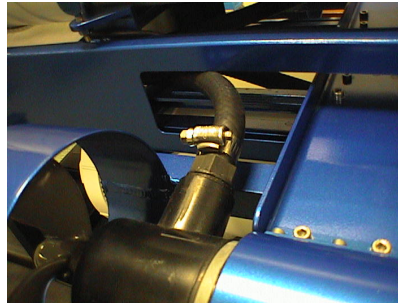


FIGURE F.3: Improvised underwater connector for motor.

F.1.4 Frame

The exoskeletal frame was built from aluminium and welded together. The frame was pressure tested to ensure no leaks. Allowing water to enter the frame would upset the buoyancy and stability of the vehicle and would also prove very difficult to remove afterwards. The main body of the frame is shown in Figure F.4.

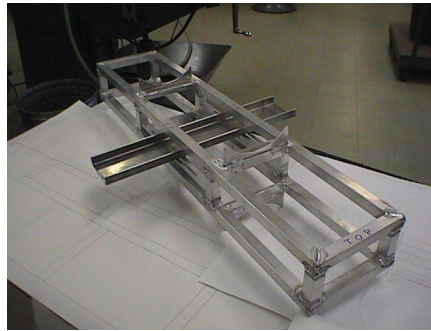


FIGURE F.4: The main body of the frame.

The vertical motors were each attached to the frame via their own mounts (Figure F.5) and their propellers protected by shrouds attached to these mounts. An adjustable mount (Figure F.6) was built for the horizontal motors for easily repositioning of the motors in an optimal position. The horizontal motors attach on either side of this mount.



FIGURE F.5: Vertical motor mount.

In order to hold the two hulls in place on the frame, aluminium straps were machined and supports welded onto the frame.



FIGURE F.6: The adjustable mount for the forward motors.

F.1.5 Motor Controllers

The motor controllers were built on two separate circuit boards. The smaller circuit board consists of logic circuits and connects to servo ports on the back of the Eyebot controller (Figure F.7). The larger board contains the MOSFETs for the H-bridges (Figure F.8). Both circuits connect together via a ribbon cable.



FIGURE F.7: Motor controller logic circuit board on the back of the Eyebot.



FIGURE F.8: MOSFET motor controller board.

Due to the high current consumption of the motors, the MOSFETs dissipate a large amount of heat. Hence, a large aluminium heat sink was attached to the MOSFETs. However, to prevent the build up of heat in the hull, it was decided to have an external heat sink protruding through the end cap (Figure F.9) and connected to the inner heat sink. This configuration would allow the external heat sink to be cooled by the water. This would then create a large temperature differential which would allow heat to flow to the outside and prevent the internal temperature from rising too high and causing damage to components.

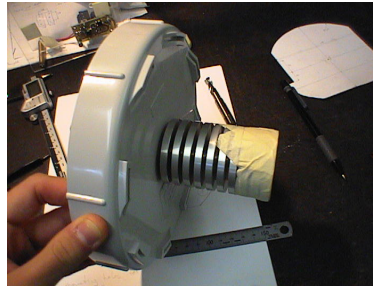


FIGURE F.9: Heat sink attached to end cap.

F.1.6 Power Board

A power board was built firstly to distribute power to the vehicle, secondly, to ensure the batteries discharged evenly, and thirdly, to allow onboard power to be disconnected from all circuits. The power distribution board was attached to the battery frame as shown in Figure F.10.

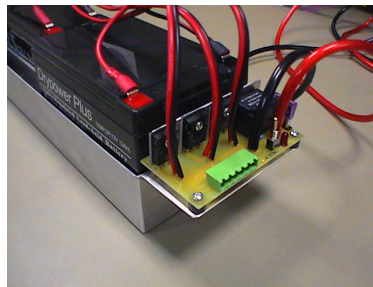


FIGURE F.10: Power board positioned on battery frame.

F.1.7 Regulators

Two voltage regulators were built for the Eyebot controller and the mini PC. Since the batteries supply 12V, regulators were needed to reduce the voltage to 7V and 5V for the Eyebot and PC respectively.

F.2 Uniting the Components

With most of the main parts and components built, the next step was to unite all the mechanical and electronic components (Figure F.11). The main problem encountered was the mounting of electronic components within the hulls and their connections. This was a very intricate process because components had to use up the available internal space conservatively and at the same time be positioned in such a way that was conducive to their removal from the hull.

Components in the upper hull were positioned on the Perspex boards in such a way to minimise space consumption. Due to cables running between the two boards, both boards

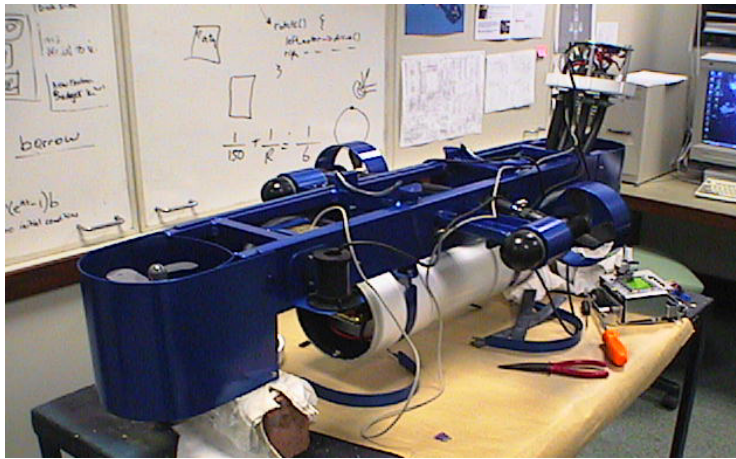


FIGURE F.11: Uniting the mechanical and electronic components.

were joined together via spacers (Figure F.12) so that they would slide out together.

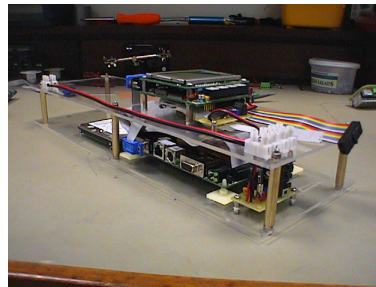


FIGURE F.12: Perspex board joined together via spacers.

To enable electronic components to be easily removed, two plates with mating connectors were constructed to allow the components on the Perspex boards to slide into the hull and mate blindly with the connectors situated in the rear. As such, no cables would have to be disconnected by hand to remove components for inspection or maintenance.

However, it was found that the Perspex boards were too flexible to enable satisfactory mating of the two connector plates. Therefore, the Perspex boards were replaced with machined aluminium plates. This provided a more sturdy and robust rack for the electronic components (Figure F.13).

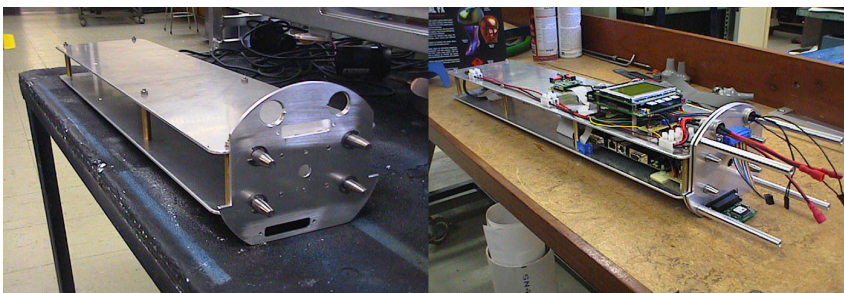


FIGURE F.13: (Left) Aluminium component rack. (Right) Rack with components.

One end cap from the upper hull was chosen for external connections. Both end caps could not be used for through-hull connections as this would result in cables becoming twisted when either end cap was removed. The end cap that was chosen had threaded plastic connectors affixed to it to house cables for the four motors, power from the lower hull, the lower hull leak monitor probes, the camera and other external devices (Figure F.14). The lower hull only required connectors on its end cap for the power cables and leak monitor probes.



FIGURE F.14: The external connections on upper hull's end cap.

Having acquired or built all the necessary components for the vehicle, a revised analysis of the total mass and volume revealed that the anticipated mass of 25kg had been an underestimate. The revised total mass of the vehicle was found to be closer to 35kg which meant that there was doubt as to whether or not the current volume of the vehicle would be able to produce a large enough buoyant force to counteract the vehicle's weight.

Therefore, a decision was made to increase the length of the upper hull to 75cm, thereby significantly increasing the volume of the vehicle and hence, the maximum allowable mass. This proved to be a minor setback with machining of the new PVC tube and other associated modifications being relatively straightforward.

F.3 Summary of Design and Construction

The final mechanical design schematics of the AUV can be seen in Figure F.15. In testing the components and the vehicle itself, the following was performed:

- All electronic components were tested and verified both individually and in combination with each other before mounting them into the hull
- The upper and lower hulls were each separately pressure tested for watertight integrity
- The whole vehicle was tested in water with the hulls and external connections checked for leakage
- The temperature inside the upper hull with all components operating was checked

- Software was written for controlling the speed and direction of the motors as well as for the leak monitor and power monitor
- Electronic components and all the motors were tested on the vehicle while underwater

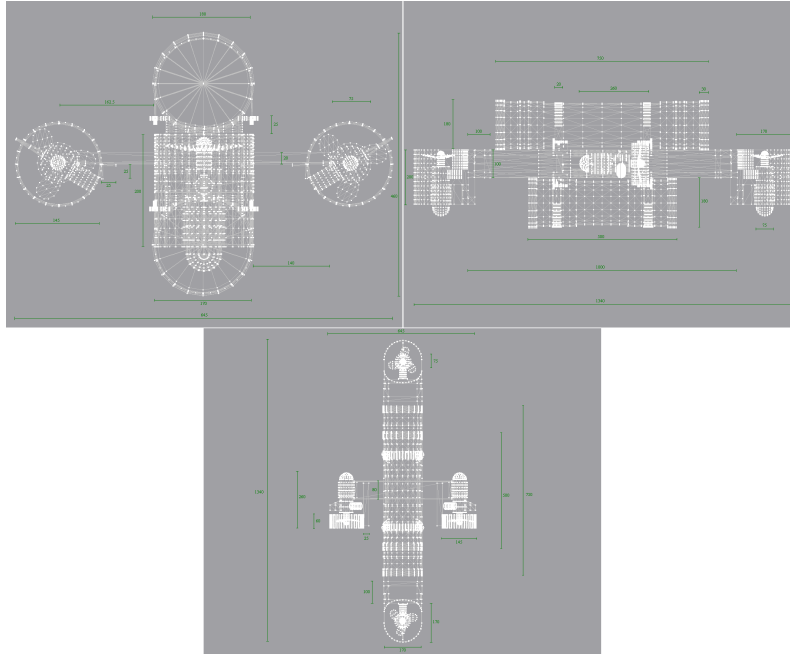


FIGURE F.15: Final design schematics. (Top left) Front view. (Top right) Portside view. (Bottom) Top view.

Testing of the electronic components and motors proved to be successful both in and out of the water. No leaks were found in the hulls or external connections, and the temperature readings inside the upper hull did not exceed undesirable levels. Indeed, very few minor modifications had to be made to the vehicle after initial testing.

Indeed, the mass and volume estimations as seen in Appendix D were significant underestimates. The mass of the vehicle in the end was 35kg. Although the vehicle was originally designed to have a maximum mass of 30kg, the fact that much more volume was added to the vehicle than was originally anticipated meant that the buoyant force remained greater than the weight of the vehicle.

The final painted vehicle undergoing testing can be seen in Figures F.16 and F.17. A flowchart of the process involved in designing and constructing the *Mako* AUV is shown in Figure F.18.

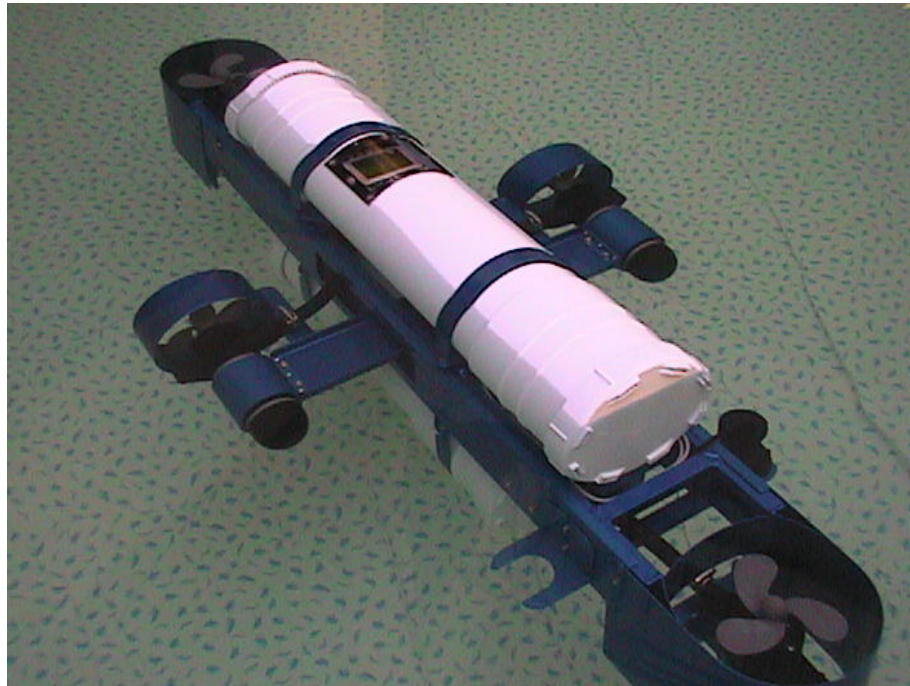


FIGURE F.16: The *Mako* undergoing underwater testing.

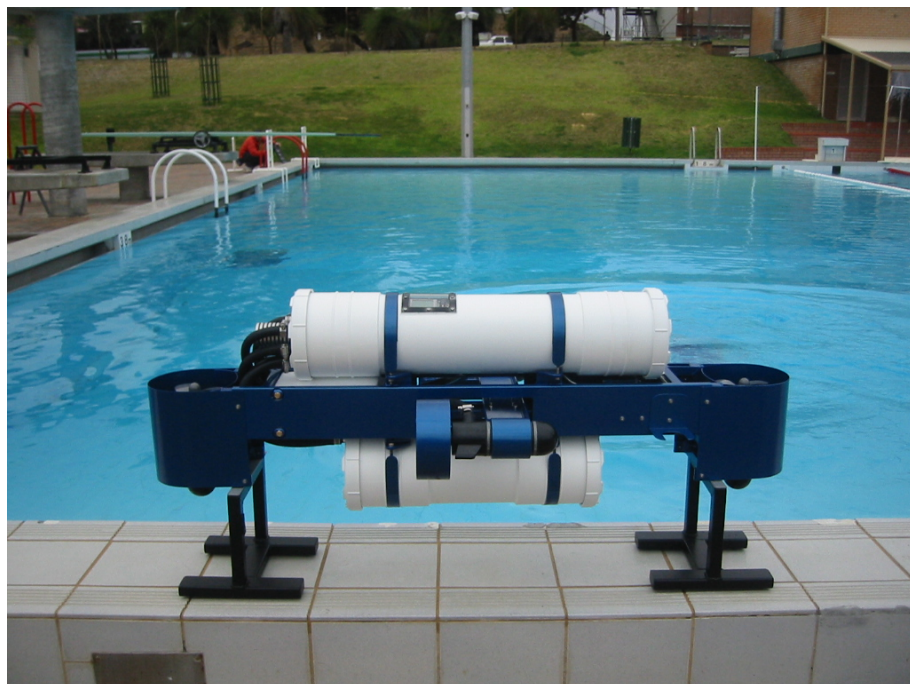


FIGURE F.17: Testing at local swimming pool.

AUV Design and Construction Flowchart

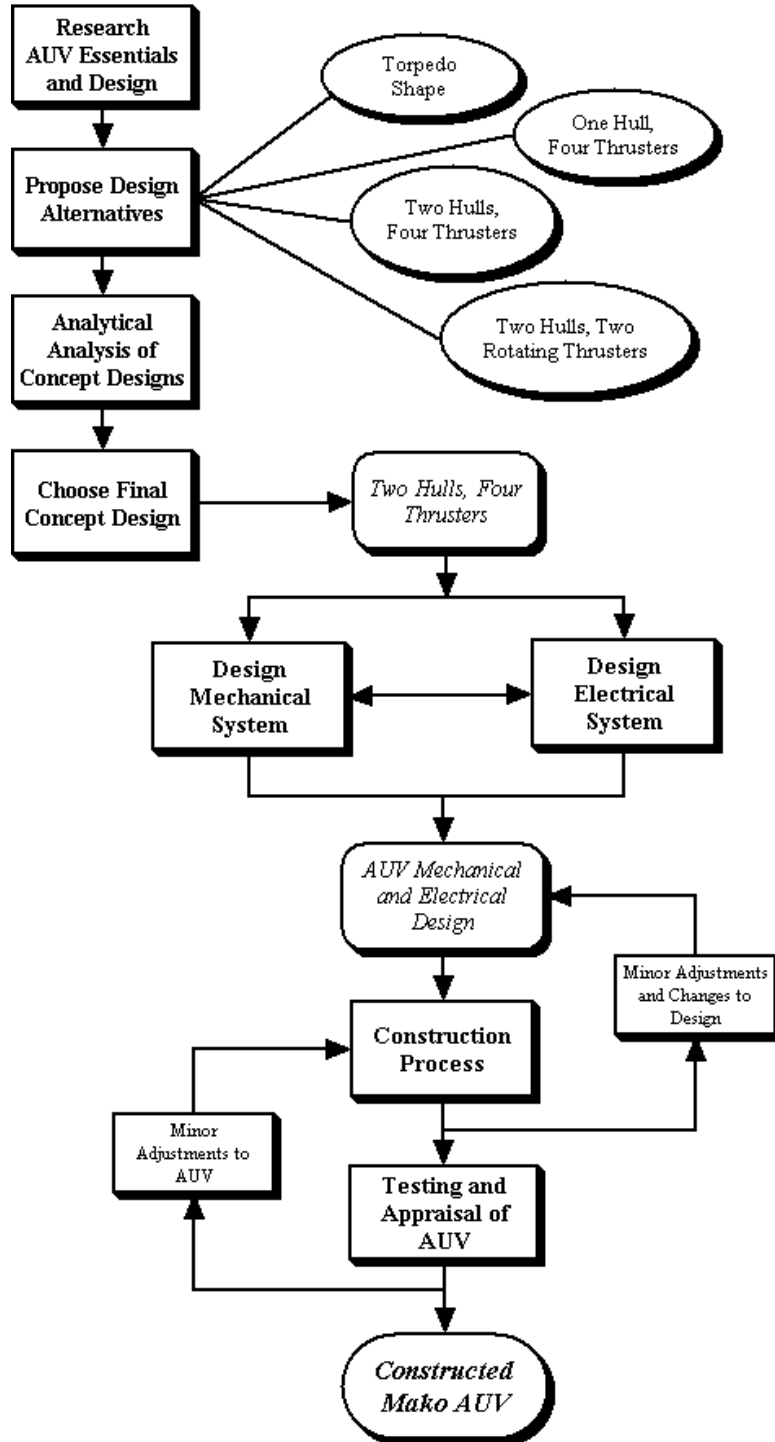


FIGURE F.18: Design and construction flowchart.

Appendix G

CDROM Listing

The contents of the CDROM submitted with this thesis are listed in this appendix.

CDROM directory contents:

- **Construction**
 - Contains photos of the construction of the *Mako* in chronological order
- **Source Code**
 - Contains the software written in C++ for the thrust measurement, system identification, sensor feedback, and remote control of the *Mako*
- **Testing**
 - Contains test footage and photos
- **Identification and Simulations**
 - Contains system identification and controller simulation software with results
- **Thesis**
 - *Design, Modelling and Control of an Autonomous Underwater Vehicle* Honours Thesis
 - Published paper associated with this thesis, *The Autonomous Underwater Vehicle Initiative - Project Mako*
 - Thesis source code in LATEX format including all figures
 - Interim report for this thesis
- **Miscellaneous**
 - Contains various pictures including design schematics and computer renderings

References

- [1] O. Xu. Autonomous underwater vehicles (auvs). Report, The University of Western Australia, 2004.
- [2] J. Yuh. Design and control of autonomous underwater robots: A survey. [online], 2000. Available: http://neuron-ai.tuke.sk/~hudecm/PDF_PAPERS/DesignAndControlOfAutonomousUnderwaterrobotsASurvey.pdf/.
- [3] Autonomous underwater vehicles. [online], 2003. Available: http://www.geo-prose.com/ALPS/white_papers/alt.pdf/.
- [4] Bluefin robotics. [online], 2004. Available: <http://www.bluefin.com/auv.htm/>.
- [5] Nps center for auv research. [online], 2003. Available: <http://www.cs.nps.navy.mil/research/auv/>.
- [6] Nekton research ltd. [online], 2003. Available: <http://www.nektonresearch.com/>.
- [7] W. Naeem et al. Lqg/ltr control of an autonomous underwater vehicle using a hybrid guidance law. In *International Federation on Automatic Control Journal*, 2003.
- [8] C. Silpa-Anan. Autonomous underwater vehicle: Vision and control. Master's thesis, The Australian National University, 2001.
- [9] S. Ahmad and R. Sutton. Dynamic modelling of a remotely operated vehicle. In *Proceedings of the 1st IFAC workshop on guidance and control of underwater vehicles GCUV'03*, pages 47–52, 2003.
- [10] P. Ridao et al. Model identification of a low-speed uuv. In *Control Applications in Marine Systems*. International Federation on Automatic Control, 2001.
- [11] M. Caccia et al. Modeling and identification of open-frame variable configuration unmanned underwater vehicles. In *IEEE Journal of Oceanic Engineering*, volume 25, pages 227–240, 2000.
- [12] G. Indiveri. *Modelling and Identification of Underwater Robotics Systems*. PhD thesis, University of Genova, 1998.

- [13] J. Healey and D. Lienard. Multivariable sliding model control for autonomous diving and steering of unmanned underwater vehicles. In *IEEE Journal of Oceanic Engineering*, volume 18, pages 327–339, 1993.
- [14] S. Feijun and S. Smith. Automatic design and optimization of fuzzy logic controllers for an autonomous underwater vehicle. In *OCEANS'2000 MTS/IEEE*, 2000.
- [15] T. Fossen and I. Fjellstad. Robust adaptive control of underwater vehicles. In *3rd IFAC Workshop on Control Applications in Marine Systems*, 1995.
- [16] D. Wettergreen et al. Autonomous guidance and control for an underwater robotic vehicle. In *Proceedings of the International Conference on Field and Service Robotics FSR'99*, 1999.
- [17] T. Bräunl. Research relevance of mobile robot competitions. *IEEE Robotics and Automation Magazine*, 6(4), 1999.
- [18] AUVSI. Association for unmanned vehicle systems international. [online], 2004. Available: <http://www.auvsi.org/>.
- [19] T. Bräunl et al. The autonomous underwater vehicle initiative - project mako. In *IEEE Conference on Robotics, Automation and Mechatronics*, 2004.
- [20] Surface ships: Principles of stability. [online], 2004. Available: http://wrc.chinalake.navy.mil/warfighter_enc/SHIPS/shipeng/stability/basics/basics.htm/.
- [21] T. Fossen. *Guidance and Control of Ocean Vehicles*. John Wiley and Sons, United States of America, 1995.
- [22] P. Brutzman. *A Virtual World for an Autonomous Underwater Vehicle*. PhD thesis, Naval Postgraduate School, 1994.
- [23] Wikipedia. [online], 2004. Available: http://en.wikipedia.org/wiki/Coriolis_effect/.
- [24] D. Grosset et al. Quasi-rigid docking of auv for underwater manipulations. In *Proceedings of the 4th International Workshop on Computer Science and Information Technologies*, 2002.
- [25] International submarine engineering web based auv designinfo. [online], 2000. Available: <http://www.ise.bc.ca/WADEsysdesign.html/>.
- [26] R. Altshuler. Orca-v: An autonomous underwater vehicle. [online], 2002. Available: <http://www.auvsi.org/competitions/2002/MIT.pdf/>.
- [27] Mit project orca. [online], 2002. Available: <http://web.mit.edu/orca/www/>.

- [28] D. Eaton et al. Nautilus: Evolution of an autonomous underwater vehicle. [online], 2003. Available: <http://www.auvsi.org/competitions/2003/WestFlorida.pdf/>.
- [29] J. Buescher et al. Cuauv: Design and implementation of an autonomous underwater vehicle for the 2003 auvsi underwater competition. [online], 2003. Available: <http://www.auvsi.org/competitions/2003/Cornell.pdf/>.
- [30] Cornell university autonomous underwater vehicle. [online], 2004. Available: <http://www.cuauv.org/>.
- [31] M. Makeev et al. Subjugator 2003. [online], 2000. Available: <http://www.auvsi.org/competitions/2003/Florida.pdf/>.
- [32] M. Nguyen. Design of an active acoustic sensor system for an autonomous underwater vehicle. Honours thesis, The University of Western Australia, 2004.
- [33] D. Lim. A vision system for an autonomous underwater vehicle. Honours thesis, The University of Western Australia, 2004.
- [34] D. Wettergreen et al. Development of autonomous underwater vehicle towards visual servo control. In *Proceedings of the Australian Conference on Robotics and Automation 2000*, 2000.
- [35] D. Juul et al. Submersible control using the linear quadratic gaussian with loop transfer recovery method. In *Proceedings of the Symposium on Autonomous Underwater Technology*, 1994.
- [36] M. Kwiesielewicz et al. Predictive versus fuzzy control of autonomous underwater vehicle. In *IEEE International Conference on Methods and Models in Automation and Robotics*, 2001.
- [37] S. Feijun and S. Smith. Design of sliding mode fuzzy controllers for an autonomous underwater vehicle without system model. In *OCEANS'2000 MTS/IEEE*, 2000.
- [38] S. Sagatun and R. Johansson. Optimal and adaptive control of underwater vehicles. In *4th Symposium on Robot Control*, 1994.
- [39] T. Fossen et al. On-board sensor-based adaptive control of small uuvs in very shallow water. In *Proceedings of the IFAC Conference on Control Applications in Marine Systems (CAMS '98)*, pages 201–207, 1998.
- [40] T. Fossen and S. Sagatun. Adaptive control of nonlinear underwater robotic systems. In *Proceedings of the IEEE Conference on Robotics and Automation*, pages 1687–1695, 1991.
- [41] T. Fossen and B. Foss. Sliding control of mimo nonlinear systems. In *Proceedings of the European Control Conference*, pages 1855–1860, 1991.

- [42] J. Healey and D. Lienard. Adaptive sliding mode control of autonomous underwater vehicles in the dive plane. In *IEEE Journal of Oceanic Engineering*, volume 15, pages 152–159, 1990.
- [43] D. Mills and C. Harris. Neurofuzzy modelling and control of a six degree of freedom auv. [online], 1996. Available: <http://www.ecs.soton.ac.uk/publications/rj/1995-1996/isis/djm/rj95.html>.
- [44] V. Filaretov et al. The sliding mode adaptive control system for autonomous underwater robot. In *Proceedings of ICAR '95*, 1995.
- [45] M. Carreras et al. *Dynamics Model of an Underwater Robotic Vehicle*. University of Girona, 2001.
- [46] J. Yuh. Modeling and control of underwater robot vehicles. In *IEEE Transactions on Systems, Man and Cybernetics*, volume 20, pages 1475–1483, 1990.
- [47] E. Broadway. Telemetry for an autonomous underwater vehicle. Honours thesis, 2004.
- [48] J. Adams and K. Rattan. Intelligent control of a direct drive robot using multi-stage pid. In *Proceedings of the 44th IEEE Midwest Symposium on Circuits and Systems*, 2001.
- [49] Rules and mission: 7th annual international autonomous underwater vehicle competition. [online], 2003. Available: http://www.auvsi.org/competitions/2004/%20AUV%20Comp/Rules/%20Mission_Final_2004.pdf/.